

# Master Thesis

Institute of Future Fuels, German Aerospace Centre (DLR)

Supervisors: Dr. Neumann, Nicole Carina

Dr. Moumin, Gkiokchan

Prof. Dr. Katharina Theis-Bröhl

## **Techno-Economic Analysis of Sustainable Ethylene Production Pathways**

Submitted by:

Onwunmelu, Uchechi Jennifer (38040)

M.Sc. Program: Process Engineering and Energy Technology,  
Hochschule Bremerhaven

Submission date: 31<sup>st</sup> march 2023

# Acknowledgements

My first appreciation goes to the Almighty God for his continuous love, support and guidance. This work would not have been possible without him.

I would like to thank my supervisors at DLR, Dr. Nicole Neumann and Dr. Gkiokchan Moumin for giving me this opportunity, also, for their patience, guidance and support. It was a pleasure working with you.

I would like to thank Prof. Dr. Katharina Theis-Bröhl for supervising this thesis and for her guidance throughout this work.

I would also like to appreciate my beloved family for their love, support and encouragement. Thank you for believing in me.

# Declaration of Authorship

I hereby declare that this thesis paper was written independently by me. I have also provided an accurate reference on the information and tools used from other sources and literature.

Cologne, 31.03.2023

Onwunmelu, Uchechi Jennifer

Signature:  \_\_\_\_\_

# Abstract

Ethylene is considered an important chemical in the chemical industry because it is a base chemical for the production of many chemicals like ethylene oxide, acetaldehyde, or ethylbenzene. As a result of this, its market demand is very large at a value of 141 Mt worldwide production of ethylene worldwide as recorded in 2015. Conventionally, ethylene is produced from fossil-based feedstock and its production process releases CO<sub>2</sub> into the atmosphere. Coupled with its large market demand, the amount of CO<sub>2</sub> emissions from the production of ethylene is considerably large at 1.51 kg CO<sub>2</sub> eq/kg of ethylene. This problem has fueled the need for developing sustainable ethylene production pathways. The sustainable pathways considered in this study were; Biogas based-oxidative coupling of methane and CO<sub>2</sub>-Oxidative coupling of methane. However, the CO<sub>2</sub>-oxidative coupling of methane (CO<sub>2</sub>-OCM) was chosen to be studied in this thesis in detail. This study was focused on carrying out a techno-economic analysis for the production of ethylene from CO<sub>2</sub>-OCM process and in further steps, comparing its economic results to other sustainable ethylene production pathways. The process simulation was done with the Aspen Plus software. Because the research of catalyst for the CO<sub>2</sub>-OCM reaction is still ongoing and no catalyst has been developed yet to give the desired industrial yield of 30 % for the C<sub>2</sub> products, it is important to investigate the economic feasibility of the process assuming the required C<sub>2</sub> yield is attainable. Thus, this work identifies the economic potential of the CO<sub>2</sub>-OCM process. The ethylene obtained from this simulation is of polymer grade with purity of 99.9 %. The economic analysis carried out after the process simulation produced a net production cost of 16.85 \$/kg of ethylene. The value of the OPEX was found to contribute 98 % to the NPC of ethylene while the CAPEX contributed 2 %. It was discovered that the cost of SNG in the process was the major cost driver for the NPC of ethylene. Sensitivity analysis was done by varying operational hours, CO<sub>2</sub> cost and SNG cost to investigate their effect on the NPC of ethylene. More attention was paid to SNG as the major cost driver of the process. Depending on the assumed SNG cost, ethylene from the CO<sub>2</sub>-OCM process can be considerably more expensive than fossil ethylene and the BG-OCM pathway. A further analysis for the CO<sub>2</sub>-OCM process was done by replacing its SNG feedstock with biomethane which costs lesser at 0.82 \$/kg and this resulted in an NPC of 1.86 \$/kg of ethylene. This result showed that the CO<sub>2</sub>-OCM process may be competitive as a sustainable pathway for ethylene production if biomethane instead of SNG is utilized as feedstock or if SNG can be provided at a considerably low cost of 0.74 \$/kg. This work thus shows that low SNG cost is a basic prerequisite if a shift away from the fossil ethylene production pathway to the CO<sub>2</sub>-OCM pathway is necessary.

# Table of Content

Abstract .....	iv
Table of Content.....	v
List of Figures .....	vii
List of Tables.....	ix
Glossary.....	xi
1. Introduction .....	1
1.1 Motivation .....	4
2. State of the Art .....	6
2.1 CO <sub>2</sub> Utilization Technologies .....	7
2.2 Solar Energy.....	10
2.3 Ethylene Production .....	14
3. Methodology .....	23
3.1 Process simulation.....	23
3.2 Economic analysis.....	30
4. Results and Discussion.....	39
4.1 Process simulation.....	39
4.2 Economic Analysis.....	46
5. Conclusion and Outlook.....	59
Publication bibliography .....	62
Appendix A .....	69

Appendix A.1 CO <sub>2</sub> -OCM Catalysts .....	69
Appendix B .....	70
Appendix B.1: Process Simulation.....	70
Appendix B.2: Stream results.....	72
Appendix B.3: Energy Analysis .....	80
Appendix C .....	82
Appendix C.1 Equipment sizing and costing .....	82
Appendix C.2 sensitivity analysis .....	84

# List of Figures

Figure 1: Annual CO <sub>2</sub> Emission from 1750 – 2020 (Ritchie et al. 2020). .....	2
Figure 2: Ethylene and its derivatives (Torres Galvis and Jong 2013). .....	10
Figure 3: DNI distribution of different countries in world (Global Solar Atlas 2023).....	12
Figure 4: Different concentrating solar technologies. Adapted from (Abanades et al. 2021).....	13
Figure 5: Different production pathway of conventional ethylene production (arescotx.com). .	14
Figure 6: Equilibrium conversion of methane to ethane and ethylene with respect to change in temperature and CO <sub>2</sub> :CH <sub>4</sub> ratio (Wang and Zhu 2004). .....	20
Figure 7: Block diagram of the CO <sub>2</sub> -OCM ethylene production plant.....	23
Figure 8: Design spec of ethylene yield from reactor. ....	25
Figure 9: Equilibrium reactions in the absorber column. ....	26
Figure 10: Thermal requirement at different lean loading levels (Abu-Zahra et al. 2007). .....	28
Figure 11: Complete process flow diagram. ....	40
Figure 12: Process flow diagram and simulation results of the OCM reactor .....	41
Figure 13: Process flow diagram for the CO <sub>2</sub> absorption section. ....	41
Figure 14: Process flow diagram of DEMTH column .....	43
Figure 15: Process flow diagram of COSEP column .....	44
Figure 16: Process flow diagram of C2SPLIT column. ....	44
Figure 17: Composite curves from Aspen Energy analyzer for pinch point analysis. ....	45
Figure 18: Summary of equipment cost. ....	48
Figure 19: OPEX Breakdown. The inner pie-chart shows the specific OPEX contributions. The outer pie-chart shows the percentage of specific OPEX covered by the sale of By-Products. The ‘remaining’ section of the outer pie-chart is the percentage of specific OPEX not covered by the sale of By-products.....	51

Figure 20:CAPEX and OPEX contribution to the Net production cost. ....	52
Figure 21: Ethylene Price vs operational hours of the plant. ....	53
Figure 22: Ethylene price vs CO <sub>2</sub> sources.....	54
Figure 23: Ethylene price comparison.....	58

# List of Tables

Table 1: CSE Technologies with their respective concentration ratios and temperature ranges extracted from <sup>(a)</sup> (Abanades et al. 2021), <sup>(b)</sup> (Chu and Meisen 2011), <sup>(c)</sup> (Romero and González-Aguilar 2014) .....	13
Table 2: Specifications for CO <sub>2</sub> absorber column. ....	26
Table 3: Specifications for stripper column. ....	27
Table 4: Specifications for DEMTH column. ....	29
Table 5: Specifications for COSEP column. ....	29
Table 6: Specifications for C2SPLIT column. ....	30
Table 7: Parameters required for costing of Equipment.....	32
Table 8: Simulation results for CO <sub>2</sub> absorption section. ....	42
Table 9: Heat demand comparison of this study with literature simulation values.....	42
Table 10: Simulation result of the DEMTH column. ....	43
Table 11: Simulation results of the COSEP column. ....	43
Table 12: Simulation result of the C2SPLIT column.....	45
Table 13: Purchasing and installation cost of OCM reactor and heat exchangers. The heat exchangers described as PEX are process heat exchangers where both hot and cold process streams are cooled and heated up simultaneously.....	47
Table 14: Purchasing and installation cost of multi-compressor, pump and expander. ....	47
Table 15: Purchasing and installation cost for Distillation and flash columns. ....	48
Table 16: Plant production and parameters.....	49
Table 17: Demand and cost of utilities. CST demand represents the heat demand for the OCM reactor which is supplied by solar towers. Heat demand represents the heat demand for the stripper which is supplied by the parabolic trough.....	49

Table 18: By-Product cost.....	50
Table 19: Operational expenditure summary. ....	51
Table 20: CO <sub>2</sub> sources, cost adapted from <sup>(a)</sup> (Fu et al. 2010), <sup>(b)</sup> (Psarras et al. 2017) <sup>(c)</sup> (Giglio et al. 2015) <sup>(d)</sup> (Fasihi et al. 2019) and their corresponding ethylene production prices.....	53
Table 21: Summary of SNG cost scenarios.....	55
Table 22: Comparison of CO <sub>2</sub> -OCM and BG-OCM. ....	57
Table 23: Comparison of CO <sub>2</sub> -OCM and BG-OCM (2).....	57
Table 24: Comparison of Biogas price in the BG-OCM study and a literature source (Leme and Seabra 2017).....	57

# Glossary

**AEL**

Alkaline Electrolyzer

**ACC**

Annual Capital Cost

**ACCR**

Annual Capital Charge Ratio

**BG-OCM**

Biogas-based Oxidative Coupling of Methane

**CCS**

Carbon Capture and Storage

**CCU**

Carbon Capture and Utilization

**CEPCI**

Chemical Engineering Plant Cost Index

**CPP**

Catalytic Pyrolysis Process

**CSE**

Concentrated solar energy

**CSP**

Concentrating Solar Power

**CST**

Concentrating Solar Thermal

**DAC**

Direct Air Capture

**DCC**

deep catalytic cracking

**DNI**

Direct Normal Irradiance

**DOE**

Department of America

**ELECTNRTL**

Electrolyte Non-Random-Two-Liquid

**ESC**

Ethane Steam Cracking

**FCI**

Fixed Capital Investment

**FTO**

Fischer Tropsch to Olefins

**GDP**

Gross Domestic Product

**GHG**

Greenhouse gas	<b>SOEC</b>
<b>HEN</b>	Solid oxide electrolysis cells
Heat Exchanger Network	<b>SOC</b>
<b>MTO</b>	Solid oxide cell
Methanol to Olefins	<b>SRK</b>
<b>NDCs</b>	Soave–Redlich–Kwong
Nationally Determined Contributions	<b>UNFCCC</b>
<b>NPC</b>	United Nations Framework Convention on Climate Change
Net Production Cost	<b>USD</b>
<b>OCM</b>	United States Dollars
Oxidative Coupling of Methane	<b>WC</b>
<b>OECD</b>	Working Capital
Organization for Economic Co-operation and Development	
<b>OPEX</b>	
Operational Cost Expenditure	
<b>PCC</b>	
Post-Combustion Capture	
<b>PtG</b>	
Power to Gas	
<b>TAC</b>	
Total annualized Cost	
<b>TCI</b>	
Total Capital Investment	

# 1. Introduction

The natural Carbon cycle (C-cycle) represents an equilibrium of the Carbon dioxide (CO<sub>2</sub>) uptake and release that occurs naturally, which maintains the CO<sub>2</sub> concentration in the atmosphere at a constant level of 270 ppm (Aresta and Dibenedetto 2021). The greenhouse effect on the Earth's surface keeps it warm, and without this, the Earth would be at a temperature of  $-18^{\circ}\text{C}$ . The anthropogenic greenhouse effect leads to climate change, which results in a rise in the Earth's temperature, which causes global warming, rise in sea levels, food security, health problems, etc. (Yoro and Daramola 2020).

CO<sub>2</sub> emission from natural sources are greater in amount compared to the CO<sub>2</sub> emitted as a result of human activities, however, these natural CO<sub>2</sub> emissions are balanced out by nature. The extra amount of CO<sub>2</sub> emissions caused by human activity cannot be balanced out by nature, hence results in the accumulation of CO<sub>2</sub> in the atmosphere at undesired amounts (Yoro and Daramola 2020). A major contributor of CO<sub>2</sub> accumulation in the atmosphere is caused by the increased industrialization and robust growth of economies in the world which drives the high demand of energy usage (Aresta 2010). Major CO<sub>2</sub> emissions contributors can be divided into several sectors; the Power sector, the transportation sector, the agricultural sector and the manufacturing sector (Aresta and Dibenedetto 2021). The source of CO<sub>2</sub> emissions in the power industry is the production of electricity from fossil-based sources. In the transportation industry, fossil fuels are combusted for use in automobiles and jets. These emissions from the fossil fuel combustion contain mainly CO<sub>2</sub> emissions to the atmosphere. In 2019, the amount of CO<sub>2</sub> emitted from combustion of fossil fuel amounted to about 58.7 billion tons. In the manufacturing industry, CO<sub>2</sub> is emitted from waste disposal of manufacturing processes, energy utilization from fossil fuel for supply of heat to processes, etc. The agricultural industry contributes the least CO<sub>2</sub> emissions compared to other industries (Yoro and Daramola 2020).

In 2017, the amount of production from the chemical, petrochemical and pharmaceutical industry amounted to 5.7 US Dollars (USD) with predictions to quadruple in 2060. This shows how important these industries are in the economy of the world. The reliance of the chemical and petrochemical industry on fossil fuels and fossil feedstock makes it a major contributor to CO<sub>2</sub> emissions in the industry, while iron and steel production, alongside cement production are regarded as lesser contributors in comparison (Saygin and Gielen 2021). The chemical and petrochemical sector produces chemicals, plastics, fibers and several other kinds of products. The production of chemicals alone accounts for about 1.1 Gt of CO<sub>2</sub> emissions annually, these

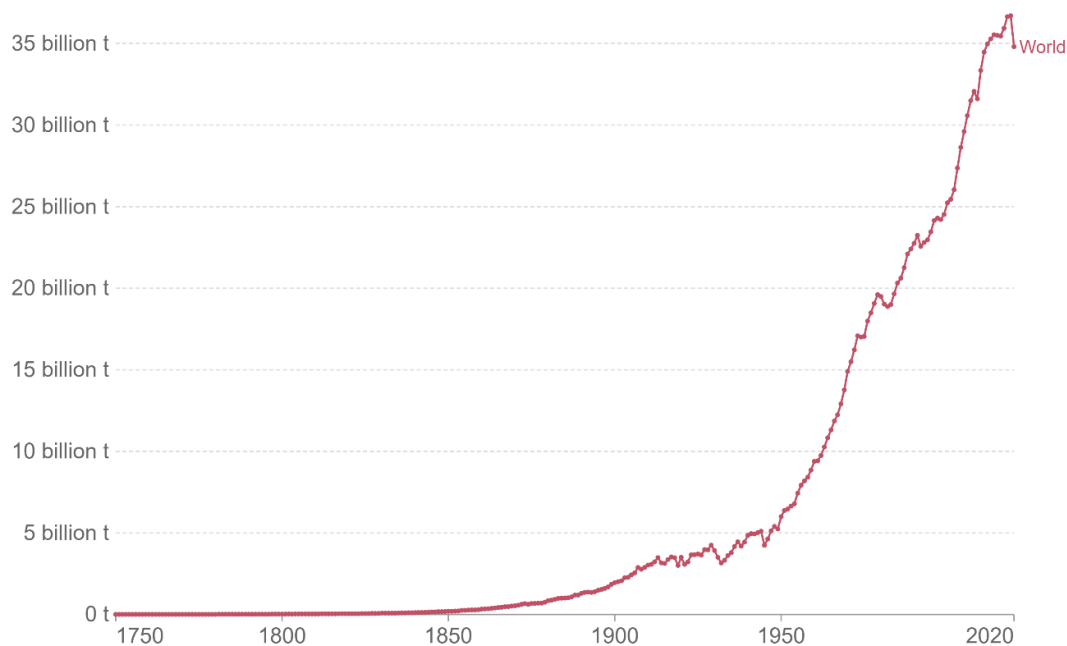
emissions are not only calculated for the production of chemicals but also for its usage and waste disposal. Also, indirect CO<sub>2</sub> emission from electricity supply resulted in about 0.6 Gt of CO<sub>2</sub> annually. In 2017, the chemical and petrochemical sector consumed 46.8 exajoules (EJ) of energy, including non-energy use (Saygin and Gielen 2021). According to (Aresta 2010), carbon-based fossil fuels account for about 80 – 85 % of energy sources.

From Figure 1, it can be seen that CO<sub>2</sub> emissions from fossil fuels and industries have been on a constant rise from 1750s up until the 1900s, after which there has been a rise and fall of CO<sub>2</sub> emissions. In general, over the years the amount of CO<sub>2</sub> emissions from fossil fuels and industry up until 2020 is about 35 billion tones, this is a clear increase from the zero CO<sub>2</sub> emissions in the 1750s. Studies have shown that if the concentration of CO<sub>2</sub> in the atmosphere continues to increase, it could lead to irreversible changes in climate. In order to stabilize the global mean temperature, there has to be an immediate action of reduction or elimination of CO<sub>2</sub> emissions into the atmosphere (Wilcox 2012).

## Annual CO<sub>2</sub> emissions

Carbon dioxide (CO<sub>2</sub>) emissions from fossil fuels and industry. Land use change is not included.

Our World  
in Data



Source: Global Carbon Project

OurWorldInData.org/co2-and-other-greenhouse-gas-emissions/ • CC BY

Figure 1: Annual CO<sub>2</sub> Emission from 1750 – 2020 (Ritchie et al. 2020).

CO<sub>2</sub> concentration in the atmosphere as at the year 2019 was recorded as 410 ppm, before the industrial age the CO<sub>2</sub> atmospheric concentration was 273 ppm. There have been several policies put into place to help regulate the amount of CO<sub>2</sub> concentration in the atmosphere, policies like the European Union (EU) 2030 and 2050 CO<sub>2</sub> atmospheric concentration target. The target is to

get the CO<sub>2</sub> concentration in the atmosphere to a stabilized 450 ppm and a limiting global warming level of 1.5 °C. In order to achieve this target, the global Greenhouse gas (GHG) emission should not exceed the limit of 270 Gt in CO<sub>2</sub> equivalent (Gt<sub>CO<sub>2</sub>eq</sub>). If the CO<sub>2</sub> emission annually is a 30 Gt/y CO<sub>2</sub> emission equivalent, then the 270 Gt<sub>CO<sub>2</sub>eq</sub> limit will be reached in a few years (Aresta and Dibenedetto 2021).

The Paris Climate Agreement is an international effort to set the goal of the maintenance of global temperature rise to below 2 °C above pre-industrial levels. This agreement was signed by several countries like China, US, also the EU and this is a step in the right direction to reduce GHG emissions. This agreement does not only serve as a pledge to the parties involved but it also obliges them to communicate intended efforts and take responsibility into putting these efforts to action (Schreurs 2016). The parties are obliged to make an update every five years of their Nationally Determined Contributions (NDCs) to the United Nations Framework Convention on Climate Change (UNFCCC). In 2021, the new and updated NDCs that were submitted to the UNFCCC accounted for over 40 % of global CO<sub>2</sub> emissions, the updated NDCs also had more targets or larger number of sectors to be covered for GHGs emission reduction. These pledges vary in scope depending on the countries involved, some pledges are made towards the specific kind of GHG emissions to be reduced, which sectors emissions can be reduced from and which sectors are excluded, use of carbon dioxide removal techniques, time frames for these emission reductions, etc. More governments are making pledges towards net zero GHG emissions by 2050, these countries including the EU account for about 70 % of the global CO<sub>2</sub> emissions (International Energy Agency 2021).

In the 1997 Kyoto protocol, the European Union made a commitment to reduce its GHG emissions to eight percent compared with 1990 emission levels. In 2008, the EU announced its 2020 target which involved reducing GHG emissions to 20 % compared to 1990 emission levels, with an energy consumption mix that includes 20 % of renewables and an improved energy efficiency of 20 % (Schreurs 2016). To put the EU on the track to achieving climate neutrality by 2050, GHG emissions should be reduced by 55 % by 2030. For the EU, this means not only reducing emission in high emitting sectors like coal power stations and energy-intensive industries but also in other sectors like transportation, agriculture and construction where reduction emission challenges exist (European Commission 2011).

Reduction of CO<sub>2</sub> emission and accumulation in the atmosphere can be achieved through several measures like energy efficiency, fuel substitution from coal sources to oil and gas, as coal has higher CO<sub>2</sub> emission than petroleum or natural gas because it contains more carbon, the use of advanced technologies to produce electricity, the use of renewable energy sources, CO<sub>2</sub> capture,

storage and utilization, etc. All these measures mentioned earlier can only provide short to medium term emission reduction individually but if combined, could lead to an effective CO<sub>2</sub> emission reduction method. Energy efficiency in terms of better energy conversion from chemical to electrical, also the concept of energy saving and responsible use of energy would help reduce emissions (Aresta 2010). Coal is used in the power sector for electricity production, the use of coal is advantageous because as a raw material it is readily available. However, coal has higher CO<sub>2</sub> emissions than petroleum or natural gas because it contains more carbon. Therefore, the idea to replace coal source with oil and gas in the power industry would also help to reduce CO<sub>2</sub> emissions. A better alternative would be the use of renewable energy as energy source for industries. For example, one of the ways to reduce emissions in the cement industry is by the replacement of fuel from coal with biomass or co-gasified coal and biomass (Yoro and Daramola 2020). Biomass can also be used to produce fuel that is suitable for automobiles and jets in the transportation. Renewable energy sources like wind, solar, hydro or geothermal can be used as alternative energy sources in industries, even though the extent of its availability and application is largely dependent on geographical and time factors (Aresta 2010).

Petrochemical industries produce fuels and chemicals that can be used as feedstock for production of other chemicals. The production of these products releases a substantial amount of CO<sub>2</sub> to the atmosphere. If the CO<sub>2</sub> from these processes are captured and not released into the atmosphere, it helps reduce its emissions. Apart from the petrochemical industries, there are other chemical processes that emit CO<sub>2</sub> and so the technology of capturing this gas before it gets into the atmosphere has a huge potential to reduce CO<sub>2</sub> emissions (Yoro and Daramola 2020). Another technology considered to have a huge reduction potential is the utilization of these captured CO<sub>2</sub> to replace the use of carbon feedstock from fossil resources in the chemical industry (Kätelhön et al. 2019). In order to meet the net-zero emission target, it is estimated that about 1.6 Gt CO<sub>2</sub> and 7.6 Gt CO<sub>2</sub> per year should be captured in 2030 and 2050 respectively (International Energy Agency 2021).

## 1.1 Motivation

Chemical and petrochemical industries are one of the largest contributors of CO<sub>2</sub> into the atmosphere compared to other industries, this makes carbon capture and utilization technologies even more important in its implement in these industries. One of the ways to reduce their carbon footprint is by replacing its carbon-based feedstock with captured CO<sub>2</sub>. In the utilization of CO<sub>2</sub>, the market size and demand of the end product is important, as it consumes more CO<sub>2</sub> than

chemicals that have lesser market size and demand. Ethylene is known as a base chemical for many chemicals in the chemical industry, thereby making the demand and market size of ethylene very high. With an ethylene production in 2015 of 141 Mt and CO<sub>2</sub> emissions of 1.51 kg CO<sub>2</sub> eq/kg of ethylene produced, it can be seen how significant ethylene production is to the contribution of CO<sub>2</sub> emissions into the atmosphere and how much CO<sub>2</sub> can be avoided by replacing its fossil-based feedstock with captured CO<sub>2</sub>. The need for sustainable ethylene production can therefore not be overemphasized.

In this study, a techno-economic analysis will be carried out on a sustainable ethylene production pathway to evaluate its feasibility for industrial scale production. This would be achieved by carrying out a process simulation of the desired process and also a cost estimation and economical evaluations based on the process simulation carried out.

## 2. State of the Art

Carbon Capture and Storage (CCS) is the capture of CO<sub>2</sub> from emission sources, transportation and storage of this captured CO<sub>2</sub> in geological formations. The aim of CCS is to prevent the emission of CO<sub>2</sub> into the atmosphere (Anderson and Newell 2004). CO<sub>2</sub> is a main product from combustion processes, it can be captured from different sources depending on the operating conditions and combustion processes involved. There are several CO<sub>2</sub> capture categories; Post-Combustion Capture (PCC), oxyfuel combustion capture and pre-combustion capture. PCC involves the capture of CO<sub>2</sub> from combustion process plants like in thermal power generation plants, fossil fuels plants, biomass plants, etc. (Koytsoumpa et al. 2018). In oxyfuel combustion capture, pure oxygen is used to combust fuels instead of using air. When pure oxygen is used for the combustion, high CO<sub>2</sub> concentrations can be obtained (Anderson and Newell 2004). Pre-combustion capture is the separation of CO<sub>2</sub> from a conversion process. An example would be the separation of the CO<sub>2</sub> generated from water gas shift reaction with hydrogen as co-product (Koytsoumpa et al. 2018).

The cost of CCS depends on the combustion process involved and the component of the off-gas stream. CCS technologies are generally less expensive when higher concentrations of CO<sub>2</sub> is available for capture and lower operating temperatures are used. This means that not all sectors that contribute to the CO<sub>2</sub> emissions are compatible with CCS technologies, if their CO<sub>2</sub> concentration is low (Anderson and Newell 2004). Thermal power plants have large CO<sub>2</sub> emissions, accounting for about 40 % of total Organization for Economic Co-operation and Development (OECD) CO<sub>2</sub> emissions while the transportation sector accounted for 29 %. In 2014, total OECD CO<sub>2</sub> emissions for fuel combustion accounted for 11.9 Gt CO<sub>2</sub>, from which oil, coal and gas contribute largely (Koytsoumpa et al. 2018). Technologies for CO<sub>2</sub> capture like absorption, adsorption, membrane technology and air separation exist, even though their applications are dependent on several factors like the concentration of CO<sub>2</sub> in the gas mixture, the type of plant involved, the environment of CO<sub>2</sub>, etc. For example, membrane technology application is better with high concentrations of CO<sub>2</sub> and would therefore not be appropriate to use for direct air capture where the CO<sub>2</sub> concentration is relatively small. Membrane technology can also be used for high temperature and pressure applications. Whereas, absorption and adsorption technologies are best applied in low temperature CO<sub>2</sub> capture applications (Wilcox 2012).

CO<sub>2</sub> is compressed after capture for transportation, storage or utilization. It could be transported by rail, ship, truck or pipeline depending on the amount of compressed CO<sub>2</sub>, pressure and temperature of compressed CO<sub>2</sub> and distance to be transported. Pipeline is suitable for large scale transportation applications, it is good for operating pressures above 7.38 MPa. The typical pressure and temperature for ship transportation are 0.7 MPa and – 50 °C respectively (Wilcox 2012). Storage options for transported CO<sub>2</sub> include depleted oil and gas fields (geological storage), Ocean, deep aquifers, enhanced coal-bed methane, active oil wells (EOR). The storage capacity, costs, storage integrity and environmental risks differ from one storage option to the other. Geological storage has considerably lower environmental risk and storage capacity compared to ocean storage (Anderson and Newell 2004).

## 2.1 CO<sub>2</sub> Utilization Technologies

The incorporation of CO<sub>2</sub> utilization to carbon capture forms the term Carbon Capture and Utilization (CCU). CCU technologies are beneficial because it is said to have the potential to reduce about 10 % of the world's current annual emission, it also produces value added products that has economic benefits and capable of job creation for people (Li et al. 2016). The utilization of CO<sub>2</sub> has application in different sectors, however, it can broadly be divided into three major uses: technological, chemical and biological use. The properties of CO<sub>2</sub> like its inertness, high density, acidic character, non-conducting, etc. makes it good for technological use. In technological use, CO<sub>2</sub> changes its phases and there is no chemical conversion of CO<sub>2</sub> to form a valuable product. Some of the technological application of CO<sub>2</sub> are found in food processing, the production of carbonated beverages, as a blowing agent in plastic and rubber production, metal fabrication, refrigeration, water neutralization and many more applications. The biological use of CO<sub>2</sub> in the production of aquatic biomass like algae. Algae can be utilized for energy production because it has high efficiency in the conversion of solar energy and can grow in either fresh or sea water thereby reducing land use (Aresta 2003). Biomass from CO<sub>2</sub> used as feedstock in biorefineries has environmental benefits due to its carbon neutrality property, it is capable of reducing GHG emissions from 39 % to 86 % percent when compared to the conventional fossil fuel route. It is said that in 2030, biotechnologies would contribute about 2.7 % to the Gross Domestic Product (GDP) within the Organization for Economic Co-operation and Development (OECD) regions hence, its economic benefits (Li et al. 2016).

CO<sub>2</sub> can be converted chemically into useful products like methanol, ethanol, polymers, etc. The conversion of CO<sub>2</sub> can be achieved by catalytic hydrogenation, electrochemical catalytic reaction,

photocatalytic reaction, etc. with all these approaches having their individual challenges (Li et al. 2016). In summary, for CO<sub>2</sub> to be utilized effectively in any process; technological, biological or chemical, this process has to reduce the overall CO<sub>2</sub> emissions, it has to be less in the consumption of energy and material, it should be ecofriendly and also economically viable (Aresta 2010).

### 2.1.1 CO<sub>2</sub> Utilization for Fuel and Chemical Production

The utilization of CO<sub>2</sub> for industrial processes is not necessarily a novel invention; CO was already utilized in the 1900s for chemical and fuel production. In the 1970s, CO<sub>2</sub> was used as an additive for the production of methanol and for the production of organic carbonates from epoxides. The utilization of CO<sub>2</sub> in 2030 is forecasted to grow up to 332 Mt/y, although this number is nothing much compared to the 35,000 Mt/y of CO<sub>2</sub> emitted, it plays a significant role in the amount of CO<sub>2</sub> avoided rather than the amount of CO<sub>2</sub> used (Aresta et al. 2016). In the middle 1980s, CO<sub>2</sub> conversions into useful products were classified into two cases based on what oxidation state the carbon atom in CO<sub>2</sub> is reduced to during the reaction. In the first class; Class A, the oxidation state of CO<sub>2</sub> either remains the same as + 4 or is reduced to + 3. Class A products usually have CO<sub>2</sub> incorporated into the product and these reactions are quasi-neutral or exothermic. Examples of some of these products in class A include; oxalic acid, organic and inorganic carbonates, carbamates, polycarbonates, polyurethanes and isocyanates. The second class; Class B, has the oxidation state of CO<sub>2</sub> reduced to + 2 or even lower and these reactions require a lot of energy. Products in class B include methane, methanol, and other higher hydrocarbons. Class A products fall into the chemicals market, while class B falls into the fuel market. CO<sub>2</sub> conversion to fuels would consume more CO<sub>2</sub> because the market size for fuels is considerably larger than that of chemicals (Aresta et al. 2016).

CO<sub>2</sub> utilization for fuel production involves the conversion of CO<sub>2</sub> to fuels like gasoline, diesel, kerosene, hydrogen, methanol, dimethyl ether (DME), oxy-methylene ethers (OMEs), Synthetic Natural Gas (SNG), etc. CO<sub>2</sub> utilization in fuel production also falls under the power to fuel technologies where hydrogen is produced from water through the use of renewable energy and is further reacted with CO<sub>2</sub>. This is also a way to balance the excess energy that is produced by renewable energy sources (Koytsoumpa et al. 2018).

CO<sub>2</sub> utilization for chemical production consumes about 110 Mt CO<sub>2</sub> per year; some of the major chemicals include urea, inorganic carbonates, salicylic acid, methanol, propylene carbonate. Although the conversion of CO<sub>2</sub> to urea and salicylic acid are pure thermal processes, there are other CO<sub>2</sub> conversion routes that require the aid of catalysts (Aresta and Dibenedetto 2007).

Certain barriers like thermodynamics and kinetics make the chemical conversion of CO<sub>2</sub> unattractive. Thermodynamically, CO<sub>2</sub> has a free energy of formation value of – 394.01 kJ/mol, this means that energy will be needed to convert it to other products. Even if this thermodynamic barrier is overcome, some CO<sub>2</sub> conversion routes still need the help of catalysts to overcome the kinetic barrier (Aresta 2003). The thermodynamic energy input required to convert CO<sub>2</sub> to chemicals is large and is not considered economical to produce this energy through fossil fuel. Also, considering the fact that fossil fuel energy contributes to CO<sub>2</sub> emissions, the use of renewables such as solar as energy source is considered (Ganesh 2013). Chemicals are grouped into two based on their production volumes. Bulk chemicals have a global production volume of over 10 000 tons per annum while fine chemicals have considerably lesser production volume. This information is important as the production value and the market size of a chemical can affect the amount of CO<sub>2</sub> utilized or avoided in the process (Otto et al. 2015). CO<sub>2</sub> can serve as a direct feedstock for several groups of chemicals like acyclic carbonates, cyclic carbonates, polycarbonates, carbamic acids, isocyanates, hydrocarbons, etc. (Aresta 2010). There are other chemicals which can be produced from the methanol route, base chemicals like ethylene, propylene, benzene, toluene, xylene which are further synthesized to produce other intermediate chemicals like ethylene oxide, ethylene glycol, polypropylene, styrene, acetone, etc. (Kätelhön et al. 2019).

The production of ethylene however, is of importance as it serves as a base chemical to many products in the petrochemical industry. Figure 2 shows products like surfactants, detergent, ethylene benzene, ethylene glycol, polyethylene, ethylene oxide, etc. Ethylene is known as one of the largest volume petrochemical that has a wide range of application. (Alshammari et al. 2016). In 2015, the production of ethylene worldwide was recorded at 141 Mt and this worldwide consumption is expected to increase. Conventional ethylene production by steam cracking of naphtha and thermal cracking of ethane emits 1.51 kg CO<sub>2</sub> eq/kg of ethylene, this value is expected to increase significantly with increase in demand and production of ethylene. CCU technology for ethylene production has the potential to reduce the carbon footprint of conventional ethylene by about 236 %. This makes the study of sustainable ethylene production routes important. (Ioannou et al. 2020).

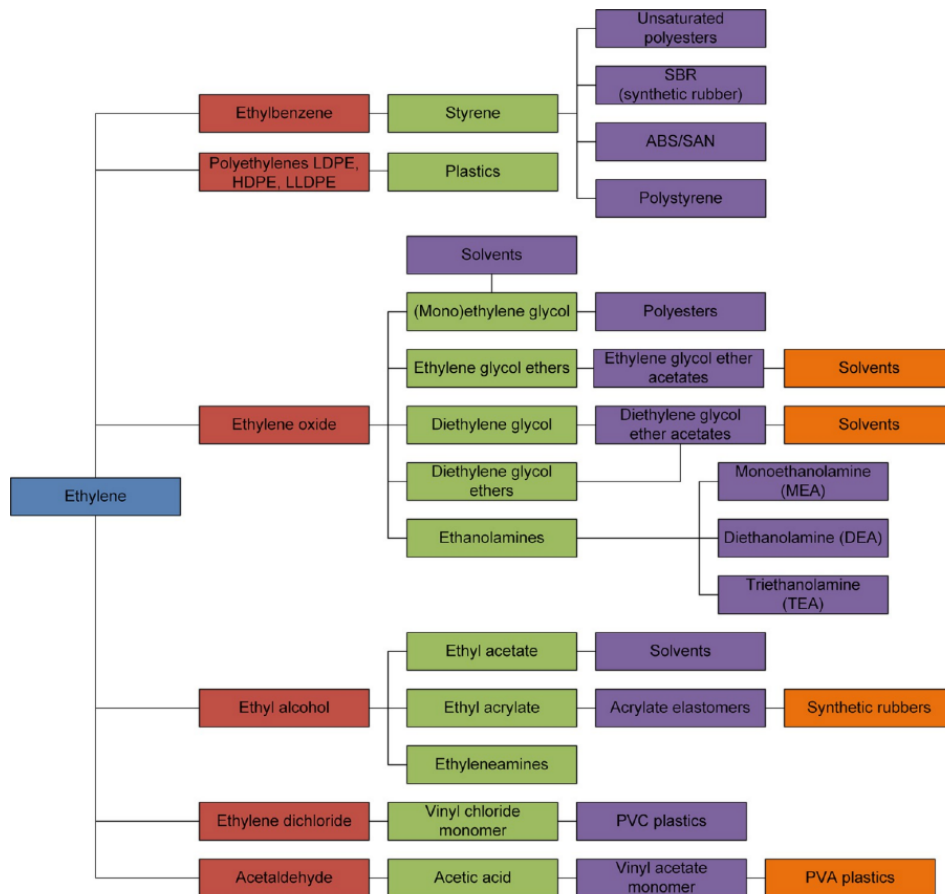


Figure 2: Ethylene and its derivatives (Torres Galvis and Jong 2013).

## 2.2 Solar Energy

The Sun's energy is the most abundant energy on Earth and this energy can be used for various applications. Energy emitted from the Sun in the form of radiation is about  $3.8 \cdot 10^{23}$  kW and the amount that reaches the Earth is  $1.08 \cdot 10^{14}$  kW, which is about 60 % of the Sun's total radiation (Sonawane and Bupesh Raja 2018). All other renewable sources of energy like wind, biomass, etc. have their origins from the Sun. The amount of solar energy that the Earth surface receives in one day is enough to satisfy the world's demand for more than 20 years. As the world's demand for energy keeps on increasing, solar energy could be a solution to this demand because of its abundance (Chu and Meisen 2011). In recent years, there has been an increased interest in alternative energy sources because of the CO<sub>2</sub> emissions involved in the use of fossil fuel. Solar energy is of particle interest because of its abundance and no environmental pollution (Sonawane and Bupesh Raja 2018).

Different solar energy technologies like photovoltaic systems and solar thermal energy systems exist. Photovoltaics convert solar radiation into electric power with the help of semiconductors. Photovoltaic solar technology is commercialized and widely used for electricity generation (Chu and Meisen 2011). The main technologies that convert solar radiation into heat are the concentrating and non-concentrating solar thermal technologies. The flat plate collector is an example of a non-concentrating solar technology that is used for domestic heating and air conditioning. It has the problem of excessive heat loss therefore its low temperature applications are in the range of 100-200°C. Solar concentrators use receivers that have minimized surface aperture which reduces excessive heat loss, it concentrates the radiation of the Sun on a smaller area thereby increasing radiation flux. This makes concentrating solar technologies applicable for higher range of temperatures than non-concentrating technologies. Generally, concentrating solar technologies can be used to generate electrical power or heat. The application of concentrating solar thermal technology for electrical power production is referred to as Concentrating Solar Power (CSP) and that for heat production is Concentrating Solar Thermal (CST) energy (Abanades et al. 2021).

### 2.2.1 Concentrated Solar Energy

Process heat required in chemical industries represents a large percentage (two-thirds) of the general energy consumption in industries. Concentrated solar thermal systems can be used to provide heat for industrial processes, this provides a substitution of fossil fuel conventionally used as heat source, thereby reducing CO<sub>2</sub> emissions (Häberle 2012). One megawatt of installed concentrating solar thermal plants avoids about 688 tons and 1360 tons of CO<sub>2</sub> when compared to the conventional plants that use natural gas and coal respectively (Romero and González-Aguilar 2014). Total radiation from the Sun is a sum of its direct and diffused radiation on the Earth's surface. When the radiation from the Sun to the Earth's surface is not scattered by the atmosphere, it is referred to as direct and the part of the radiation that gets to Earth's surface after being scattered by the Atmosphere or aerosol particles is referred to as diffused or indirect radiation (Duffie et al. 1980).

Concentrated solar energy (CSE) captures the direct radiation from the Sun, its application is best suited in areas where weather conditions are favorable and are not cloudy or dusty (Sonawane and Bupesh Raja 2018).

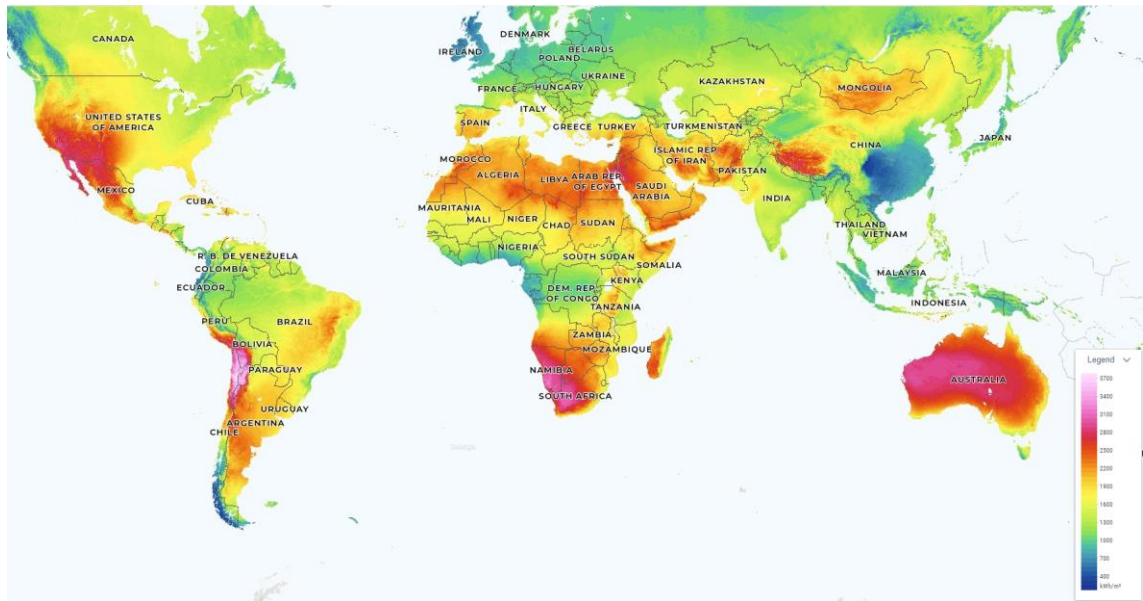


Figure 3: DNI distribution of different countries in world (Global Solar Atlas 2023).

Figure 3 shows the Direct Normal Irradiance (DNI) distribution, the regions with higher DNIs that are best for CSE applications are highlighted in pink and red. CSE technologies have huge capital investments and can easily get degraded in unfavorable environmental conditions. Installed in the CSE technologies are solar collectors which absorb radiation from the Sun and convert this radiation into heat. The converted heat is then transferred to a fluid which can be utilized in process equipment or sent to a solar thermal storage tank (Sonawane and Bupesh Raja 2018). A solar collector consists of a receiver and a concentrator. The part of the collector that absorbs the radiation and converts the energy to the required form is the receiver, the concentrator is responsible for directing the radiation to the receiver, the radiation enters the concentrator through an aperture. The concentration ratio is the ratio of the area of the aperture to the receiver area of the collector. The higher the concentration ratio, the higher the temperature at which the energy is delivered by the CSE technology (Duffie et al. 1980).

Figure 4 shows from a–d, major concentrating solar technologies that are widely commercialized: parabolic trough, linear Fresnel, central tower and parabolic dish respectively. The parabolic trough and linear Fresnel reflectors have a one-axis tracking technology, while the central tower and parabolic dish concentrators have a two-axis tracking technology (Abanades et al. 2021). It is required for collectors to have tracking systems, this enables the collectors to follow the Sun and concentrate solar radiation onto the receivers. Parabolic trough is a mature solar technology that is made of reflective sheet material that is bent into a parabolic shape.

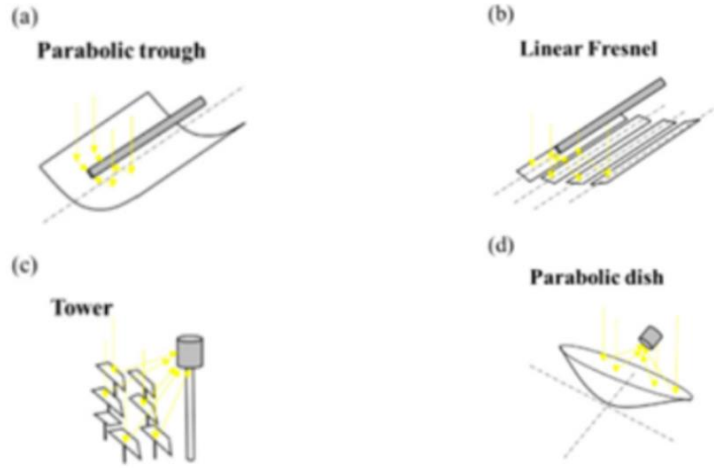


Figure 4: Different concentrating solar technologies. Adapted from (Abanades et al. 2021).

It produces long collector modules and its collectors can be oriented in particular directions like east-west or north-south depending on the application and the amount of energy required. The linear Fresnel uses an array of linear mirror strips to concentrate light onto a receiver. Its reflectors are flat or curved and is relatively cheaper than the glass used in parabolic reflector. It also has little structural requirement because it is not built so high above the ground. The disadvantage of the linear Fresnel reflector to the parabolic reflector is that it is less efficient in converting solar energy and it is difficult to include the heat storage capacity to its system design (Chu and Meisen 2011). The linear Fresnel and parabolic trough are within the temperature ranges of 150 – 400 °C, the parabolic dish and central receiver collector are within the temperature ranges of 300 – 1500 °C.

Table 1: CSE Technologies with their respective concentration ratios and temperature ranges extracted from (a) (Abanades et al. 2021), (b) (Chu and Meisen 2011), (c) (Romero and González-Aguilar 2014)

CSE technology	Concentration ratio	Temperature range (°C)
linear Fresnel	50 – 100 <sup>(a)</sup>	150 – 350 <sup>(c)</sup>
Parabolic trough	50 – 100 <sup>(a)</sup>	150 – 400 <sup>(c)</sup>
parabolic dish	600 – 2000 <sup>(b)</sup>	1500 <sup>(b)</sup>
Central receiver collector	30 – 1500 <sup>(b)</sup>	300 – 1000 <sup>(c)</sup>

The different temperature ranges and concentration ratio for these concentrating technologies are shown in Table 1. Both the parabolic dish and central receiver collectors are point-focus collectors. The dish in parabolic dish reflector, tracks the sunrays into the receiver and the receiver absorbs this solar energy and converts it to thermal energy. The parabolic dish can achieve temperatures up to 1500°C. Its major advantage is that it has a higher concentration ratio than the parabolic trough and linear Fresnel and is more efficient. The central receiver collector, also known as heliostat field uses concave mirrors on the heliostats to reflect the incident solar

radiation to the receiver. Its advantage is that it minimizes thermal-energy transport requirements by transferring the solar radiation to a single receiver, it also has relatively high concentration ratios like the parabolic dish. It is easy to include a heat storage capacity to its system design unlike the linear Fresnel. The inclusion of a storage system to collectors is important because it reduces the inconsistency of the solar radiation received. Solar radiation is not available during the night and so a storage system helps to extend the use of these technologies even during the night hours (Chu and Meisen 2011).

## 2.3 Ethylene Production

Different technological pathways exist for the production of ethylene conventionally. They include steam cracking, dehydrogenation of ethane, catalytic pyrolysis process (CPP) and deep catalytic cracking (DCC). Out of these technologies, steam cracking is regarded as the leading technology for ethylene production (Zhao et al. 2021). As can be seen from Figure 5 below, there are various feedstock, which can be used in the steam cracking process; light hydrocarbons derived from natural gas which includes ethane, propane and butane, crude oil refinery products like naphtha and gas oil.

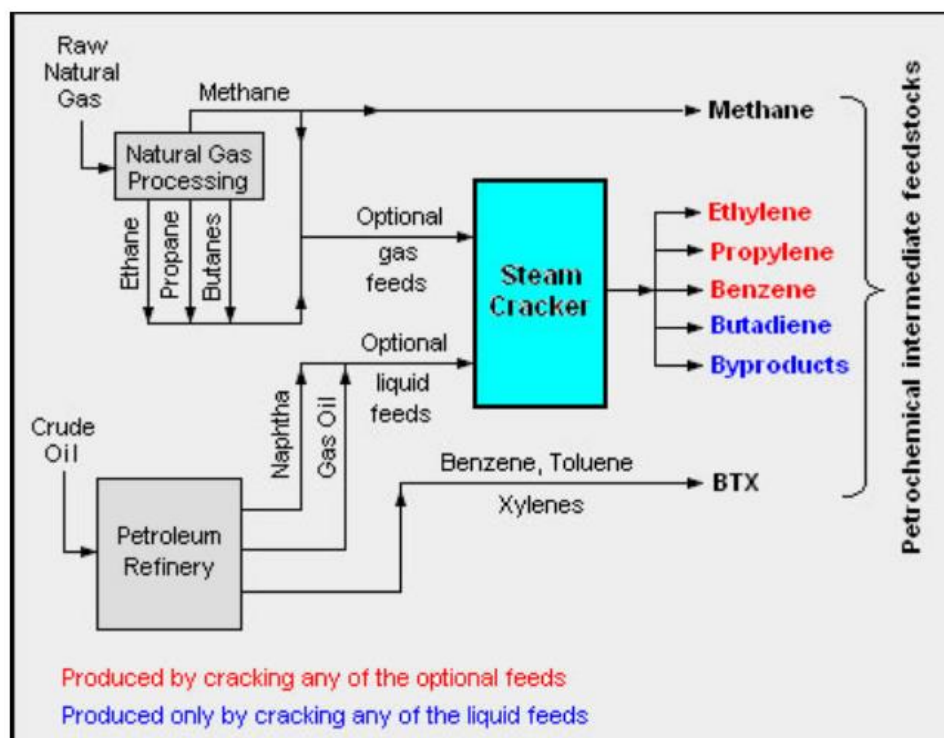


Figure 5: Different production pathway of conventional ethylene production (arescotx.com).

Steam cracking is divided into two types, based on the feedstock to the reactor: 1) the steam cracking of mixed petroleum referred to as PSC. In PSC, liquefied petroleum gas is mixed with naphtha as the feedstock to the reactor. 2) The ethane steam cracking (ESC), where ethane is the feedstock to the reactor. In general, the feedstock to the tubular reactor reacts with steam. This results in the breakdown of the large molecules into smaller molecules like methane, ethylene, propylene, etc. as seen in Figure 5 below. These products are further separated to achieve the target product, which is ethylene, propylene or both based on the demand. ESC is known to produce fewer byproducts and has lower cost compared to PSC (Zhao et al. 2021).

Steam cracking has an operating temperature of (790 – 850) °C, a yield of about 80 % and (23 – 24) % of ethylene with ethane and naphtha as feedstock respectively. Some sustainable pathways have been developed to produce ethylene from fossil-free feedstock, in order to reduce CO<sub>2</sub> emissions from the conventional ethylene production (Zhao et al. 2021). They include methanol to olefins (MTO), O<sub>2</sub>-oxidative coupling of methane (O<sub>2</sub>-OCM), CO<sub>2</sub>-oxidative coupling of methane (CO<sub>2</sub>-OCM) and Fischer-Tropsch synthesis to olefins (FTO). These sustainable ethylene production pathways will be discussed in the sections below.

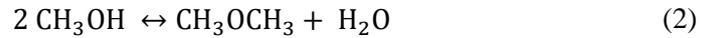
### 2.3.1 Ethylene from Methanol

Methanol has a production volume of about 1.5 million tons. It has one of the largest production volumes in the chemical industry. It is used as a platform chemical to produce various products like formaldehyde, methyl-tert-butyl ether (MTBE), acetic acid, ethylene, etc. its production is expected to increase to 2.17 million tons in 2050 (Dechema et al. 2017). Conventionally, methanol is produced from synthesis gas by reforming of natural gas. The sustainable low-carbon pathway of methanol production is through the hydrogenation of CO<sub>2</sub>, with CO<sub>2</sub> as a carbon source. Captured carbon reacts with hydrogen obtained from the electrolysis of water with renewable electricity to produce methanol (Dechema et al. 2017). Reverse water gas shift reaction can also be used to convert CO<sub>2</sub> and hydrogen into syngas which can further produce methanol. The equation for the direct hydrogenation reaction can be seen below. The commercially available catalyst used for methanol production is Cu/ZnO/Al<sub>2</sub>O<sub>3</sub> (Zhao et al. 2021).



Ethylene is produced from methanol in the methanol to olefins (MTO) reaction. The direct production of olefins from CO<sub>2</sub> and Hydrogen is at a Technological Readiness Level (TRL) of 3 – 4, this means that the technology has not yet been commercialized. The MTO reaction

process is a two-step reaction, first reaction is the dehydration of methanol to dimethyl ether (DME) and water as seen in below and the second step involves the conversion of DME to olefins (Dechema et al. 2017). The reactions steps can be seen the equations 2–4 below:



Apart from ethylene, propylene and butene being the main olefins produced methane, ethane, propane, heavier hydrocarbons and aromatics are also produced as a by-product of this reaction. The operating conditions of the MTO reactions are (350 – 500) °C and (2 – 3) bar, temperature and pressure respectively. Suitable catalysts like SAPO-34 and ZSMS-5 are used in this reaction, although SAPO-34 is considered more efficient in terms of activity, selectivity and robustness. The yield in olefins for the MTO reaction is affected by the type of catalyst used, the operating temperature and the gas space velocity (Dimian and Bildea 2018). Apart from the exothermic nature of the MTO reaction, there is also the issue of coking and this occurs when large particles are unable to pass through the porous catalyst, thereby causing them to remain in the porous holes of the catalyst. This coke formation reduces the efficiency of the catalyst. Hence, the suggestion of a fluidized bed reactor over a fixed bed reactor which provides adequate mixing and uniform temperature throughout the reactor (Yu and Chien 2016).

### 2.3.2 Ethylene from Fischer Tropsch Synthesis

Fischer Tropsch synthesis to olefins produces low-olefins, which include ethylene, propylene and butylene, among other ranges of products. (Liu et al. 2020). Considering CO<sub>2</sub> as the carbon source, this reaction occurs in two steps; the reverse water gas shift reaction and Fischer Tropsch reaction. CO<sub>2</sub> reacts with hydrogen to produce CO and water; this reaction is endothermic and it favors the production of CO at high temperatures. Methane could be formed as a by-product of this reaction depending on the catalyst used (Billig et al. 2019).



A high selectivity of 60 % for low olefins from the total product is obtained when the reaction is supported by iron nanoparticles and a H<sub>2</sub>/CO molar ratio of one. The conversion rate of CO usually is about (70 – 80) wt. % (Liu et al. 2020).

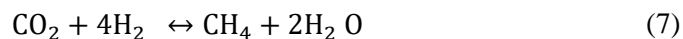


There are two types of FT synthesis reaction; high-temperature FT (HTFT) and low-temperature FT (LTFT). HTFT occurs at operating temperatures and pressure between (300 – 500) °C and 2 MPa respectively, it works best with iron-based catalysts. HTFT favors the production of gasoline and linear olefins. LTFT occurs at operating temperature and pressure between (200 – 240) °C and (2.7 – 4.5) MPa respectively. It works well with either iron or cobalt-based catalysts and favors the production of linear paraffin. The typical molar ratio for LTFT of H<sub>2</sub>/CO is about 1.7 (Dry 2002).

### 2.3.3 Oxidative Coupling of Methane

The production of chemicals and liquid fuels from methane is of considerable interest and importance to the petrochemical industry. Methane is currently being used for heating, power generation, ammonia, and methanol synthesis. One of the major problems with the conversion of methane is its stability and this makes it resistant to reactants (Carlos Colmenares 2010).

It is produced from the reaction of hydrogen and CO<sub>2</sub>. The three reactions that take place in the reactor are shown below. These reactions are promoted by the help of a nickel-based catalyst and are affected by the pressure, temperature and feed inlet ratio of the reactants (Billig et al. 2019). In the process designed by Baltruweit, two separate reactors are used for the methanation reaction so as to increase the rate of CO<sub>2</sub> conversion; first one is an isothermal reactor and the second, adiabatic. The first reactor is operated at 395 °C and the second at 350 °C, this is followed by a CO<sub>2</sub> removal unit for unconverted CO<sub>2</sub> and drying of the gas to remove water (Billig et al. 2019). The product gas contains mainly CH<sub>4</sub> and Hydrogen.

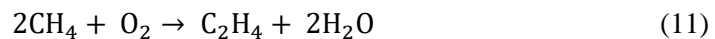
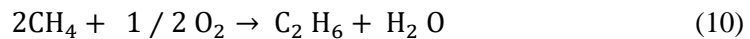


Methane can also be obtained from biogas; raw biogas produced contains a large percentage of methane, although this percentage varies depending on the feedstock used for biogas production. Other components of biogas like CO<sub>2</sub>, CO, H<sub>2</sub>S, O<sub>2</sub>, NH<sub>3</sub> and N<sub>2</sub> are present in smaller amounts compared to methane. Biogas can be also be purified to remove these unwanted components, thereby achieving higher purity for biomethane. In this study, methane from both sources discussed above will be considered as feedstock for the OCM reaction.

### 2.3.4 Ethylene from O<sub>2</sub>-OCM

Oxidative coupling of methane (OCM) for ethylene production was conventionally done with oxygen as the oxidant. Oxygen oxidative coupling of methane (O<sub>2</sub>-OCM) was first discovered by Keller and Bhasin in 1982 and since then there have been over 2000 publications on O<sub>2</sub>-OCM (Arinaga et al. 2021). The O<sub>2</sub>-OCM reaction occurs at temperatures between 800 – 870 °C, with operating pressure at atmospheric pressure of 1 bar. The reactant stoichiometric ratio of CH<sub>4</sub>:O<sub>2</sub> is maintained at 2:1, this is because high amount of oxygen can lead to high heat release and a lower selectivity of the required product. In order to improve the selectivity and to control the temperature in the reactor, a diluent usually N<sub>2</sub>, CO<sub>2</sub> or steam, can be used (Teixeira Penteadó 2021).

The mechanism of methane conversion to ethylene, involves the production of ethane by the coupling of methyl radicals formed on the surface of a metal catalyst and the ethane produced is further dehydrogenated to form ethylene. Equations 10 and 11 show the formation of C<sub>2</sub> products through OCM (Arinaga et al. 2021).



The metal oxide catalysts used for this reaction are Li/MgO, La<sub>2</sub>O<sub>3</sub>/CaO and Mn–Na<sub>2</sub>WO<sub>4</sub>/SiO<sub>2</sub>, although Li/MgO is not fit for industrial purposes because it is unstable and deactivates strongly. Mn–Na<sub>2</sub>WO<sub>4</sub>/SiO<sub>2</sub> on the other hand is known to be an excellent catalyst for industrial processes. This is because of its stability at high temperatures and its high methane conversion and selectivity of (20 – 30) % and (70 – 80) % respectively. It has been able to achieve a maximum of 24.5 % yield of C<sub>2</sub> products in a packed-bed membrane reactor (Teixeira Penteadó 2021).

O<sub>2</sub>-OCM has some challenges like the over oxidation of hydrocarbon products to CO and CO<sub>2</sub> (CO<sub>x</sub>) and low yield of C<sub>2</sub> products. The problem of low yield is linked to the over-oxidation of C<sub>2</sub> products to CO<sub>x</sub> products, therefore several researches have been geared towards suppressing the formation of these CO<sub>x</sub> products (Arinaga et al. 2021). This induced gas phase oxidation means that in order to achieve high conversions of methane to C<sub>2</sub> products, a high partial pressure of oxygen is required and when this happens, the methane and methyl radicals are converted to carbon oxides hence a reduced selectivity of C<sub>2</sub> products (Asami et al. 1995).

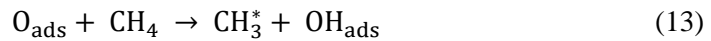
Alternative oxidants for OCM reaction like CO<sub>2</sub>, N<sub>2</sub>O, SO<sub>2</sub> have been investigated, the idea was to replace oxygen with softer oxidants that would not over-oxidize the C<sub>2</sub> products. N<sub>2</sub>O is a greenhouse gas and its utilization in the industry to reduce GHG emissions is appreciated. N<sub>2</sub>O is

a milder oxidant and so reduces over-oxidation of the C<sub>2</sub> products unlike in O<sub>2</sub>-OCM reaction however, N<sub>2</sub>O is expensive and this reduces its application possibilities on an industrial scale also, there is the problem of the product stream being diluted with N<sub>2</sub> (Arinaga et al. 2021).

### 2.3.5 Ethylene from CO<sub>2</sub>-OCM

The first researchers to introduce CO<sub>2</sub> as an oxidant for the OCM reaction were Aika and Nishiyama (Cai and Hu 2019), this reaction is called CO<sub>2</sub>-Oxidative coupling of methane (CO<sub>2</sub>-OCM). The use of CO<sub>2</sub> as an oxidant reduces the over-oxidation problem of O<sub>2</sub>-OCM, its selectivity of C<sub>2</sub> products are comparable to that of O<sub>2</sub>-OCM and it has lower C<sub>2</sub> yields compared to that of O<sub>2</sub>-OCM (Arinaga et al. 2021).

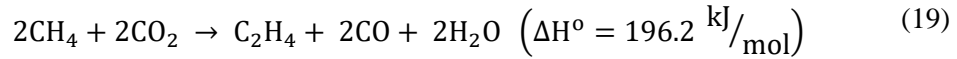
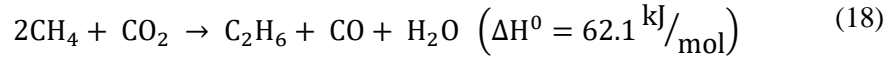
Aika and Nishiyama (Cai and Hu 2019) utilized the oxygen in CO<sub>2</sub> to produce a negative Gibbs free energy of the total reaction. They proposed that the conversion mechanism of methane involved two surface reactions where both CH<sub>4</sub> and CO<sub>2</sub> are activated. CO<sub>2</sub> is decomposed on the surface of the catalyst to form oxygen active species (O<sub>ads</sub>) and CO, also the C-H bond of CH<sub>4</sub> is also broken by the attack of the oxygen active species produced earlier on the C-H bond of CH<sub>4</sub> on the surface of the catalyst to produce methyl radicals. These methyl radicals further combine to form ethane and ethane is dehydrogenated to ethylene. It is also proposed that the activation of CH<sub>4</sub> could be because of lattice oxygen from the catalyst. This conversion mechanism of methane to ethane formation, can be seen in the equations 12–15 below (Cai and Hu 2019).



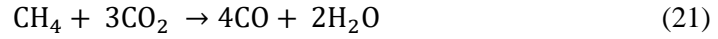
The presence of CO<sub>2</sub> in the reaction reduces catalyst deactivation which causes the formation of hot-spots in reactors, it reduces appearance of unwanted side reactions and over oxidation of the C<sub>2</sub> products (Takht Ravanchi and Sahebdehfar 2021). Another advantage of CO<sub>2</sub> in this reaction is that it removes the hydrogen that is frequently formed during the dehydrogenation of ethane to ethylene in OCM reactors and converts it to water, thereby improving the yield of ethylene and shifting the equilibrium to the forward reaction (Arinaga et al. 2021), as can be seen in equation 16 and 17



The overall reaction of CO<sub>2</sub>-OCM is seen in equations 18 and 19 below:



In addition, CO can be produced from the unwanted side reactions shown in equations 20 and 21



One disadvantage is that the CO<sub>2</sub>-OCM reaction is endergonic in nature and the stability of CO<sub>2</sub> makes the reaction more complex than the O<sub>2</sub>-OCM reaction (Arinaga et al. 2021). From thermodynamic calculations, equilibrium conversions of methane to ethane and ethylene is possible at about 800 °C and a CO<sub>2</sub>:CH<sub>4</sub> ratio of 2 to produce a yield of 15 % and 25 % respectively. The equilibrium conversion of methane can be increased with increase in temperature and CO<sub>2</sub>:CH<sub>4</sub> ratio. This is shown in Figure 6 below concerning the reaction temperature and the CO<sub>2</sub>:CH<sub>4</sub> ratio. The dotted lines represent ethane (C<sub>2</sub>H<sub>6</sub>) and the solid lines represent ethylene (C<sub>2</sub>H<sub>4</sub>). The curves a and c represent a CO<sub>2</sub>:CH<sub>4</sub> ratio of 1 and curves b and d represents CO<sub>2</sub>:CH<sub>4</sub> of 2. If the yields of 15 % and 25 % of ethane and ethylene respectively can be achieved, the combined C<sub>2</sub> yield would be enough to be considered for economic evaluations as the target C<sub>2</sub> yield required for economic evaluations is about 30 % (Wang and Zhu 2004).

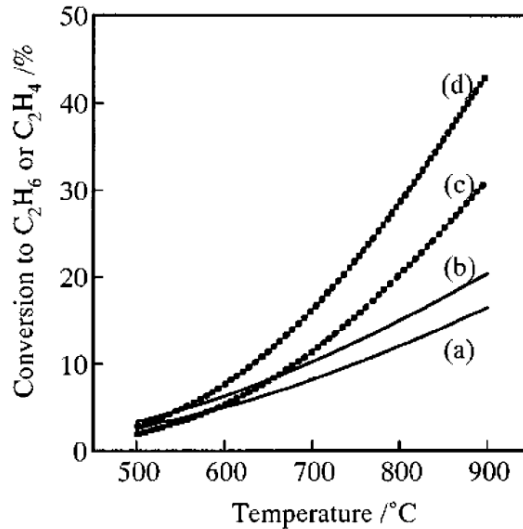


Figure 6: Equilibrium conversion of methane to ethane and ethylene with respect to change in temperature and CO<sub>2</sub>:CH<sub>4</sub> ratio (Wang and Zhu 2004).

Experimental values have shown that the target yield value is not yet obtainable because of kinetic limitations. This problem highlights the need of development of effective catalyst that will activate both CH<sub>4</sub> and CO<sub>2</sub> and improve selectivity of C<sub>2</sub> products.

### 2.3.5.1 CO<sub>2</sub>-OCM Catalysts

Aika and Nishiyama (Arinaga et al. 2021) discovered through isotopically labelled reaction, with the addition of CO<sub>2</sub> over PbO-based catalysts that only CO and C<sub>2</sub> hydrocarbons were produced and it was therefore deduced that C<sub>2</sub> hydrocarbons were formed from methane and CO from CO<sub>2</sub>. These Pb catalyst were further compared with a methyl radical precursor under OCM conditions with O<sub>2</sub> as an oxidant and later with CO<sub>2</sub> added to the reaction. It was discovered that the reaction with only O<sub>2</sub> as an oxidant resulted in the formation of CO<sub>2</sub> as the only product and reaction with added CO<sub>2</sub> yielded C<sub>2</sub> products. This showed the ability of CO<sub>2</sub> to reduce over-oxidation of methyl radicals. The ability of basic oxides to increase C<sub>2</sub> selectivity in the presence of CO<sub>2</sub> was observed by Suzuki (Arinaga et al. 2021).

Asami (Cai and Hu 2019) investigated monometallic metal oxides with a pure CO<sub>2</sub>-OCM reaction and discovered that rare earth metals improved the selectivity of C<sub>2</sub> products most. In another study, he investigated lanthanide oxides and discovered that praseodymium (Pr) and terbium (Tb) oxides increased the yields of C<sub>2</sub> products (Arinaga et al. 2021). ZNO and Cao catalysts were also investigated; CaO was unable to adsorb CO<sub>2</sub> even though alkaline earth metals are supposed to be good absorbers of CO<sub>2</sub>. This was because CaO cannot donate electrons, which CO<sub>2</sub> requires for activation. ZnO however was able to activate CO<sub>2</sub> due to its defects, which are formed during the splitting of methane. Even though CO<sub>2</sub> activation was possible, ZnO was not efficient for splitting methane and this resulted to low C<sub>2</sub> yields with selectivity less than 5% (Cai and Hu 2019).

There are also researches on binary oxides like La<sub>2</sub>O<sub>3</sub>/ZNO, which showed that the addition of ZNO to La increased the selectivity of C<sub>2</sub> products to above 90%. Afterwards, basic oxide and redox-active oxides were developed a binary oxide system for the CO<sub>2</sub>-OCM reaction where the basic oxide increases chemisorption of CO<sub>2</sub> and the redox-oxide was responsible for the dissociation of CO<sub>2</sub> into CO and O\* (Arinaga et al. 2021). Wang's group investigated CaO/CeO<sub>2</sub> binary catalyst and it was reported to have more 5 % yield of C<sub>2</sub> and selectivity of (60 – 70) %, this is an obvious improvement from the low methane conversion and C<sub>2</sub> selectivity that were observed from CaO mono-catalyst. It was proposed that the Ca<sup>2+</sup> site of the catalyst adsorbed

CO<sub>2</sub>, while the Ce<sup>3+</sup> site was responsible for producing active oxygen species which is responsible for the conversion of methane to C<sub>2</sub> products (Cai and Hu 2019).

Investigation of tertiary catalysts have not been left out either. Amin's group investigated Ca-Mn/CeO<sub>2</sub> and it showed that the presence of CaO was responsible for increasing the basicity of the catalyst system and this increases the adsorption of CO<sub>2</sub>. The Ce<sup>3+</sup> and Mn<sup>2.7+</sup> site of the catalyst activated CO<sub>2</sub>, which resulted in the production of oxygen active species responsible for forming methyl radicals (Cai and Hu 2019). Other examples of binary oxide catalysts that have investigated can be found in the table at the appendix that summarizes CO<sub>2</sub>-OCM catalysts. (CaO-Cr<sub>2</sub>O<sub>3</sub>, CaO-CeO<sub>2</sub>, CaO-ZnO, Sr-Mn).

# 3. Methodology

This chapter contains the process simulation and economic evaluation of the CO<sub>2</sub>-OCM production plant for ethylene production.

## 3.1 Process simulation

The process simulation of the plant was done with the Aspen Plus V12.1 simulation software. The production process of ethylene is divided into three major sections; (1) reaction of methane and CO<sub>2</sub> in the OCM reactor, (2) CO<sub>2</sub> absorber section and (3) product upgrading section where ethylene is separated from the other by-products. Figure 7 shows the block diagram of the process which will be replicated in the Aspen Plus simulation. The produced off-gas from the CO<sub>2</sub>-OCM reactor contains ethane, ethylene, CO, water, unconverted methane and CO<sub>2</sub>. This off-gas is further sent into a CO<sub>2</sub> removal section where the CO<sub>2</sub> is absorbed and separated, then recycled back to the CO<sub>2</sub>-OCM reactor. The remaining off-gas goes to the product upgrading section where methane, CO and ethane are separated from ethylene. Recovered methane is recycled back to the reactor.

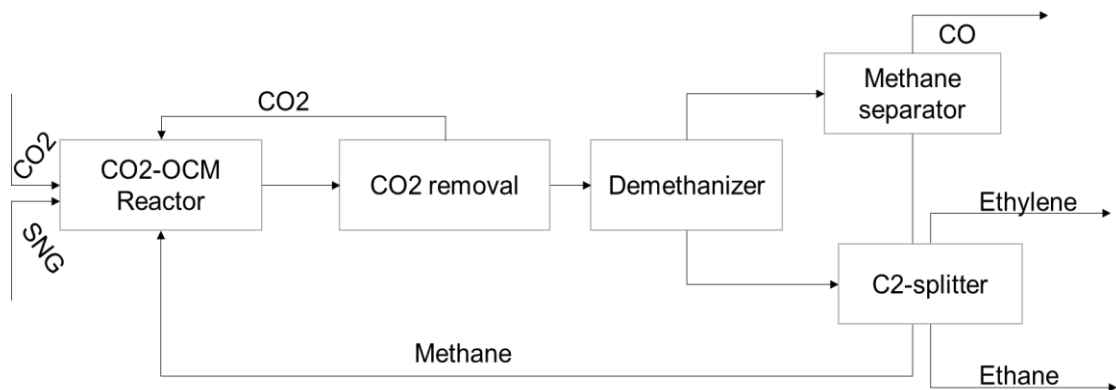


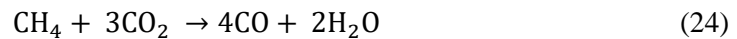
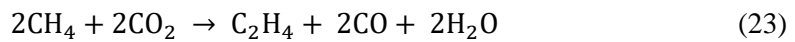
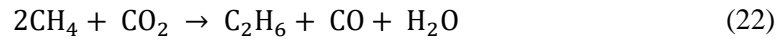
Figure 7: Block diagram of the CO<sub>2</sub>-OCM ethylene production plant.

The property models used for the process simulation are Soave–Redlich–Kwong (SRK) and Electrolyte Non-Random-Two-Liquid (ELECNRTL). SRK is a cubic equation of state property method used in phase equilibrium calculations. It is widely known for its applications in gas processing, refinery, petrochemicals and in ethylene plants. It is said to be well suited for non-polar mixtures like hydrocarbons, light gases, CO<sub>2</sub>, etc. (Haydary 2019). Since these gases are a major component of the gases present in this process simulation, SRK was chosen as a suitable property method to provide accurate representation of the components in the system. SRK was

used for modelling all the equipment in the process except for the CO<sub>2</sub> removal section; the absorber and the stripper, where the ELECNRTL model was used. The sections below show how each section of the process was modelled using Aspen Plus.

### 3.1.1 CO<sub>2</sub>-OCM Reactor

The reactor for the process was modelled with an R-Stoic reactor from Aspen Plus and the SRK property method was used in the reactor. Due to the unavailability of kinetic data for the process in literature, a kinetic reactor was not used. The equations used to model the reactor are shown below. Equations 22 and 23 are the overall reaction for the CO<sub>2</sub>-OCM reaction, equation 24 represents the unwanted side reaction that occurs in the reactor (Wang and Zhu 2004). This equation shows that CO is also a product of methane conversion and not only the conversion of CO<sub>2</sub>.



The operating temperature and pressure for the reactor were specified as 800 °C and 1 bar respectively, methane and CO<sub>2</sub> entered the reactor at room temperature and pressure (25 °C and 1 bar). To produce the desired thermodynamic yield of 15 % and 25 % of ethane and ethylene respectively from the reactor (Wang and Zhu 2004), design spec and calculator from the flow sheeting options in Aspen Plus were used. As can be seen in Figure 8 below, a yield of 25 % was specified for ethylene. FC<sub>2</sub>H<sub>4</sub> represents the mole flow of ethylene from the reactor, FCH<sub>40</sub> is the initial mole flow of methane to the reactor and FCH<sub>4</sub> is the unconverted mole flow of methane from the reactor. The same procedure is repeated for the calculation of the specified yield of ethane required.

The recycle streams from the downstream where methane and CO<sub>2</sub> are separated were recycled back to the OCM reactor. To make up for the amount of methane and CO<sub>2</sub> that were converted in the first cycle and was not recycled back to the reactor, another design spec was created. This varies the input to the reactor in such a way that it makes up for the converted methane and CO<sub>2</sub>, thereby keeping the amount of methane and CO<sub>2</sub> which goes into the reactor at a constant amount.

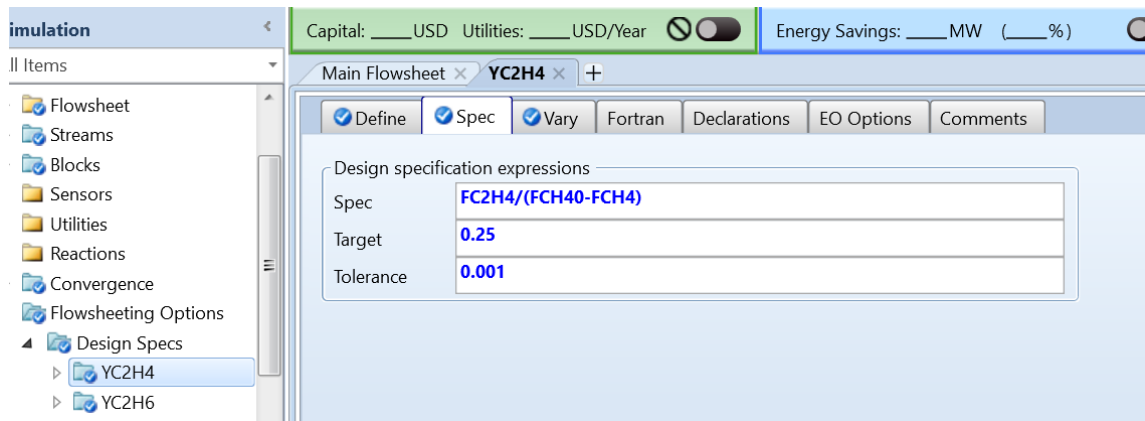


Figure 8: Design spec of ethylene yield from reactor.

The off-gas from the reactor is sent into a heat exchanger where the temperature is cooled from 800 °C to 40 °C. This cooled off-gas is further sent into a flash separator where water is separated from the gas at the bottom product and the off-gas leaves from the top of the flash separator to the CO<sub>2</sub> removal section.

### 3.1.2 CO<sub>2</sub> Removal

The CO<sub>2</sub> removal section consists of the CO<sub>2</sub> absorber column and the stripper column, with a heat exchanger and pump between them; this can be seen in Figure 13. In the CO<sub>2</sub> absorber column, CO<sub>2</sub> is removed from the inlet gas to the absorber and leaves with the solvent at the bottom of the absorber. This bottom product, which is rich in CO<sub>2</sub>, goes through a pump and a heat exchanger to increase its pressure and temperature respectively before entering the stripper. In the stripper, the solvent is regenerated and CO<sub>2</sub> is separated from the solvent. The solvent leaves as the bottom product and is recycled back to the absorber, while the top product containing majorly CO<sub>2</sub> and water leaves from the top of the stripper to a flash separator where water and CO<sub>2</sub> is further separated.

For the design of both the absorber and stripper, Electrolyte Non-Random-Two-Liquid model with Redlich-Kwong equation (ELECNRTL) was used as the property method and ASME 1967 steam table correlations (STEAM-TA) for free water method. The ELECNRTL method was chosen because it is a versatile electrolyte method that has been used in literature for CO<sub>2</sub> removal (Al-Malah 2016). Monoethanolamine (MEA) solvent was used for the absorption of CO<sub>2</sub>. Absorption using MEA is a well-known, commercialized technology in several chemical industries for CO<sub>2</sub> capture (Svinhufvud 2022). The ELECNRTL method and MEA solution were entered into the simulation at the properties section of the Aspen Plus software.

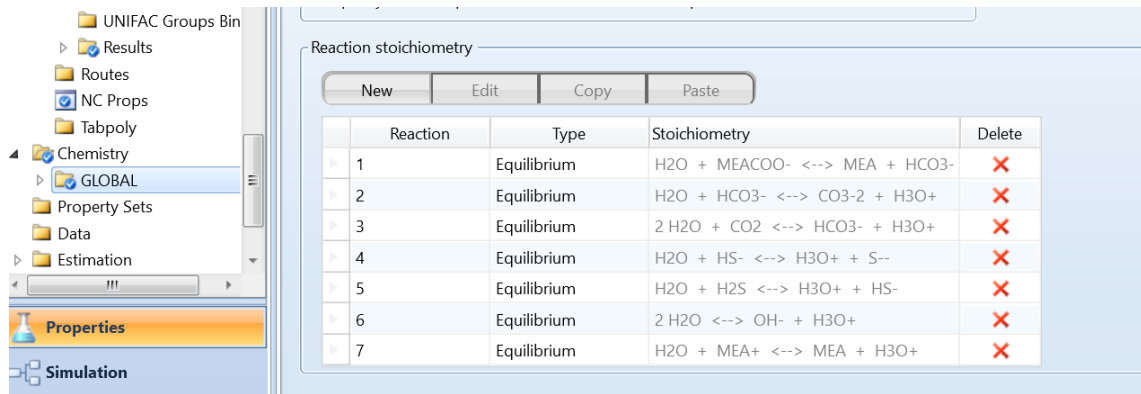


Figure 9: Equilibrium reactions in the absorber column.

The electrolyte wizard was used to propose reactions and constants, the equilibrium reactions can be seen in Figure 9.

### 3.1.2.1 CO<sub>2</sub> Absorber

The lean solvent entering the CO<sub>2</sub> absorber contains 30 % wt. of MEA, 67 % wt. of water and 3 % wt. of CO<sub>2</sub>. The weight percent of MEA in the lean solvent is used based on a model from literature for CO<sub>2</sub> removal process (Abu-Zahra et al. 2007). The lean solvent enters the column at 42 °C and 1.15 bar, while the off-gas enters at 40 °C and 1 bar. The absorber column is designed using a Radfrac column in Aspen Plus. The specifications of the column were based on the specifications for a CO<sub>2</sub> absorber design in the ASPEN MEA report (Charles W. White 2003). The column was designed as an equilibrium-based column, with 10 stages, no condenser or reboiler. The lean solvent enters the column from the top at stage 1, while the off-gas enters the column from the bottom at stage 10. The condenser pressure was operated at 1 bar. The summary of these specifications can be found in Table 2 below.

Table 2: Specifications for CO<sub>2</sub> absorber column.

Absorber	Radfrac column
Type	Equilibrium-based
Condenser	No condenser, 1 bar
Number of stages	10
Lean-solvent inlet stage	Stage 1
Off-gas inlet stage	Stage 10

The bottom product from the CO<sub>2</sub> absorption column, which is rich in CO<sub>2</sub>, goes into a pump where its pressure is increased to 2.4 bar and further sent to a heat exchanger where its temperature

is increased to 96 °C. The solution that leaves the heat exchanger then goes into the Stripper column.

### 3.1.2.2 Stripper Column

The outlet solution from the heat exchanger enters at 96 °C and 2.4 bar at stage 1 of the stripper column. The specifications for the column, number of equilibrium stages, type of condenser and reboiler and condenser pressure were taken from the ASPEN MEA report (Charles W. White 2003). The value for the boil up ratio, distillate to feed ratio and feed entry stage were obtained from (Svinhufvud 2022). Table 3 below shows a summary of the specifications used for the design of the Stripper column.

Table 3: Specifications for stripper column.

Stripper	Radfrac column
Type	Equilibrium-based
Condenser	Partial vapor, 1.77 bar
Reboiler	Kettle
Number of stages	12
Boil up ratio	0.26
Distillate to feed ratio	0.12

The top product of the stripper contains majorly CO<sub>2</sub> and water which was further cooled down in a heat exchanger to 40 °C and then sent to a flash separator where CO<sub>2</sub> was separated from water. The bottom product from the stripper contains the regenerated MEA solution, it is cooled down in a heat exchanger to 42 °C where it is recycled back to the absorber column as lean solution. From literature, it is estimated that the lean loading which is the ratio of moles of CO<sub>2</sub> carrying species to the moles of all MEA carrying species, to be within the range of 0.12 – 0.4 mol/mol (Svinhufvud 2022). The equation for calculating this value can be seen in equation 25

$$\text{lean loading} = \frac{[\text{CO}_2] + [\text{HCO}_3^-] + [\text{CO}_3^{2-}] + [\text{MEACOO}^-]}{[\text{MEA}] + [\text{MEA}^+] + [\text{MEACOO}^-]} \quad (25)$$

The lean loading value affects the amount of energy is required in the reboiler of the stripper to strip CO<sub>2</sub> from the MEA solution. This is because, the mole ratio of CO<sub>2</sub> in the lean solution, is the amount of CO<sub>2</sub> that was not removed from the rich CO<sub>2</sub> solvent that enters the column. The lower the value, the more thermal energy that is required at the reboiler of the stripper column and vice versa (Abu-Zahra et al. 2007). Figure 10 shows how different lean level flowrate ratios affect

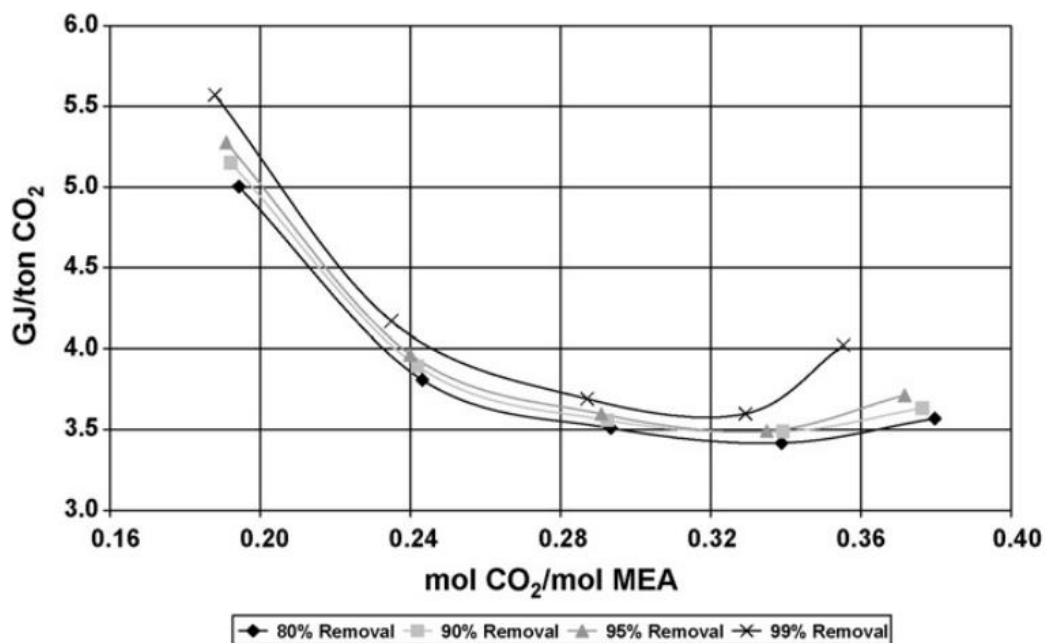


Figure 10: Thermal requirement at different lean loading levels (Abu-Zahra et al. 2007).

the thermal energy requirement of a stripper column. The plots on the graph represent different percentages of CO<sub>2</sub> removal, the higher the value, the higher the thermal energy requirement. In summary, both the amount of CO<sub>2</sub> removed and the lean loading value affects the thermal energy requirement of the column.

### 3.1.3 Product Separation and Upgrade

In this section, the goal is to separate the off-gas mixture which contains methane, CO, ethane and ethylene, in order to achieve the main product of the process which is ethylene. The off-gas from the CO<sub>2</sub> absorber section is sent to a multistage compressor where the pressure is increased to 30 bar and afterwards to a heat exchanger where the gas is cooled to  $-90$  °C. This cooled high-pressure gas is then sent into the DEMTH column. Three distillation columns represented as Radfrac columns in Aspen Plus were used in this section; the DEMTH, COSEP and C<sub>2</sub>-split columns. For the design of the three distillation columns, a short-cut distillation column was used to first determine the initial specification for the column and these were fine-tuned with the design specs used later on.

In the DEMTH column, methane and CO is separated from ethane and ethylene, with the former as the top product and the later as the bottom product. The design specifications used for the design of the column is shown in Table 4, the column is designed as equilibrium based. Design

specifications were also added for the for the column to ensure that 99.9 % of the ethylene and maximum of 0.1 % of methane is recovered in the bottom product.

*Table 4: Specifications for DEMTH column.*

<b>DEMTH</b>	<b>Radfrac column</b>
Type	Equilibrium-based
Condenser	Partial vapor, 29 bar
Reboiler	Kettle
Number of stages	26
Reflux ratio	0.6
Distillate to feed ratio	0.888
Mole fraction of methane in bottom product	0.0001
Mole recovery of ethylene in bottom product	0.999

The top product from the DEMTH then goes into the COSEP column where methane is separated as the bottom product from CO, which is the top product. Methane is further purged in a SEP column, heated up in a heat exchanger and recycled back to the CO<sub>2</sub>-OCM reactor. Table 5 shows the specifications used to design the COSEP column. Design specs were also used in this column to ensure that the amount of CO in the bottom product is minimal. This ensures that a high purity of methane at the bottom product is achieved.

*Table 5: Specifications for COSEP column.*

<b>COSEP</b>	<b>Radfrac column</b>
Type	Equilibrium-based
Condenser	Partial vapor, 28 bar
Reboiler	Kettle
Number of stages	58
Reflux ratio	3.6
Distillate to feed ratio	0.522
Mole fraction of CO in bottom product	0.00001
Mass purity of CO in top product	0.999

The bottom product from the DEMTH column exits the column at  $-7\text{ }^{\circ}\text{C}$  and is sent into the C2SPLIT column. In the C2SPLIT column, ethane is taken out as the bottom product and ethylene as the top product.as with the other two columns, design specs were used to ensure the purity of ethylene was as required.

Table 6: Specifications for C2SPLIT column.

<b>C2SPLIT</b>	<b>Radfrac column</b>
Type	Equilibrium-based
Condenser	Partial vapor, 8 bar
Reboiler	Kettle
Number of stages	60
Reflux ratio	2.954
Distillate to feed ratio	0.602
Mole purity of ethylene in top product	0.9997
Mole recovery of ethylene in top product	0.99

### 3.1.4 Heat Integration

After the process simulation was completed, the Aspen Energy Plus analyzer was used for the energy analysis of the process. The aim is to perform a heat integration for the process in order to reduce the amount of external utilities required for the plant. A minimum temperature difference between hot and cold fluids was selected as 10 °C. The process has a large range of temperature; from the OCM reactor at 800 °C to the product upgrading section of – 90 °C, it is possible to use the heat off-gas from the OCM reactor to heat up downstream sections that require heat.

## 3.2 Economic analysis

In this section, the economic evaluation of the CO<sub>2</sub>-OCM process is explained. The aim of an economic analysis, is to determine how feasible a production process is economically. Data from the process simulation obtained in the process simulation section, is used to for the economic evaluation of the CO<sub>2</sub>-OCM pathway. For the O<sub>2</sub>-OCM pathway, economic data were taken from literature.

To determine the net production cost of ethylene, the annualized cost method is used. This method does not consider taxes or depreciation, it assumes that the working capital is recovered at the end of the investment, therefore annualizes only the fixed cost (Towler and Sinnott 2008). Hence, for this method, the estimation of the total investment cost, the operational expenditure, total annualized cost and net cost of production is necessary.

$$C_2 = C_1 \cdot \left(\frac{I_2}{I_1}\right). \quad (26)$$

In order to predict the cost of the components for the reference year, which is 2021 used in this study, the cost index method is used. Inflation is used for this estimation. The formula for the cost index estimation is shown equation (26) where,  $C_2$  and  $C_1$  represents the cost of the component at the present year and the original year the equipment cost was evaluated respectively.  $I_2$  and  $I_1$  represent the Index value of the component at the present year and the original year. These cost estimations are discussed in detail in the sections below

### 3.2.1 Total Investment Cost (CAPEX)

The total capital investment (TCI) is the sum of the fixed-capital investment (FCI) and the working capital (WC) (Peters et al. 2003). This can be seen in equation 27. Fixed capital investment is the amount required for the designing, constructing and installation of the plant. The working capital is the amount for maintain the operations of the plant, such as maintaining inventories of feeds, products, etc. (Towler and Sinnott 2008). In several companies, the ratio of working capital to total capital investment varies; it ranges from 10–50%. This high ratio could be as a result of seasonal demand of products or high inventories maintained over appreciable periods (Peters et al. 2003). For this study, the ratio was taken as 10 %.

$$TCI = FCI + WC. \quad (27)$$

The fixed capital investment is further divided into manufacturing fixed capital (direct cost) and non-manufacturing fixed capital investment (indirect cost). Direct cost represents the capital that is required for installation of process equipment and other components need for the process. Components of direct cost include cost for site preparation, piping and instrumentation, insulation, etc. All other costs required for over construction and other components of the plant that are not related to the operation of the process are grouped under indirect cost. Example of plant components under indirect cost are warehouses, laboratories, processing buildings, etc. (Peters et al. 2003)

$$FCI = \text{Direct cost} + \text{Indirect cost} . \quad (28)$$

To estimate the direct cost, the estimation of the size and cost of the equipment is a prerequisite. In the sections below, the different equipment used in this study will be sized. The required parameters for costing of each equipment is summarized in Table 7 .

Table 7: Parameters required for costing of Equipment.

Equipment	Parameter for sizing
Reactor	Exchanger area
Heat Exchanger	Exchanger area
Columns	Diameter and height
Compressor	Work/duty
Expander	Work/duty

### 3.2.1.1 Reactor

Sizing and cost estimation of the reactor in this study was carried out by considering the reactor unit as an equivalent of a heat exchanger. The area of the reactor was determined as a heat exchanger. The sizing of the heat exchanger is discussed in the next section.

### 3.2.1.2 Heat exchangers

The sizing of heat exchangers requires the calculation of the heat exchanger area. This is shown by equation 29, where  $\dot{Q}$  is the heat duty of the exchanger and this value is obtained from the Aspen Plus simulation,  $k$  is the heat transfer coefficient estimated from approximate design values of overall heat transfer coefficients from (Ulrich and Vasudevan 2004),  $\Delta T_{o \log mean}$  is the logarithmic mean temperature difference.

$$A = \frac{\dot{Q}}{k \cdot \Delta T_{o \log mean}} \quad (29)$$

The logarithmic mean temperature difference is calculated as shown in equation 30. where  $h$  is hot fluid and  $c$  is cold fluid. The numbers 1 and 2 represent inlet and outlet temperatures respectively of either hot or cold fluid.

$$\Delta T_{o \log mean} = \frac{(T_{h1} - T_{c2}) - (T_{h2} - T_{c1})}{\ln\left(\frac{T_{h1} - T_{c2}}{T_{h2} - T_{c1}}\right)} \quad (30)$$

The calculated heat exchanger area is used to estimate the cost of the heat exchanger using the correlation chart from (Peters et al. 2003).

### 3.2.1.3 Columns

Columns in this section includes the CO<sub>2</sub> absorber, the stripper, distillation columns for the demethanizer, C<sub>2</sub>-splitter, COSEP and flash drums used for the separation of water from off-gas. As stated in Table 7 above, the diameter and height are required parameters for the cost estimating of the column. For the estimation of the diameter and height, the columns are designed as tray columns in this study. Equation 31 shows how the diameter is estimated (Seader et al. 2011)

$$\left( \frac{4VM_g}{\pi P_g \mu_f f \left(1 - \frac{A_d}{A}\right)} \right)^{0.5}, \quad (31)$$

where V is the maximum molar vapor rate of the column and this data is obtained from Aspen Plus, M<sub>g</sub> is the gas molecular weight, μ<sub>f</sub> is the flooding velocity, f is the flooding fraction, which is taken as 0.8 for this study, A<sub>d</sub> is the liquid down comer area, A is the tray cross sectional area and P<sub>g</sub> is the density of the gas.

The value of the ratio of the liquid down comer area to the tray cross sectional area is determined by the value of the abscissa ratio F<sub>LV</sub>, which is estimated as shown below. Where L and M<sub>L</sub> are the liquid flowrate and average molecular mass of the liquid respectively

$$F_{LV} = \left( \frac{LM_L}{VM_g} \right) \cdot \left( \frac{P_g}{P_l} \right)^{0.5}. \quad (32)$$

For  $F_{LV} \leq 0.1, \frac{A_d}{A} = 0.1$

$$0.1 \leq F_{LV} \leq 1.0, \frac{A_d}{A} = 0.1 + \left( \frac{F_{LV} - 0.1}{9} \right)$$

$$F_{LV} \geq 1.0, \frac{A_d}{A} = 0.2$$

The flooding velocity μ<sub>f</sub> is estimated as shown in equation 33 below. P<sub>l</sub> is the liquid density and C is the capacity of Soudes and Brown (Seader et al. 2011)

$$\mu_f = C \cdot \left( \frac{P_l - P_g}{P_g} \right)^{0.5}. \quad (33)$$

The capacity parameter is estimated as shown in equation 34 below where F<sub>st</sub> is given as the surface tension factor, F<sub>f</sub> is the foaming factor, C<sub>f</sub> is the flooding correlation and F<sub>HA</sub> value is dependent on the value of  $\frac{A_d}{A}$

$$C = F_{st} \cdot F_F \cdot F_{HA} \cdot C_f. \quad (34)$$

For  $\frac{A_d}{A} > 0.1, F_{HA} = 1.0,$

$$0.06 \leq \frac{A_d}{A} \leq 0.1, F_{HA} = 5 \cdot \left(\frac{A_d}{A}\right) + 0.5.$$

To estimate the height of the column, the number of stages obtained from the Aspen simulation is multiplied by the tray spacing which is taken as 24 inch in this study. A constant height of 4 ft is added above the top tray for the removal of entrained liquid and 10 ft below the bottom tray to account for bottoms surge capacity (Seader et al. 2011). The equation can be seen below

$$H = ((N - 1) \cdot \text{tray spacing}) + \text{height above and below the column}. \quad (35)$$

The correlation graph for vessels from (Peters et al. 2003) was used to estimate the cost of the column with the calculated volume of column estimated in equation 36

$$V = \frac{H\pi D^2}{4}. \quad (36)$$

To estimate the overall cost of the column, the cost of the internals is evaluated. The value for the cost of trays varies depending on the diameter of the column. This value was obtained from the DACE price booklet (Dutch Association of Cost Engineers 2017) and is multiplied by the number of trays from the aspen simulation. This cost is added to the cost of the column to obtain the overall equipment purchase cost of the column.

$$V = \frac{2LM_L t}{P_L}. \quad (37)$$

Cost estimation of the flash drums are achieved by estimating the volume of the drum. This volume is determined based on the liquid residence time  $t$ , which is taken as a minimum of 5 mins in this study. Equation 37 shows the formula for the estimation of the volume of the flash drum. This volume is then used to determine the cost of the vessel using the correlation chart in (Peters et al. 2003)

#### 3.2.1.4 Compressors and Expanders

The duty of the compressor obtained from the Aspen Plus simulation is used to estimate the cost of the compressor using the correlation chart from (Peters et al. 2003). The same procedure was repeated for the cost estimation of the expander and pump.

Correlation charts used for the base cost estimation for equipment are based in 2002. After the equipment is bought, it is transported to and installed at the plant site, the cost that covers this operation is known as the installation cost. It is usually greater than the purchased equipment cost by a certain factor referred to as the Lang factor. The Lang factor has different values for different industries as the cost of installation differs from process to process. For process plants, it ranges between the values of 4 – 5, depending on if the plant is a solid type plant or a fluid type plant (Peters et al. 2003). In this study, a Lang factor value of 4 is used. With the Lang factor multiplied with the equipment cost, the fixed capital investment can be estimated. The equation can be seen below

$$FCI = \sum \text{Equipment cost} \cdot \text{Lang factor} . \quad (38)$$

The sum of the all the equipment cost multiplied by the Lang factor, added to working capital which is estimated as 10 % of the FCI in this study gives the CAPEX value of the process.

### 3.2.2 Operational Expenditure (OPEX)

The operational expenditure is the sum of the variable cost of production and fixed cost of production. The variable cost of production is the cost that is related to the manufacturing operation of the plant, it means that these costs are usually incurred as the operation of the plant is on. The fixed cost of production on the other hand is not dependent on the operation of the plant. This cost can be incurred even if the operation of the plant is off. These costs can be affected by inflation except for depreciation which is calculated based on tax regulations (Peters et al. 2003). Variable production cost is made up of cost for raw materials required in the process, utilities like process heaters, steam, cooling waters, etc., packaging and shipping cost. A good efficiency of plant design and its operation can aid in the reduction of the cost for variable production. Example of fixed production cost include operating labor, supervision, maintenance, property taxes and insurance, rent of land or buildings, plant overhead cost (Towler and Sinnott 2008)

$$OPEX = \text{Variable cost of production} + \text{Fixed cost of production} . \quad (39)$$

The annual cost of labor is a function of the plant capacity. The plant capacity is used to estimate the employee-hours per day per step, the number of process steps of the plant discussed previously, to obtain the total-employee-hours per day, then multiplies this value, this is further converted to per year. The labor cost is then calculated from this value, also considering the location of the plant and labor rate for that location. This cost is then added to the supervised labor

cost, which is estimated as 15 % of the labor cost to obtain the total annual labor cost. In this study, the fixed cost of production is estimated by summing the percentages of the labor, insurance and maintenance cost. The values for the insurance and maintenance cost are taken as 2 % and 4 % respectively. The labor percentage value is obtained by dividing the annual cost of labor by the CAPEX value. The same procedure is repeated for evaluating the percentage value of the variable OPEX; the sum of the utilities and raw material is divided by the CAPEX. The summation of the percentage values of the variable and fixed OPEX multiplied the CAPEX, gives the OPEX value for the process.

### 3.2.3 Total annualized cost

The annualized cost is the amount that should be paid back annually in order to repay the initial investment of the plant, in addition with the compound interest which is the expected return on the capital (Towler and Sinnott 2008). Assuming that an amount P, invested over a period of time, n and at interest rate, i, would yield a certain amount, then A is the regular payment that has to be made annually in order to generate the same sum of money over the same period of time, that would have been generated by investing P. The ratio of A to P is known as the annual capital charge ratio (ACCR) (Towler and Sinnott 2008). This is the fraction of the principal that must be paid annually to repay the principal and its accumulated interest over a period of n. In this study, the interest rate is estimated at 8 % and the number of operation years is estimated at 20 years

$$ACCR = \frac{A}{P} = \frac{[i(1+i)^n]}{[(1+i)^n - 1]} \quad (40)$$

To calculate the annualized capital cost (ACC), the annual capital charge ratio is multiplied with the total fixed capital cost

$$ACC = ACCR \cdot \text{Total fixed capital cost.} \quad (41)$$

Finally, the total annualized cost (TAC) or the total cost of production is calculated as shown in the equation below

$$TAC = \text{Operating Cost} + ACC \quad (42)$$

For the estimation of the refrigeration duty, the total annualized cost is calculated. The cost for the refrigeration utility itself is not estimated because it is a one-time inventory, therefore the calculation of the installed equipment cost and the energy consumed by the equipment is calculated by the cost correlation developed by (Luyben 2017). the TAC is calculated by

multiplying this cost with the energy transferred from the refrigerant, this value is obtained from the simulation.

$$\text{Cost } (\$/\text{GJ}) = \exp[2.452 - 0.01863 \cdot T(^{\circ}\text{C})] \quad (43)$$

This cost correlation equation is estimated for a period of ten years, where T is the temperature the process needs to be cooled down to. If the payback period is smaller, the refrigeration cost is expected to be higher because the refrigeration system will be more cost intensive.

$$\text{TAC } (\$/\text{y}) = \text{Energy} + \frac{\text{Installed equipment cost}}{10 \text{ years}}. \quad (44)$$

Estimating with a payback period of ten years, it is said that the capital cost and energy cost are about 50 % each. Therefore, the calculated TAC for the refrigeration cost is divided by two to obtain the capital cost and then a new capital cost is calculated based on 20 years payback period and added to the energy cost. Thereby giving a cost for 20 years payback period.

### 3.2.4 Net Production Cost

The production cost of ethylene is calculated by subtracting the value of by-product cost from the total annualized cost and dividing it by the amount of ethylene produced per year. This is shown in the equation below

$$\text{NPC} = \frac{\text{TAC} - (\text{By} - \text{product cost})}{\text{Ethylene Production per annum}}. \quad (45)$$

### 3.2.5 Sensitivity Analysis

In this study, the effects of uncertainties are investigated. The sensitivity analysis forecasts how changes in components such as raw materials cost, operating costs, etc. will affect the cash flows and viability of the project. It identifies which parameters affect the viability of the project with a variation of range of these parameters. Here, the major cost drivers are identified and varied to observe how these changes affect the cost of ethylene production.

The results from the economic analysis shows components that are the cost drivers for the CAPEX and OPEX of the process. The result also shows which of the CAPEX or the OPEX affects the net cost of production of ethylene the most. With these components identified, a sensitivity analysis is done by varying the range of cost of these components to obtain the best values, which would result in a decrease of the NPC of ethylene. This analysis also shows the range of cost the

components within which the process will not be economically viable. More attention is paid to the main cost driver of the process, which is the component that contributes the most to the NPC of ethylene. Its sensitivity analysis result shows the optimum value of this component at which the NPC of ethylene is minimum and conditions could lead to obtaining the optimum value of the main cost driver.

# 4. Results and Discussion

In this section the results of the process simulation and economic analysis carried out in the previous chapter will be displayed and discussed. The economic results obtained from the process simulation data of the CO<sub>2</sub>-OCM process will be compared to the economic results of the Biogas-based Oxidative Coupling of methane (BG-OCM) results from (Teixeira Penteadó 2021).

## 4.1 Process simulation

The result for the complete process simulation of the CO<sub>2</sub>-OCM process is shown in Figure 11. Figure 11 shows all the sections of the process described in chapter 3, it also includes the heat integration done in the simulation, and the red dotted lines indicate these. The green lines are the raw materials inlet into the process; methane, CO<sub>2</sub> and Lean MEA solution. The black lines are the streams in the process. The light blue lines show the products from the process. The results of all the process sections and heat integrations done will be discussed in this section.

### 4.1.1 OCM Reactor

The expected thermodynamic yield of the CO<sub>2</sub>-OCM reaction as discussed in Chapter 3 is 25 % and 15 % yield of ethylene and ethane respectively. As expected, methane has an overall conversion of about 41 % and a corresponding yield of 25 % and 15 % yield of ethylene and ethane respectively (see Figure 12). This result matches the thermodynamic yield in literature. The legend in Figure 12 shows symbols that represent the temperature, pressure and mass flow values of the process. This legend is valid for the other figures of the process shown in this section.

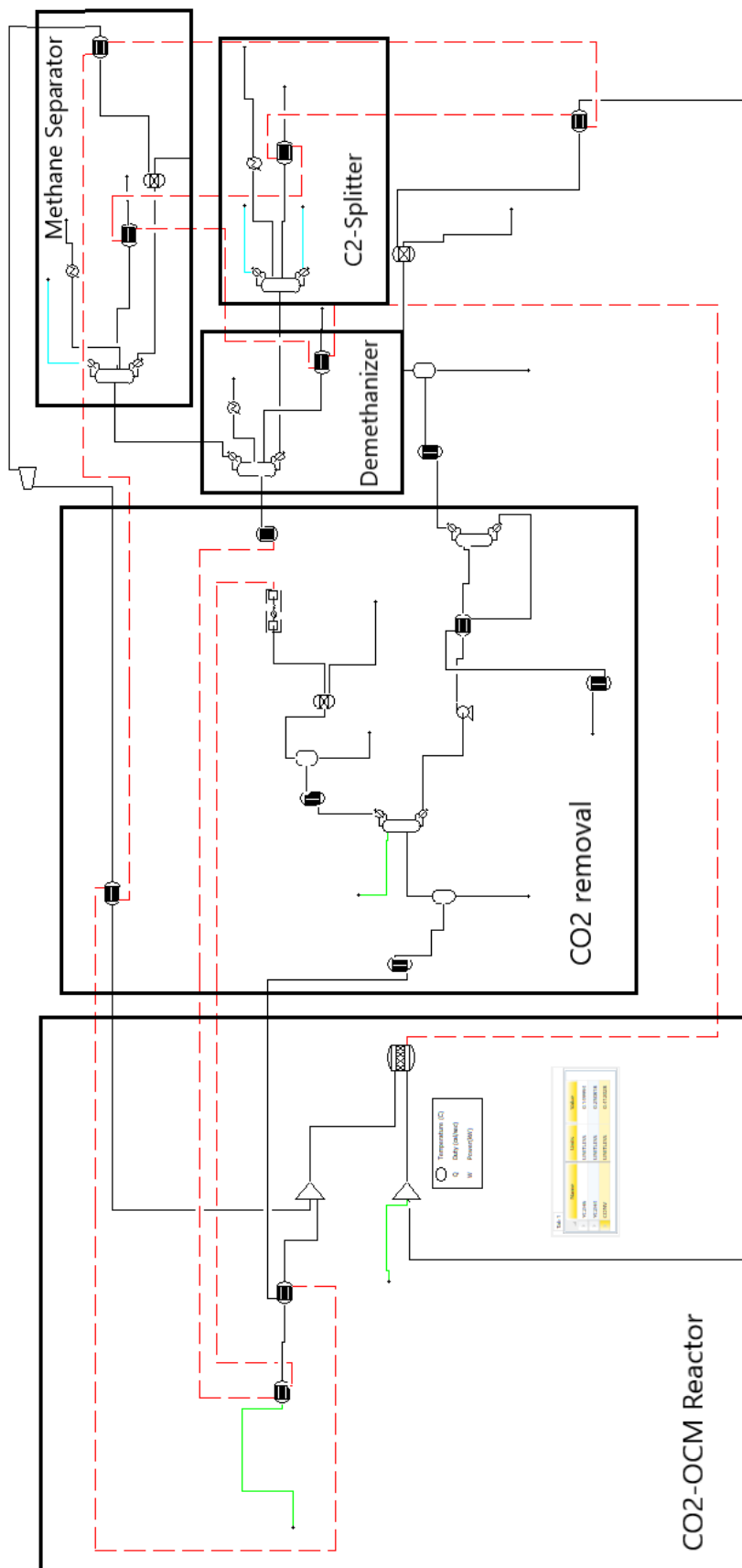
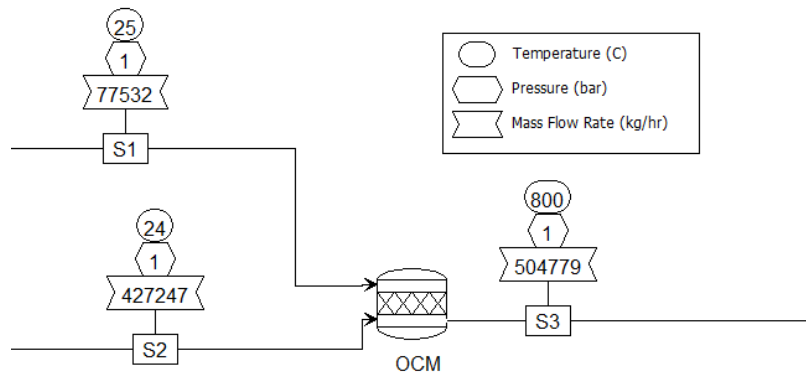


Figure 11: Complete process flow diagram.



Name	Units	Value
YC2H6	UNITLESS	0.150032
YC2H4	UNITLESS	0.249831
CONV	UNITLESS	0.409106

Figure 12: Process flow diagram and simulation results of the OCM reactor

#### 4.1.2 CO<sub>2</sub> Absorption section

The result for the CO<sub>2</sub> absorption section can be seen in Figure 13. It shows the absorption and stripper column, also the heat exchanger and pump in-between them, which was used for increasing the temperature and pressure respectively of the rich solution entering the stripper. As discussed in the chapter 3, the lean solution is expected to be within a certain mol ratio range of 0.12 – 0.4 mol/mol of CO<sub>2</sub>/MEA.

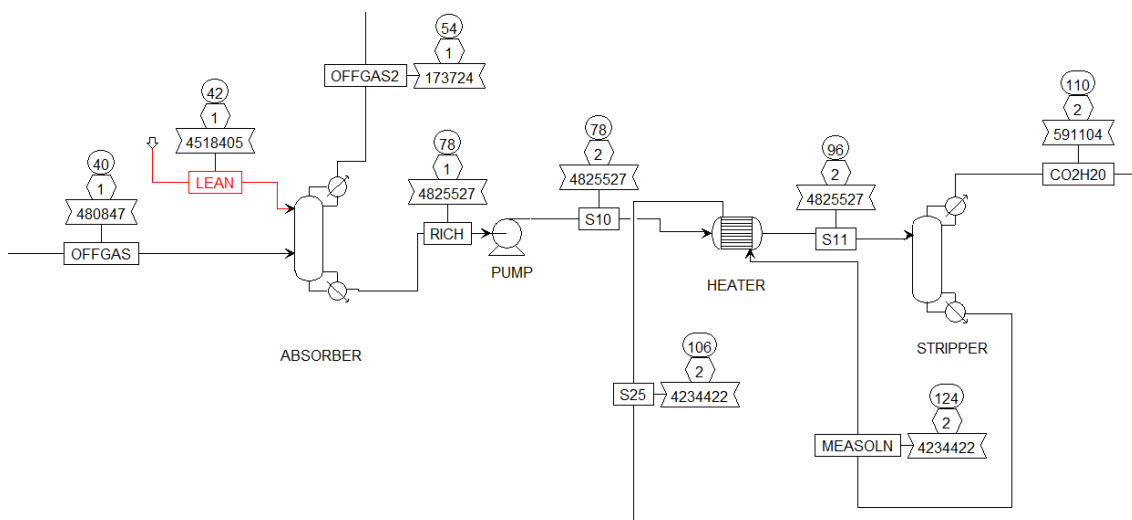


Figure 13: Process flow diagram for the CO<sub>2</sub> absorption section.

The lean ratio of 0.145 mol/mol CO<sub>2</sub>/MEA obtained from the simulation is within the required range in literature (Table 8). This value was calculated using equation 25. The rich loading ratio represents the amount of CO<sub>2</sub>/MEA that was removed from the off-gas.

Table 8: Simulation results for CO<sub>2</sub> absorption section.

CO <sub>2</sub> Absorption section	Results
Lean loading (MEASOLN)	0.145
Rich loading (Rich)	0.455
Mass % of CO <sub>2</sub> removed	99.98%

From Table 8, the amount of CO<sub>2</sub> absorbed by MEA is 99.98 wt.% which is really efficient, but this means accordingly that a high amount of energy would be required by the stripper column to separate CO<sub>2</sub> from the MEASOLN, in order to achieve the required lean ratio range that was obtained. Therefore, the energy consumption of the stripper was compared to other Aspen Plus simulation models for CO<sub>2</sub> absorption.

Table 9: Heat demand comparison of this study with literature simulation values.

	CO <sub>2</sub> -Natural Gas	CO <sub>2</sub> -Syngas IGCC	Rate-Based MEA	Literature	This study	
<b>Captured CO<sub>2</sub></b>	117517.94	121266.35	96	6050.7	60.441	kg/h
<b>Heat Demand</b>	334722.22	219444.44	142.52	7326.8	117.857	kW
<b>Ratio</b>	2.84	1.80	1.48	1.21	1.949	kW/(kg/h)

The first three columns; CO<sub>2</sub>-Natural gas, CO<sub>2</sub>-Syngas IGCC and Rate-Based MEA results were obtained from Aspen Plus examples in the Aspen Plus software for CO<sub>2</sub> absorption. The fourth and fifth column represent simulation data that were obtained from literature (Charles W. White 2003) and this study's simulation respectively. It can be seen that the ratio of stripper column's heat demand to the CO<sub>2</sub> captured is within the range of 1– 3 kW/(kg/h), which is the same for the four simulations. This result validates the heat demand for the stripper column in this study.

### 4.1.3 Product Upgrade section

The first column into which the compressed and cooled gas from the CO<sub>2</sub> absorption section goes is the DEMTH column, where light products are separated from C<sub>2</sub> products. From Figure 14, stream S8 contains methane and CO as the top products, while stream S9 contains ethylene and ethane as bottom products. The specifications given in chapter 3 were 0.0001 mole fraction of

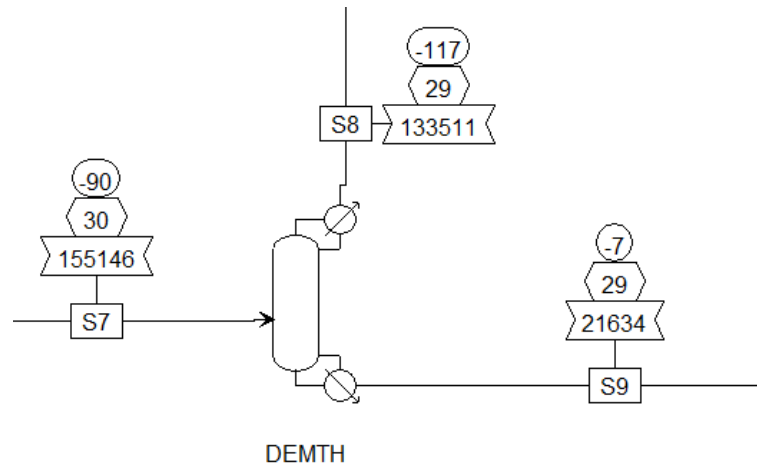


Figure 14: Process flow diagram of DEMTH column

methane and 99.99 mol.% recovery for ethylene in the bottom product. Table 10 shows that 99.9 mol.% of ethylene was recovered from the column, this value is quite high and acceptable. This shows that the DEMTH column was efficient in the separation of the products.

Table 10: Simulation result of the DEMTH column.

DEMTH	Result
Mole fraction of methane in bottom product	0.0001
Mole flow of ethylene in	455.41 kmol/h
Mole flow of ethylene out	454.92 kmol/h
Mole recovery % of ethylene	99.9

The top product containing methane and CO is further sent to the COSEP column where methane is separated from CO and recycled back to the OCM reactor. As can be seen from Figure 15, S8 is the stream from DEMTH column and CO is produced as the top product while methane is the bottom product. From the design specifications given in Chapter 3, mole fraction of CO in the bottom product is expected to be 0.00001 and the mass purity of CO in the top product, 0.999.

Table 11: Simulation results of the COSEP column.

COSEP	Results
Mole fraction of CO in bottom product	0.00001
Mass fraction of CO in top product	0.999
Mass fraction of Methane in bottom product	0.999

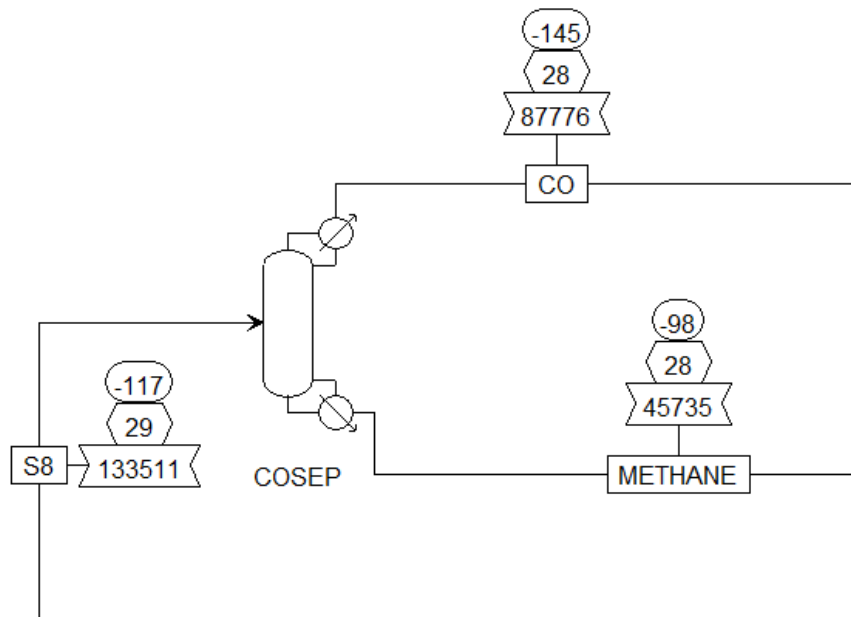


Figure 15: Process flow diagram of COSEP column

Table 11 shows the simulation results obtained from the Aspen simulation, with mass fractions of CO in top product and methane in bottom product as 0.999 and 0.999 respectively. This result shows high purity of both CO and methane, it also shows the COSEP column separated the light products sufficiently.

The bottom product from the DEMTH (S9) goes into the C2SPLIT column where ethylene is separated from ethane. As seen in Figure 16, S9 is the bottom product stream from DEMTH column, ethylene is the top product and ethane is the bottom product.

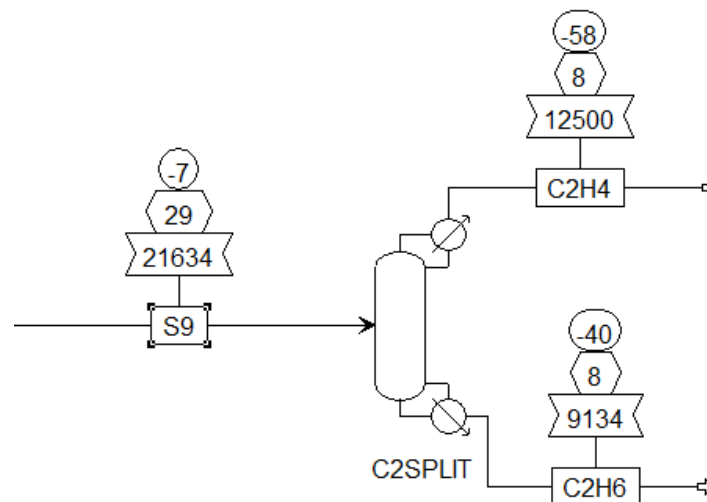


Figure 16: Process flow diagram of C2SPLIT column.

The design specifications given in chapter 3 for the C2SPLIT column were; mole purity of ethylene as 0.9997 and mole recovery of ethylene as 0.99 in the top product. Table 12 shows the simulation results from the column, with the mole purity and mole recovery of ethylene matching the design specifications. It can be seen also that the mass fraction of ethylene in the top product is 0.9996, this agrees with the required purity for polymer-based ethylene of 99.9% (Mohsenzadeh et al. 2017).

Table 12: Simulation result of the C2SPLIT column.

C2SPLIT	Result
Mole purity of ethylene in top product	0.9997
Mole of ethylene in	454.95 kmol/h
Mole of ethylene out	450.40 kmol/h
Mole recovery of ethylene in top product	0.99
Mass fraction of ethylene in top product	0.9996

#### 4.1.4 Heat Integration

The result from Aspen Energy Analyzer for the composite curve is shown in Figure 17. The blue line represents the cold streams that need to be heated up and the red line represents hot streams that need to be cooled down. The point where the two lines meet or are closest is referred to as the pinch point.

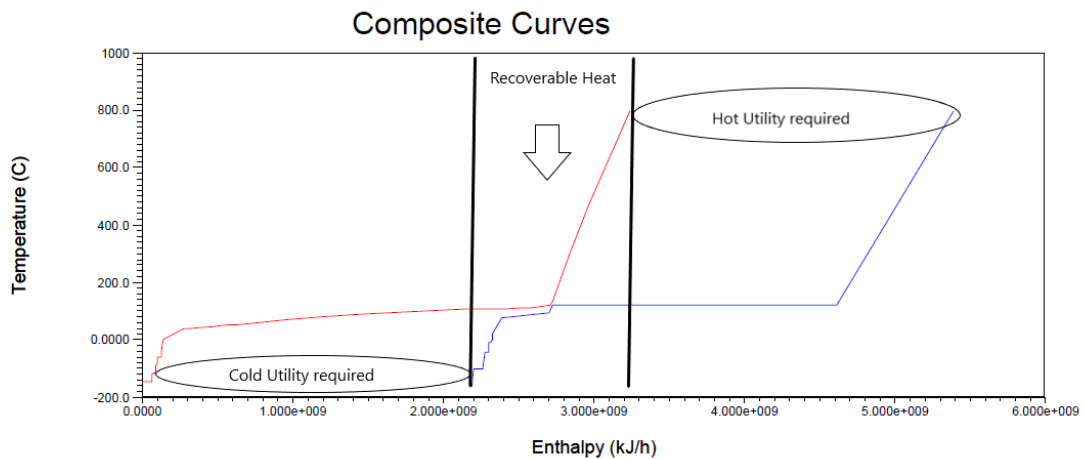


Figure 17: Composite curves from Aspen Energy analyzer for pinch point analysis.

Figure 17 shows three sections of the composite curve; hot utility required, cold utility required and recoverable heat. The range (x-axis) where the blue curve is not below the red curve requires

hot utility and the range (x-axis) where no blue curve is below the red curve requires cold utility. These regions require external utility into the process and process heat transfer is not feasible. However, the recoverable heat region shows areas where heat can be recovered and process heat transfer is feasible. From the energy savings suggestion on Aspen Plus, the cooler after the OCM reactor, where the off-gas is cooled from 800 °C – 40 °C has recoverable thermal energy. This hot stream was then utilized as heat source for heater exchangers that needed hot utility, also for the reboilers at the distillation section. This heat integration reduced the external heat demand for these heat exchangers and also the cooling demand for the cooler after the OCM reactor. After the heat integration, external heating utility was only required for the OCM reactor and the reboiler at the stripper. The calculated energy savings after the heat integration was 10 %.

The energy savings calculations, process simulation design before and after heat integration and the stream results can be found in Appendix B.

## 4.2 Economic Analysis

In this section, the results of the economic analysis done in chapter 3 will be displayed and discussed. They include; equipment sizing and costings results, CAPEX, OPEX results and Net production cost of ethylene. Parameters for carrying out sensitivity analysis will also be discussed and their results will be shown in this section.

### 4.2.1 CAPEX

The OCM reactor was modelled as a heat exchanger and so its sizing and costing results were included with the heat exchangers in this process. Table 13 shows the purchased equipment and installation costs. The number of parallel units represents the number of equipment units that would be purchased and installed in parallel. This is done solely for the purpose of cost estimation in order to reduce the size of the calculated areas of some of the heat exchangers that exceeded the correlation range in the cost estimation chart. The table for the calculation of the heat exchanger area can be found in Appendix C. The next equipment sizing and costing results was done for the compressors, pump and expander. B3 is the expander and B12a – c is the multi-compressor used in the simulation. For the sake of cost estimation, each compression stage of the multi-compressor was estimated as one compressor, the sum of their cost would give the cost of one multi-compressor unit used in the simulation.

From Table 14, it can be seen that compressors cost more than the expander or pump. The power duty used for cost estimation of these equipment can be found in Appendix C.

*Table 13: Purchasing and installation cost of OCM reactor and heat exchangers. The heat exchangers described as PEX are process heat exchangers where both hot and cold process streams are cooled and heated up simultaneously.*

Equipment	Number of parallel units	Equipment Cost M\$	Installation Cost M\$
B10 (PEX)	1	0.01	0.03
Cooler1	2	0.3	1.18
B13 (cooler)	1	0.1	0.37
Heater (PEX)	2	0.3	1.25
B11 (cooler)	4	0.7	2.60
Cooler3	11	1.7	6.87
B14 (PEX)	1	0.01	0.02
Cooler2	1	0.04	0.17
B5 (PEX)	1	0.01	0.04
B1 (PEX)	1	0.01	0.02
B4 (PEX)	1	0.02	0.10
OCM Reactor	2	0.3	1.26

*Table 14: Purchasing and installation cost of multi-compressor, pump and expander.*

Equipment	Number of parallel units	Equipment Cost M\$	Installation Cost M\$
Pump	1	0.029	0.17
B3 (expander)	1	0.367	2.19
B12a (multi-compressor)	2	5.288	63.07
B12b (multi-compressor)	2	5.727	68.31
B12c (multi-compressor)	2	5.711	68.11

The purchasing and installation cost for distillation and flash columns can be found in Table 15. The cost of internals calculated was added to the purchasing cost of the distillation column before the installation cost was calculated. It can be seen that installation of the CO<sub>2</sub> absorber and stripper cost more than the other columns. This is because the CO<sub>2</sub> absorber section has a higher mass flowrate than other sections as a result of the lean solution added to the process for the absorption of CO<sub>2</sub> and therefore it required larger columns. The calculation for the volume of the columns that was used for the estimation of its cost can be found in the Appendix C.

Table 15: Purchasing and installation cost for Distillation and flash columns.

Equipment	Number of parallel units	Cost for internals M\$	Equipment Cost M\$	Installation Cost M\$
CO <sub>2</sub> absorber	3	0.09	0.7	2.95
Stripper	4	0.16	1.1	4.33
DEMTHT	1	0.01	0.1	0.53
COSEP	3	0.20	0.5	1.94
C2SPLIT	1	0.02	0.1	0.36
Quench	1		0.02	0.09
B6	1		0.02	0.09
B7	1		0.1	0.29

After the installation cost for all the equipment was calculated, the FCI and working capital was then calculated to give a sum of 226 M\$ and 23 M\$ respectively.

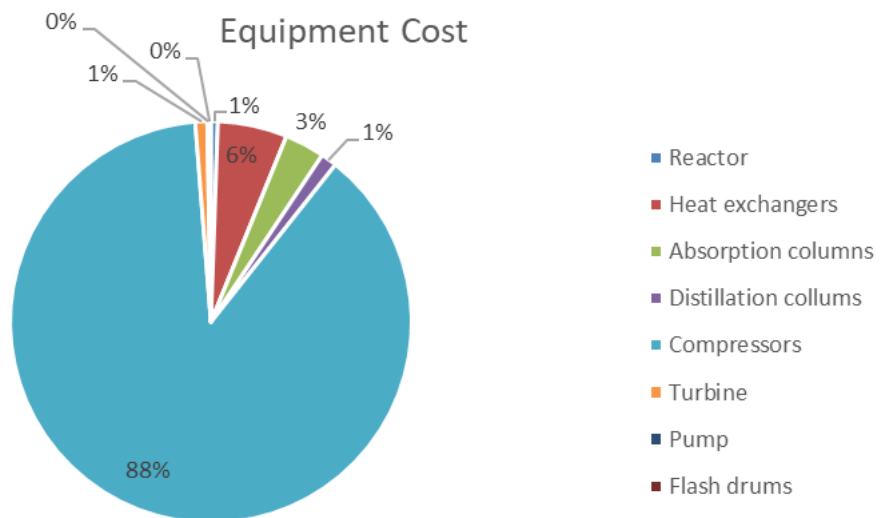


Figure 18: Summary of equipment cost.

The sum of the FCI and the working capital gives a value of 249 M\$, which is the CAPEX of the plant. Figure 18 shows a summary of the equipment purchase cost for the process. It can be seen that compressor cost contributes 88 % to the total equipment cost, while the heat exchanger contributes the second highest with a value of 6 %.

#### 4.2.2 OPEX

Values for the plant production and its parameters are shown in Table 16. The annual ethylene production is 81250 t/a, with a total plant capacity of 713716.155 t/a which includes ethylene

production and by-products from the plant. 20 years is given as its operational years, with an interest rate of 8 % and a calculated annuity as shown in Table 16.

Table 16: Plant production and parameters.

<b>Production</b>		Unit
Full load hours	6500	h/a
Ethylene production	81250000	kg/a
Plant capacity incl. By-products	713716155.4	kg/a
<b>Parameters</b>		
Operation years	20	a
Interest	8	%
Annuity	0.1018522	-

The plant capacity includes both the mass flows of ethylene produced and the by-products. The mass flows of the by-products can be found in Table 18. The data for the variable cost of the process is shown in Table 17. The utilities used in the process include: medium pressure steam for the stripper column, heat for the OCM reactor, electricity for the multi-compressor, expander and pump, cooling water for the coolers and flash drums, and refrigerants for the condensers of the distillation columns and the cooler2 before the DEMTH column. SNG and CO<sub>2</sub> are the raw materials for this process. The values of the demands for the utilities were obtained from Aspen Plus simulation and the raw material flowrates were obtained from calculations based on the desired scale of the plant.

Table 17: Demand and cost of utilities. CST demand represents the heat demand for the OCM reactor which is supplied by solar towers. Heat demand represents the heat demand for the stripper which is supplied by the parabolic trough.

<b>Variable/Energy</b>		Unit
CST demand	72	MJ/kg
Heat demand	75	MJ/kg
Electricity demand	9.313	MJ/kg
SNG demand	32037.4	kg/h
CO <sub>2</sub> demand	124319	kg/h
Cooling demand	191.273	MJ/kg
CST cost	25	\$/MWh
Heat cost	25	\$/MWh
Electricity cost	103	\$/MWh
SNG cost	6.729	\$/kg
CO <sub>2</sub> cost	0.02	\$/kg
Cooling cost	0	\$/MWh

Electricity cost was obtained from an online source (Globalpetrolprices.com 2022), with Morocco as the choice country. The cost of cooling water was obtained from BEniVer, a project which is part of the “Energiewende im Verkehr” funding initiative, whose main goal is to set same boundary conditions used for estimation of techno-economic analysis. The source of CO<sub>2</sub> was assumed to be from a pure source like a biogas upgrading plant. According to (Fu et al. 2010), industrial processes like ammonia, fermentation processes, produce an almost pure CO<sub>2</sub> and the CO<sub>2</sub> cost from such processes takes into account the cost for compression which is required for the transportation and storage of CO<sub>2</sub>. The SNG cost was obtained from literature (Vega Puga et al. 2022); a power to gas (PtG) methanation plant which utilized an alkaline electrolyzer for its hydrogen production. More details about the SNG cost are discussed in the sensitivity analysis section of this chapter.

The heat demand for the OCM reactor is represented as the CST demand in Table 17 with a value of 72 MJ/kg, this value is converted to a heat demand of 250 MW. In order to estimate the number of solar towers required to supply this heat demand, one solar tower is estimated to provide 40 MW of the heat demand. It is assumed that a solar tower is operated for 8 hours, therefore 3 solar towers are needed to cover a 24-hour operation per day. Dividing the 250 MW heat demand by 40 MW heat supplied per tower and multiplying by 3 towers needed for a 24-hour operation would result to a total of about 19 towers required. A cost of 25 \$/MWh for the CST heat was estimated from (Frantz et al. 2020) where the techno-economic analysis of an optimized design of a centrifugal particle receiver was carried out, this cost is also assumed to be the same for the heat supplied by the parabolic trough to the stripper column. The overall cost of each utility and raw material per year is shown in Table 19.

Table 18: By-Product cost.

<b>By-Product</b>	<b>Kg/h</b>	<b>Market Price (\$/kg)</b>	<b>Factor</b>	<b>M\$/a</b>
Ethane	9187.54	0.077	0.7	3.2
CO	88114.95	0.641	0.7	256.9
Total				260.1

Table 18 shows the by-products obtained in the process and how much is generated from its sales per year. The market price of both ethane and CO were obtained from (Teixeira Pentead0 2021) and (Jouny et al. 2018) respectively. Table 19 shows the OPEX summary which contains both the variable and the fixed cost. The total OPEX calculated for the plant is 1604 M\$/a.

Table 19: Operational expenditure summary.

OPEX Summary	M\$/a
Heat	83.0
SNG cost	1401.2
CO <sub>2</sub> cost	16.3
Electricity	21.6
Refrigeration	93.0
Labor	1.8
Insurance	5.0
Maintenance	10.0
Replacements	0.0
Remaining	130.7
By-Products	- 260.1

Figure 19 shows the OPEX breakdown of the process, the SNG cost represents 88 % of the OPEX, followed by 5 % for the heat cost and 4 % for refrigeration cost. The contribution of CO<sub>2</sub> and electricity to the OPEX is quite little at a value of 1 % each. The fixed costs have the least effect on the OPEX. Figure 19 also shows that the sale of by-products covers about 16 % of the OPEX cost, which leaves a remaining amount of 84 % OPEX. It is obvious that the cost of SNG is the main cost driver of the OPEX.

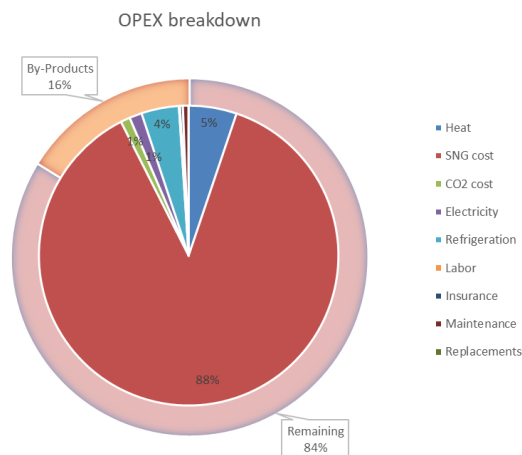


Figure 19: OPEX Breakdown. The inner pie-chart shows the specific OPEX contributions. The outer pie-chart shows the percentage of specific OPEX covered by the sale of By-Products. The 'remaining' section of the outer pie-chart is the percentage of specific OPEX not covered by the sale of By-products.

### 4.2.3 Net Production Cost

With the results of the CAPEX and OPEX obtained, the net production cost was calculated at 16.85 \$/kg of ethylene produced. From Figure 20, it can be seen that the contribution of the OPEX to the net production cost is 98 % and that of the CAPEX is 2 %. These values are shown in Figure 20.

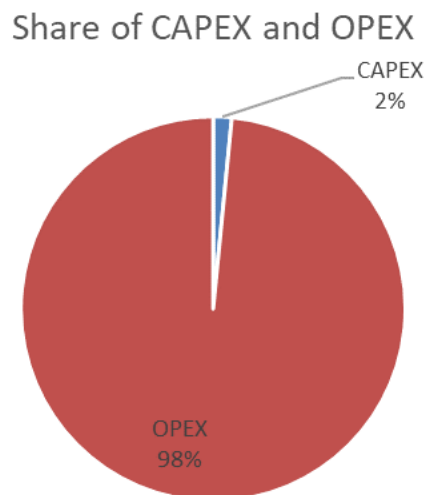


Figure 20: CAPEX and OPEX contribution to the Net production cost.

### 4.2.4 Sensitivity Analysis

The net production cost for ethylene discussed above represents the base case for the plant. Its operation is 6500 hours annually, with the SNG and CO<sub>2</sub> cost of 0.41 €/kWh and 20 €/t respectively. For the sensitivity analysis carried out in this section, the cost of SNG, cost of CO<sub>2</sub> and the operational hours of the plant were varied to obtain their effect on the NPC of ethylene.

Firstly, the operational hours were varied. As can be seen from Figure 21, the ethylene price reduces with increase in operational hours. It is observed that the relative CAPEX and OPEX reduces with increase in operational hours and vice versa when the operational hours is reduced. This could be because of increase in ethylene production capacity and sale of by-products when the operational hours are increased.

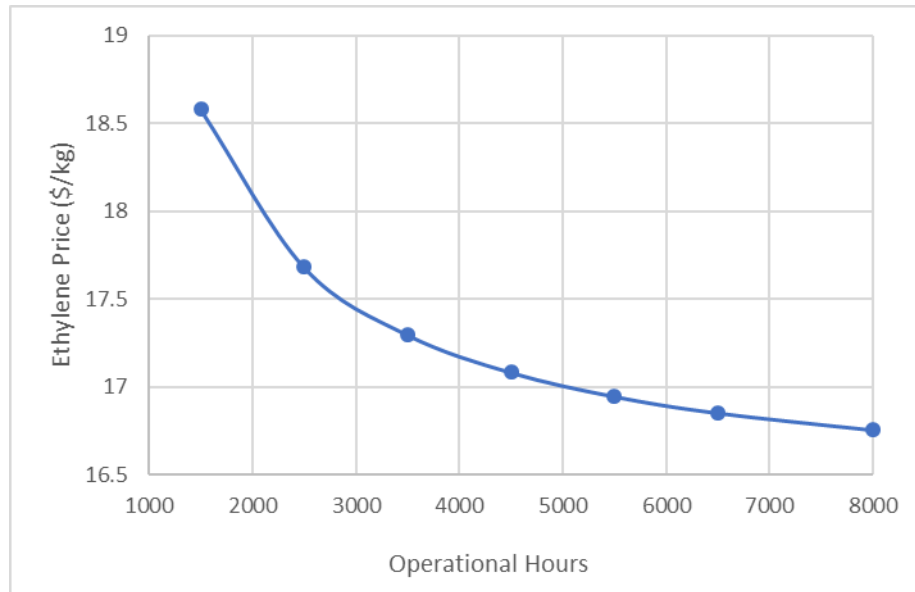


Figure 21: Ethylene Price vs operational hours of the plant.

The second sensitivity analysis was done by varying CO<sub>2</sub> cost from different industrial sources as shown in Table 20. The cost of CO<sub>2</sub> is a sum of its capture, compression and transportation cost, although the capture cost represents about (60 – 80) % of the total cost. The cost of CO<sub>2</sub> separation is inversely proportional to the CO<sub>2</sub> concentration and purity of the treated stream. Industrial processes are known to produce higher CO<sub>2</sub> concentrations than power generation, therefore they have lesser cost of separation than power generation. Cost of compression is estimated at (4 – 10) \$/t for various CO<sub>2</sub> sources (Psarras et al. 2017). As can be seen from Figure 22, CO<sub>2</sub> cost from Direct air capture (DAC) source has the highest ethylene price because of its high CO<sub>2</sub> cost shown in Table 20.

Table 20: CO<sub>2</sub> sources, cost adapted from <sup>(a)</sup>(Fu et al. 2010), <sup>(b)</sup>(Psarras et al. 2017)<sup>(c)</sup>(Giglio et al. 2015),<sup>(d)</sup>(Fasihi et al. 2019) and their corresponding ethylene production prices.

Industry	CO <sub>2</sub> Cost (\$/t)	CO <sub>2</sub> Cost in 2021 (\$/t)	Ethylene Price (\$/kg)
Biogas <sup>(a)</sup>	36-43	18	16.85
Iron/steel <sup>(b)</sup>	50-67	43	17.12
Glass <sup>(b)</sup>	59-65	63	17.35825
NGCC <sup>(c)</sup>	43	66	17.38709
Pulp/paper <sup>(b)</sup>	88	67	17.40059
Cement <sup>(c)</sup>	62	88	17.63261
DAC <sup>(d)</sup>	268-222	256	19.50399

(Fasihi et al. 2019) carried out a techno-economic analysis of low temperature DAC powered by hybrid PV-wind-battery systems in Morocco. It is projected that CO<sub>2</sub> costs from DAC in the near future will be less expensive than it is currently. Its estimated cost in 2040 and 2050 are in the range of (40 – 69) €/t and (32 – 54) €/t respectively. In summary, the higher the CO<sub>2</sub> cost, the higher the ethylene price.

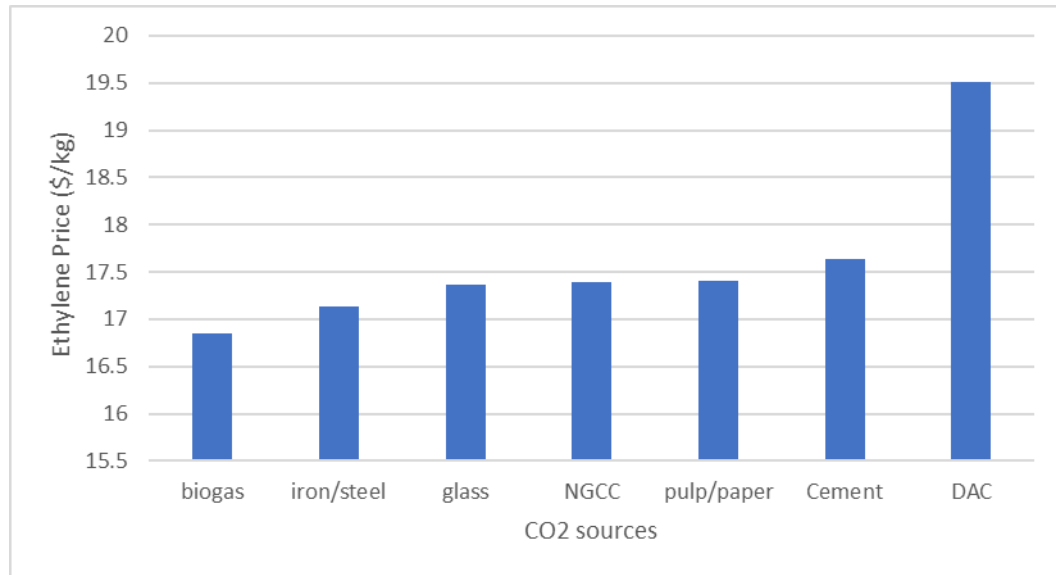


Figure 22: Ethylene price vs CO<sub>2</sub> sources.

The results obtained from the previous section shows that the OPEX contributes largely to the NPC of ethylene, furthermore, the cost of SNG is the main driver of the OPEX cost. For the sensitivity analysis based on SNG cost, the following scenarios are considered were

1. SNG from PtG plant with Alkaline electrolyzer (base-case) (Vega Puga et al. 2022).
2. SNG from PtG plant with SOEC electrolyzer (best-case) (Giglio et al. 2015).
3. Biomethane as feedstock (Leme and Seabra 2017). This is discussed in detail in the sustainable pathway comparison section of this chapter.

Based on the various SNG costs found in literature, the best-case scenario was found to be among the lower range of SNG costs, while the base-case scenario belongs to the higher SNG cost range, therefore they were chosen to investigate the effect of the wide SNG cost range on the NPC of ethylene. In addition, the two scenarios have different hydrogen production technology. The base-case was considered because it represented an SNG production technology that can be implemented in a timely manner between the two scenarios. The best-case scenario was chosen because of its low SNG cost and its prospects for the future.

Base-case SNG cost scenario with an alkaline electrolyzer (AEL) is a known mature technology for hydrogen production. From the literature source (Vega Puga et al. 2022), the cost of electricity

and CO<sub>2</sub> utilized in the plant are 46.62 \$/MWh and 18.64 \$/t respectively, with CO<sub>2</sub> source assumed to be from a biogas upgrading plant. Electricity cost was found to be one of the major cost drivers in this plant, with a value of 61 % of SNG’s cost. Other parameters like CO<sub>2</sub> cost and SNG compression had lesser impact on the price.

Solid oxide electrolysis cells (SOEC) is a promising technology for hydrogen production with high operating temperature and pressure within the range of (700 – 900) °C and 33.1 bar respectively (Giglio et al. 2015). The SOEC section was assumed to have stacks of SOEC with 1 MW<sub>el</sub> capacity each, resulting in total of 10 MW<sub>el</sub>. Electricity cost, CO<sub>2</sub> cost, SOEC stack cost and the stack degradation rate were the cost drivers in this plant.

Table 21: Summary of SNG cost scenarios.

	<b>Base-case</b>	<b>Best-case</b>	<b>Units</b>
Electrolyzer	Alkaline	SOEC	
Electrolyzer capacity	1	10	MW <sub>el</sub>
Plant availability	8000	8000	h
Electricity cost	46.62	46.62	\$/MWh
Operational lifetime	20	30	y
CO <sub>2</sub> feed cost	18.64	18.64	\$/t
CAPEX	8831.699	706-806	\$/kWh
SNG Production price	6.30	1.338	\$/kg

For both plants, the electricity cost had a big impact on the production price of SNG. In addition, the cost of CO<sub>2</sub> was a large contributor to the price of SNG in the SOEC plant. Therefore, for simplicity of comparison, the same electricity and CO<sub>2</sub> feed cost in the base-case scenario was assumed in the best case and the SNG price for the SOEC plant was obtained. The price of SNG for both scenarios are shown in Table 21. Comparing both scenarios, the SOEC case had a larger plant capacity, longer operational lifetime compared to the AEL plant. According to (Vega Puga et al. 2022), the SNG cost for the AEL plant could be reduced by 7 % with the increase of its operational lifetime from 20 to 30 years. In both cases, larger plant capacity results in lower SNG production prices although it is not stated in both studies what the percentage of reduction could be. Both cases have the same plant operational hours of 8000; however, the CAPEX value for both plants differs. The CAPEX value of the best-case scenario is about 10 times smaller than that of the base-case. The SOEC stack cost is the largest contributor to the CAPEX of the SOEC plant with 38 – 50 %, followed by the Heat Exchanger Network (HEN) with 21 – 28 %. The lower CAPEX of the SOEC plant is because of the low SOEC stack cost assumed in the study. A low SOEC stack cost of 540 \$/m<sup>2</sup> of active area was assumed as the reference cost in the study. This cost is the Department of America’s (DOE) target value for high volume scale solid oxide cell

(SOC) industrial production of above 250,000 m<sup>2</sup> annually and low SOEC degradation rate of 0.2 %/1000 h. Higher SOEC stack costs of 3500 \$/m<sup>2</sup> reflected low production volumes of 2500 m<sup>2</sup>. Degradation of SOEC cells affect both the CAPEX and also on the operating and maintenance cost. Higher SOEC stack costs and degradation rate, results in higher CAPEX and operating and maintenance cost respectively and in turn higher SNG production price. Although other factors discussed above can influence the SNG production price, the CAPEX and operating and maintenance cost of the SOEC electrolyzer appears to be a major factor for the SNG production price difference in both cases.

#### 4.2.5 Sustainable pathways comparison

The economic results of BG-OCM obtained from (Teixeira Penteadó 2021) will be compared with the economic results of the CO<sub>2</sub>-OCM in this section.

For the economic evaluation of bioethylene production from the BG-OCM process, the annualized cost method for the CAPEX was used in the study by (Teixeira Penteadó 2021) . Equipment cost was obtained from Aspen Plus economic analyzer, this cost accounts for both the equipment purchase cost and the installation cost. The sum of the equipment cost was then multiplied by a location factor of 1.7 for Brazil as the BG-OCM process was designed for Brazil. The cost of utilities and raw material are shown in Table 22 as the OPEX value for the process.

Table 22 shows the comparison of the two processes. The NPC of ethylene at 16.85 \$/kg and bioethylene at 0.51 \$/kg obtained from CO<sub>2</sub>-OCM and BG-OCM processes respectively shows that the NPC of bioethylene from the BG-OCM process is lower than ethylene from CO<sub>2</sub>-OCM. Considering the market price of conventionally produced ethylene at 1.235 \$/kg, bioethylene from this BG-OCM study is more economically competitive than fossil ethylene.

Some of the downstream processes like the DEMTH and C2SPLIT columns of the product upgrading section are similar for both the CO<sub>2</sub>-OCM and the BG-OCM. However, major differences include raw materials and by-products for the processes. The raw materials for the BG-OCM process are biogas and oxygen, while by-products are ethane and light gas; which contains majorly unconverted methane and minor amounts of CO, N<sub>2</sub>, H<sub>2</sub>. Unlike the process design for CO<sub>2</sub>-OCM in this thesis, there was no further separation of methane from other light gases and there was no recycle stream of light gases back to the reactor. This could be a contributing factor to the lower costs of ethylene from the BG-OCM process.

Table 22: Comparison of CO<sub>2</sub>-OCM and BG-OCM.

	CO <sub>2</sub> -OCM	BG-OCM	Units
C <sub>2</sub> yield	40	16.25	%
Ethylene production	81250	4625	t/a
Operation hours	6500	Not defined	h
Operational life	20	30	y
Annual. CAPEX	25.4	2.83	M\$/a
OPEX	1604.0	8.15	M\$/a
By-products	260.1	8.62	M\$/a
NPC	16.85	0.51	\$/kg

The amount of ethylene produced in CO<sub>2</sub>-OCM is about 17 times more than that produced in BG-OCM. The value of the annualized CAPEX, OPEX and by-product cost is divided by the amount of ethylene produced per year is shown in Table 23. It explains how much CAPEX, OPEX and by-products are utilized per ton of ethylene produced. The OPEX cost per ton of ethylene produced for the CO<sub>2</sub>-OCM process is about 91 % greater than that of the BG-OCM process. Considering the fact that OPEX contribution to the NPC of ethylene is 98 % in the CO<sub>2</sub>-OCM process, this could also be a contributing factor to the higher ethylene price of the process to the bio ethylene from the BG-OCM process.

Table 23: Comparison of CO<sub>2</sub>-OCM and BG-OCM (2).

	CO <sub>2</sub> -OCM	BG-OCM
Annual. CAPEX \$/t	312.125	613.9
OPEX \$/t	19742.939	1763.179
By-products \$/t	3201.745	1864.441

Another contributing factor to the lower bioethylene price of the BG-OCM process is the considerably lower cost of biogas used in the process. The biogas price in the BG-OCM study was compared to the price of biogas found in another literature (Leme and Seabra 2017) within the same region (Brazil). It was discovered that the biogas price in the BG-OCM study was quite lower than that of the second literature. This is shown in Table 24.

Table 24: Comparison of Biogas price in the BG-OCM study and a literature source (Leme and Seabra 2017).

	BG-OCM study	Literature (Leme and Seabra 2017).	
Best-case	0.0198	0.158	\$/kg
Worst-case	0.051		\$/kg

The best-case and worst-case biogas cost of the BG-OCM process represent the minimum and maximum biogas prices used in the study respectively. It can be seen that even the highest cost of biogas assumed in the BG-OCM study is lesser than the cost of biogas in literature. From the economic results of the CO<sub>2</sub>-OCM process, the price of SNG is the major cost driver. When the cost of biogas at 0.051 \$/kg used in the BG-OCM study is compared to the cost of SNG at 6.3 \$/kg

for the CO<sub>2</sub>-OCM, it can be deduced that the difference in SNG and biogas cost is majorly responsible for the corresponding difference in the NPC of ethylene and bio ethylene.

For further analysis, biomethane was replaced with SNG as the raw material in the CO<sub>2</sub>-OCM process, with the cost of biomethane was obtained from (Leme and Seabra 2017) at a price of 0.82 \$/kg. Keeping everything else in the process constant, the NPC of ethylene was estimated at 1.86 \$/kg. Although the ethylene cost from the use of biomethane as feedstock is not lower than the bioethylene cost of 0.51 \$/kg from the BG-OCM study, it shows how much the cost of either SNG or biomethane affects the NPC of ethylene from the CO<sub>2</sub>-OCM process. The same procedure was repeated for the projected cost of SNG in year 2050 at 0.051 €/kWh from (Zauner et al. 2019), the resulting NPC cost of ethylene from the CO<sub>2</sub>-OCM process was 1.64 \$/kg.

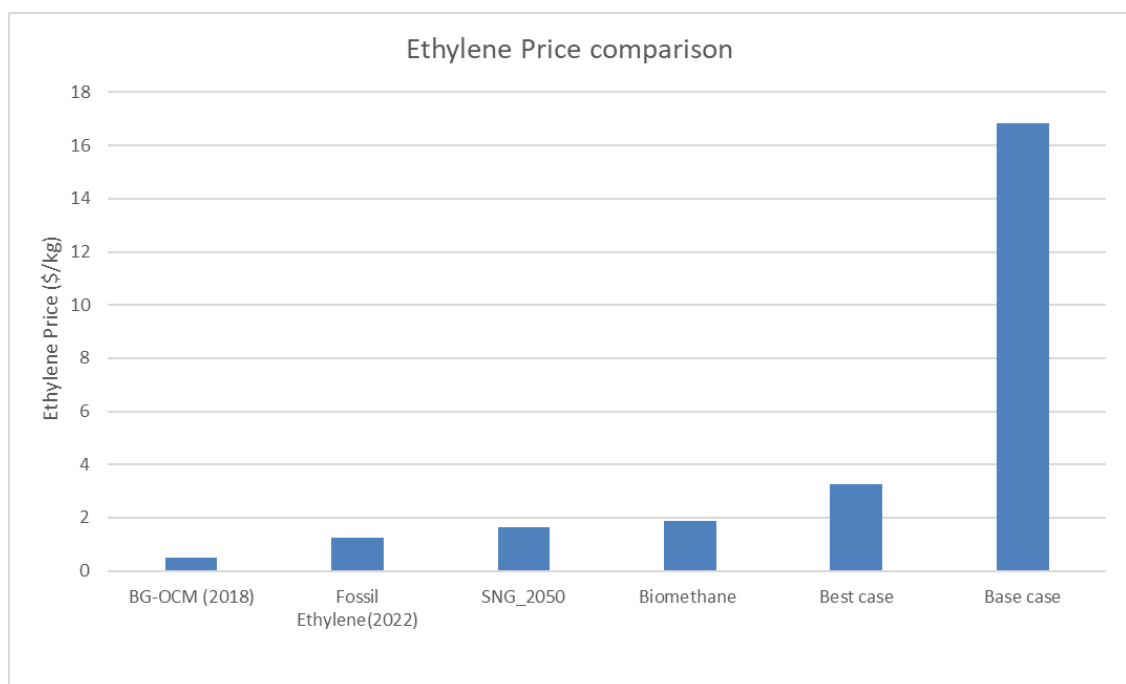


Figure 23: Ethylene price comparison.

Figure 23 shows the cost of ethylene for all production pathways discussed in this study, from the lowest (BG-OCM) to the highest cost (base case). The cost of ethylene from all cases of SNG or biomethane for the CO<sub>2</sub>-OCM process considered in this study are higher than the current market price of fossil ethylene at 1.235 \$/kg (Price of ethylene worldwide from 2017 to 2022). In summary, the use of biomethane as feedstock instead of SNG currently appears to be a more competitive approach for the CO<sub>2</sub>-OCM process.

## 5. Conclusion and Outlook

This study investigated the production of ethylene and its importance as a chemical in the chemical industry. This is due to its high market demand and its role as a base chemical for the production of other chemicals. Conventionally ethylene is produced from fossil feedstock, which releases a considerable amount of CO<sub>2</sub> into the atmosphere, and this amount becomes even more significant due to its large market demand. Therefore, the need for sustainable ethylene production pathway is necessary in order to reduce its CO<sub>2</sub> emissions in the atmosphere. Two sustainable ethylene production pathways were considered; Biogas-oxidative coupling of methane (BG-OCM) and CO<sub>2</sub>-Oxidative coupling of methane (CO<sub>2</sub>-OCM). From these two pathways, CO<sub>2</sub>-OCM was further looked into in detail.

A detailed techno-economic analysis was carried out on the CO<sub>2</sub>-OCM ethylene production pathway. The process simulation was done with the Aspen Plus V12 software. The process design was divided into three sections; OCM reaction, CO<sub>2</sub> absorption and product upgrading. The design of the OCM reactor was done based on stoichiometry and the predicted thermodynamic yield from literature. A yield of ethane and ethylene of 15 and 25 % respectively was achieved using an R-stoic reactor in Aspen Plus. The CO<sub>2</sub> absorption was designed with a Radfrac column and monoethanolamine was used as the absorbent in the absorption tower. Afterwards the off-gas containing methane, CO, CO<sub>2</sub>, ethane and ethylene were sent to the product-upgrading tower, where ethylene was separated from the mixture as the main product, CO and ethane were obtained as the by-products while methane and CO<sub>2</sub> were recycled separately back to the OCM reactor. The ethylene produced from this CO<sub>2</sub>-OCM plant is of polymer base with the required purity of 99.99 %. Heat integration was carried out after the process design to reduce the amount of external utilities required by plant.

An economic analysis was done to evaluate the feasibility of the designed process. Equipment utilized in the simulation were sized and their costs were estimated. These data were further used to calculate the CAPEX of the plant using the annualized cost method. The plant was assumed to have an annual operation hour of 6500 and an operational lifetime of 20 years. The OPEX of the plant was calculated from the cost of raw material, utilities and the fixed operational costs. The NPC of ethylene was estimated at 16.85 \$/kg. It was observed that the cost of SNG represented about 88 % of the OPEX value and the OPEX value in turn had a 98 % contribution to the NPC of ethylene, thereby making SNG the main cost driver for the NPC.

Sensitivity analysis was carried out by varying the values of the plant's operational hours between (1000 – 8000) hours, the cost of CO<sub>2</sub> from different industrial sources and the cost of SNG. Two scenarios were assumed for the cost of SNG; the base-case scenario where SNG was produced from a PtG plant with alkaline electrolyzer for hydrogen production and a best-case scenario where SNG was produced from PtG plant with SOEC electrolyzer for hydrogen production. SNG cost from the base-case scenario of 6.3 \$/kg was more than that from the best-case of 1.338 \$/kg, as such the cost of ethylene obtained from the base case was higher than that of the best case.

The economic results of ethylene from the CO<sub>2</sub>-OCM process was further compared with that from a BG-OCM process in literature. It was observed that the NPC of ethylene, the production capacity, the CAPEX and OPEX of the BG-OCM process was lesser than its corresponding values in the CO<sub>2</sub>-OCM process, although the BG-OCM had a longer project life of 30 years. This difference in price was largely attributed to the difference in cost of SNG and biogas used in CO<sub>2</sub>-OCM and BG-OCM respectively, with the maximum cost of biogas in the BG-OCM study at 0.051 \$/kg and cost of SNG at 6.3 \$/kg. The effect of SNG cost on the NPC of ethylene was investigated further, by replacing the base-case SNG cost with a cost of biomethane and a predicted cost of SNG in 2050 which resulted in a lower NPC of ethylene of 1.86 \$/kg and 1.64 \$/kg respectively.

The different costs of ethylene obtained in this study were all higher compared to the market value of fossil ethylene. The cost of bioethylene from the BG-OCM study however had a lesser value than the fossil ethylene price. It was observed that ethylene production from CO<sub>2</sub>-OCM process was not economically competitive with fossil ethylene or bioethylene from the BG-OCM study. This is not a general conclusion for all BG-OCM processes, because it was observed that the biogas cost used in the BG-OCM study was lower than the biogas cost found in literature. Biomethane would be a more economical feedstock to making the CO<sub>2</sub>-OCM process competitive than SNG, since it had lower resulting NPC, putting into consideration the availability of biomethane for such a large-scale process. Also, the potential of SNG in the future should be considered as lower prices of SNG projected in 2050 could still make SNG as feedstock to the CO<sub>2</sub>-OCM process look attractive.

The thermodynamic yield of the CO<sub>2</sub>-OCM reaction was used for the design of this process. It is however not known how lower yields and selectivity of C<sub>2</sub> products in this reaction would affect the NPC of ethylene. This would be good to investigate further because the current yield of the CO<sub>2</sub>-OCM process in literature is quite low and is not yet considered good enough for industrialization. In addition, further research is recommended for the conversion of ethane, obtained as by-product in this process, to ethylene in a subsequent downstream process. This

would improve the yield of ethylene and maybe reduce its NPC. Conventionally, ethane can be dehydrogenated to ethylene. CO<sub>2</sub>-oxidative dehydrogenation of ethane is a sustainable pathway that should be researched.

# Publication bibliography

Abanades, Stéphane; Rodat, Sylvain; Boujjat, Houssame (2021): Solar Thermochemical Green Fuels Production: A Review of Biomass Pyro-Gasification, Solar Reactor Concepts and Modelling Methods. In *Energies* 14 (5). DOI: 10.3390/en14051494.

Abu-Zahra, Mohammad R.M.; Schneiders, Léon H.J.; Niederer, John P.M.; Feron, Paul H.M.; Versteeg, Geert F. (2007): CO<sub>2</sub> capture from power plants: Part I. A parametric study of the technical performance based on monoethanolamine. In *International Journal of Greenhouse Gas Control* 1 (1), pp. 37–46. DOI: 10.1016/S1750-5836(06)00007-7.

Al-Malah, Kamal I.M. (2016): Aspen Plus®. Hoboken, NJ, USA: John Wiley & Sons, Inc.

Alshammari, Ahmad; Kalevaru, Venkata Narayana; Bagabas, Abdulaziz; Martin, Andreas (2016): Production of Ethylene and its Commercial Importance in the Global Market. In J. Davim, Hamid Al-Megren, Tiancun Xiao (Eds.): *Petrochemical Catalyst Materials, Processes, and Emerging Technologies: IGI Global (Advances in Chemical and Materials Engineering)*, pp. 82–115.

Anderson, Soren; Newell, Richard (2004): PROSPECTS FOR CARBON CAPTURE AND STORAGE TECHNOLOGIES. In *Annual Review of Environment and Resources* 29 (1), pp. 109–142. DOI: 10.1146/annurev.energy.29.082703.145619.

Aresta, Michele (2003): Carbon Dioxide Utilization: Greening Both the Energy and Chemical Industry: An Overview. In : *Utilization of Greenhouse Gases*, vol. 852: American Chemical Society (ACS Symposium Series, 852), pp. 2–39.

Aresta, Michele (2010): *Carbon dioxide as chemical feedstock*: John Wiley & Sons.

Aresta, Michele; Dibenedetto, Angela (2007): Utilisation of CO<sub>2</sub> as a chemical feedstock: opportunities and challenges. In *Dalton Transactions* (28), pp. 2975–2992.

Aresta, Michele; Dibenedetto, Angela (2021): The Carbon Dioxide Revolution. In *Carbon Dioxide Revolut*, pp. 31–43.

Aresta, Michele; Dibenedetto, Angela; Quaranta, Eugenio (2016): State of the art and perspectives in catalytic processes for CO<sub>2</sub> conversion into chemicals and fuels: The distinctive contribution of chemical catalysis and biotechnology. In *Journal of Catalysis* 343, pp. 2–45. DOI: 10.1016/j.jcat.2016.04.003.

- Arinaga, Allison M.; Ziegelski, Morgan C.; Marks, Tobin J. (2021): Alternative oxidants for the catalytic oxidative coupling of methane. In *Angewandte Chemie International Edition* 60 (19), pp. 10502–10515.
- Asami, Kenji; Fujita, Taikyu; Kusakabe, Ken-ichi; Nishiyama, Yoshiyuki; Ohtsuka, Yasuo (1995): Conversion of methane with carbon dioxide into C<sub>2</sub> hydrocarbons over metal oxides. In *Applied Catalysis A: General* 126 (2), pp. 245–255. DOI: 10.1016/0926-860X(95)00042-9.
- Billig, E.; Decker, M.; Benzinger, W.; Ketelsen, F.; Pfeifer, P.; Peters, R. et al. (2019): Non-fossil CO<sub>2</sub> recycling—The technical potential for the present and future utilization for fuels in Germany. In *Journal of CO<sub>2</sub> Utilization* 30, pp. 130–141. DOI: 10.1016/j.jcou.2019.01.012.
- Cai, Xiaojiao; Hu, Yun Hang (2019): Advances in catalytic conversion of methane and carbon dioxide to highly valuable products. In *Energy Sci Eng* 7 (1), pp. 4–29. DOI: 10.1002/ese3.278.
- Carlos Colmenares, Juan (2010): Novel Trends in the Utilization of CO<sub>2</sub> as a Reagent and Mild Oxidant in the CC Coupling Reactions. In *Current Organic Synthesis* 7 (6), pp. 533–542.
- Charles W. White (2003): ASPEN Plus Simulation of CO<sub>2</sub> Recovery Process. In.
- Chu, Yinghao; Meisen, Peter (2011): Review and comparison of different solar energy technologies. In *Global Energy Network Institute (GENI), San Diego, CA* 6, pp. 1–56.
- Dechema; Dr. Alexis Michael Bazzanella; Dr. Florian Ausfelder (2017): Low carbon energy and Low carbon energy and feedstock for the European chemical industry.
- Dimian, Alexandre C.; Bildea, Costin Sorin (2018): Energy efficient methanol-to-olefins process. In *Chemical Engineering Research and Design* 131, pp. 41–54. DOI: 10.1016/j.cherd.2017.11.009.
- Dry, Mark E. (2002): High quality diesel via the Fischer–Tropsch process – a review. In *Journal of Chemical Technology & Biotechnology* 77 (1), pp. 43–50. DOI: 10.1002/jctb.527.
- Duffie, John A.; Beckman, William A.; Worek, W. M. (1980): Solar engineering of thermal processes (Vol. 3). In *New York etc.: Wiley*.
- Dutch Association of Cost Engineers (2017): DACE Price Booklet: Cost Information for Estimation and Comparison: DACE. Available online at <https://books.google.de/books?id=d099swEACAAJ>.

European Commission (2011): Communication from the Commission to the European Parliament, the Council, the European Economic and Social Committee and the Committee of the Regions Youth Opportunities Initiative: European Commission Brussels, Belgium.

Fasihi, Mahdi; Efimova, Olga; Breyer, Christian (2019): Techno-economic assessment of CO<sub>2</sub> direct air capture plants. In *Journal of Cleaner Production* 224, pp. 957–980. DOI: 10.1016/j.jclepro.2019.03.086.

Frantz, Cathy; Buck, Reiner; Amsbeck, Lars (2020): Design and Cost Study of Improved Scaled-Up Centrifugal Particle Receiver Based on Simulation. In. ASME 2020 14th International Conference on Energy Sustainability, checked on 3/8/2022.

Fu, Qingxi; Mabilat, Corentin; Zahid, Mohsine; Brisse, Annabelle; Gautier, Ludmila (2010): Syngas production via high-temperature steam/CO<sub>2</sub> co-electrolysis: an economic assessment. In *Energy & Environmental Science* 3 (10), pp. 1382–1397.

Ganesh, Ibram (2013): Conversion of Carbon Dioxide into Several Potential Chemical Commodities Following Different Pathways - A Review. In *Materials Science Forum* 764, pp. 1–82. DOI: 10.4028/www.scientific.net/MSF.764.1.

Giglio, Emanuele; Lanzini, Andrea; Santarelli, Massimo; Leone, Pierluigi (2015): Synthetic natural gas via integrated high-temperature electrolysis and methanation: Part II—Economic analysis. In *Journal of Energy Storage* 2, pp. 64–79. DOI: 10.1016/j.est.2015.06.004.

Global Solar Atlas (2023). Available online at <https://globalsolaratlas.info/map?c=30.333445,7.03125,2>, checked on 1/10/2023.

Globalpetrolprices.com (2022). Available online at [https://www.globalpetrolprices.com/Morocco/electricity\\_prices/](https://www.globalpetrolprices.com/Morocco/electricity_prices/), checked on 3/10/2023.

Häberle, A. (2012): 19 - Concentrating solar technologies for industrial process heat and cooling. In Keith Lovegrove, Wes Stein (Eds.): *Concentrating Solar Power Technology* : Woodhead Publishing Series in Energy: Woodhead Publishing, pp. 602–619. Available online at <https://www.sciencedirect.com/science/article/pii/B9781845697693500194>.

Haydary, Juma (2019): *Chemical process design and simulation: Aspen Plus and Aspen Hysys applications*: John Wiley & Sons.

International Energy Agency (2021): Net Zero by 2050. A Roadmap for the Global Energy Sector. Edited by International Energy Agency (IEA). Available online at <https://www.iea.org/reports/net-zero-by-2050>, checked on 1/5/2023.

Ioannou, Iasonas; D'Angelo, Sebastiano C.; Martín, Antonio J.; Pérez-Ramírez, Javier; Guillén-Gosálbez, Gonzalo (2020): Hybridization of Fossil- and CO<sub>2</sub>-Based Routes for Ethylene Production using Renewable Energy. In *ChemSusChem* 13 (23), pp. 6370–6380. DOI: 10.1002/cssc.202001312.

Jouny, Matthew; Luc, Wesley; Jiao, Feng (2018): General Techno-Economic Analysis of CO<sub>2</sub> Electrolysis Systems. In *Ind Eng Chem Res* 57 (6), pp. 2165–2177. DOI: 10.1021/acs.iecr.7b03514.

Kätelhön, Arne; Meys, Raoul; Deutz, Sarah; Suh, Sangwon; Bardow, André (2019): Climate change mitigation potential of carbon capture and utilization in the chemical industry. In *PNAS* 116, Article 23, pp. 11187–11194. DOI: 10.1073/pnas.1821029116.

Koytsoumpa, Efthymia Ioanna; Bergins, Christian; Kakaras, Emmanouil (2018): The CO<sub>2</sub> economy: Review of CO<sub>2</sub> capture and reuse technologies. In *The Journal of Supercritical Fluids* 132, pp. 3–16. DOI: 10.1016/j.supflu.2017.07.029.

Leme, Rodrigo Marcelo; Seabra, Joaquim E.A. (2017): Technical-economic assessment of different biogas upgrading routes from vinasse anaerobic digestion in the Brazilian bioethanol industry. In *Energy* 119, pp. 754–766. DOI: 10.1016/j.energy.2016.11.029.

Li, Ping; Pan, Shu-Yuan; Pei, Silu; Lin, Yupo J.; Chiang, Pen-Chi (2016): Challenges and Perspectives on Carbon Fixation and Utilization Technologies: An Overview. In *Aerosol and Air Quality Research* 16 (6), pp. 1327–1344. DOI: 10.4209/aaqr.2015.12.0698.

Liu, Yuping; Kamata, Hiroyuki; Ohara, Hiroaki; Izumi, Yoshinori; Ong, Daniel Sze Wei; Chang, Jie et al. (2020): Low-Olefin Production Process Based on Fischer–Tropsch Synthesis: Process Synthesis, Optimization, and Techno-Economic Analysis. In *Ind Eng Chem Res* 59 (18), pp. 8728–8739. DOI: 10.1021/acs.iecr.0c00542.

Luyben, William L. (2017): Estimating refrigeration costs at cryogenic temperatures. In *Computers & Chemical Engineering* 103, pp. 144–150. DOI: 10.1016/j.compchemeng.2017.03.013.

- Mohsenzadeh, Abas; Zamani, Akram; Taherzadeh, Mohammad J. (2017): Bioethylene Production from Ethanol: A Review and Techno-economical Evaluation. In *ChemBioEng Reviews* 4 (2), pp. 75–91. DOI: 10.1002/cben.201600025.
- Otto, Alexander; Grube, Thomas; Schiebahn, Sebastian; Stolten, Detlef (2015): Closing the loop: captured CO<sub>2</sub> as a feedstock in the chemical industry. In *Energy & Environmental Science* 8 (11), pp. 3283–3297. DOI: 10.1039/C5EE02591E.
- Peters, Max S.; Timmerhaus, Klaus D.; West, Ronald E. (2003): Plant design and economics for chemical engineers. 5th ed. / Max S. Peters, Klaus D. Timmerhaus, Ronald West. Boston, London: McGraw-Hill (McGraw-Hill chemical engineering series).
- Price of ethylene worldwide from 2017 to 2022 (2023). Available online at <https://www.statista.com/statistics/1170573/price-ethylene-forecast-globally/>, checked on 28th march 2023.
- Psarras, Peter C.; Comello, Stephen; Bains, Praveen; Charoensawadpong, Panunya; Reichelstein, Stefan; Wilcox, Jennifer (2017): Carbon Capture and Utilization in the Industrial Sector. In *Environ. Sci. Technol* 51 (19), pp. 11440–11449. DOI: 10.1021/acs.est.7b01723.
- Ritchie, Hannah; Roser, Max; Rosado, Pablo (2020): CO<sub>2</sub> and greenhouse gas emissions. In *Our world in data*.
- Romero, Manuel; González-Aguilar, José (2014): Solar thermal CSP technology. In *Wiley Interdisciplinary Reviews: Energy and Environment* 3 (1), pp. 42–59.
- Saygin, Deger; Gielen, Dolf (2021): Zero-Emission Pathway for the Global Chemical and Petrochemical Sector. In *Energies* 14 (13). DOI: 10.3390/en14133772.
- Schreurs, Miranda A. (2016): The Paris climate agreement and the three largest emitters: China, the United States, and the European Union.
- Seader, J. D.; Henley, E. J.; Roper, D. K. (2011): Separation Process Principles. Chemical and Biochemical Operations, JohnWiley & Sons. In *Inc., New Jersey*.
- Sonawane, Pushkaraj D.; Bupesh Raja, V. K. (2018): An overview of concentrated solar energy and its applications. In *International Journal of Ambient Energy* 39 (8), pp. 898–903.
- Svinhufvud, Nina (2022): Techno-economic assessment of carbon capture and utilization in Waste-to-Energy plant.

- Takht Ravanchi, Maryam; Sahebdehfar, Saeed (2021): Catalytic conversions of CO<sub>2</sub> to help mitigate climate change: Recent process developments. In *Process Safety and Environmental Protection* 145, pp. 172–194. DOI: 10.1016/j.psep.2020.08.003.
- Teixeira Penteadó, Alberto (2021): Optimal design and evaluation of a biogas-based oxidative coupling of methane process.
- Torres Galvis, Hirsá M.; Jong, Krijn P. de (2013): Catalysts for Production of Lower Olefins from Synthesis Gas: A Review. In *ACS Catalysis* 3 (9), pp. 2130–2149. DOI: 10.1021/cs4003436.
- Towler, G.; Sinnott, R. K. (2008): *Chemical Engineering Design: Principles, Practice and Economics of Plant and Process Design*. second edition.
- Ulrich, Gael D.; Vasudevan, Palligarnai T. (2004): *Chemical Engineering Process Design and Economics: A Practical Guide*. Durham, New Hampshire, USA: Process Publishing.
- Vega Puga, Estefania; Moumin, Gkiokchan; Neumann, Nicole C.; Roeb, Martin; Ardone, Armin; Sattler, Christian (2022): Holistic View on Synthetic Natural Gas Production: A Technical, Economic and Environmental Analysis. In *Energies* 15 (5). DOI: 10.3390/en15051608.
- Wang, Shaobin; Zhu, Z. H. (2004): Catalytic Conversion of Alkanes to Olefins by Carbon Dioxide Oxidative Dehydrogenation A Review. In *Energy Fuels* 18 (4), pp. 1126–1139. DOI: 10.1021/ef0340716.
- Wilcox, Jennifer (2012): *Carbon Capture*. New York, NY: Springer New York.
- Yoro, Kelvin O.; Daramola, Michael O. (2020): Chapter 1 - CO<sub>2</sub> emission sources, greenhouse gases, and the global warming effect. In Mohammad Reza Rahimpour, Mohammad Farsi, Mohammad Amin Makarem (Eds.): *Advances in Carbon Capture*: Woodhead Publishing, pp. 3–28. Available online at <https://www.sciencedirect.com/science/article/pii/B9780128196571000013>.
- Yu, Bor-Yih; Chien, I-Lung (2016): Design and Optimization of the Methanol-to-Olefin Process. Part I: Steady-State Design and Optimization. In *Chemical Engineering & Technology* 39 (12), pp. 2293–2303.

Zauner, Andreas; Böhm, Hans; Rosenfeld, Daniel C.; Tichler, Robert (2019): Innovative large-scale energy storage technologies and Power-to-Gas concepts after optimization. In *Analysis on future technology options and on techno-economic optimization2019*.

Zhao, Zhitong; Jiang, Jingyang; Wang, Feng (2021): An economic analysis of twenty light olefin production pathways. In *Journal of Energy Chemistry* 56, pp. 193–202. DOI: 10.1016/j.jechem.2020.04.021.

# Appendix A

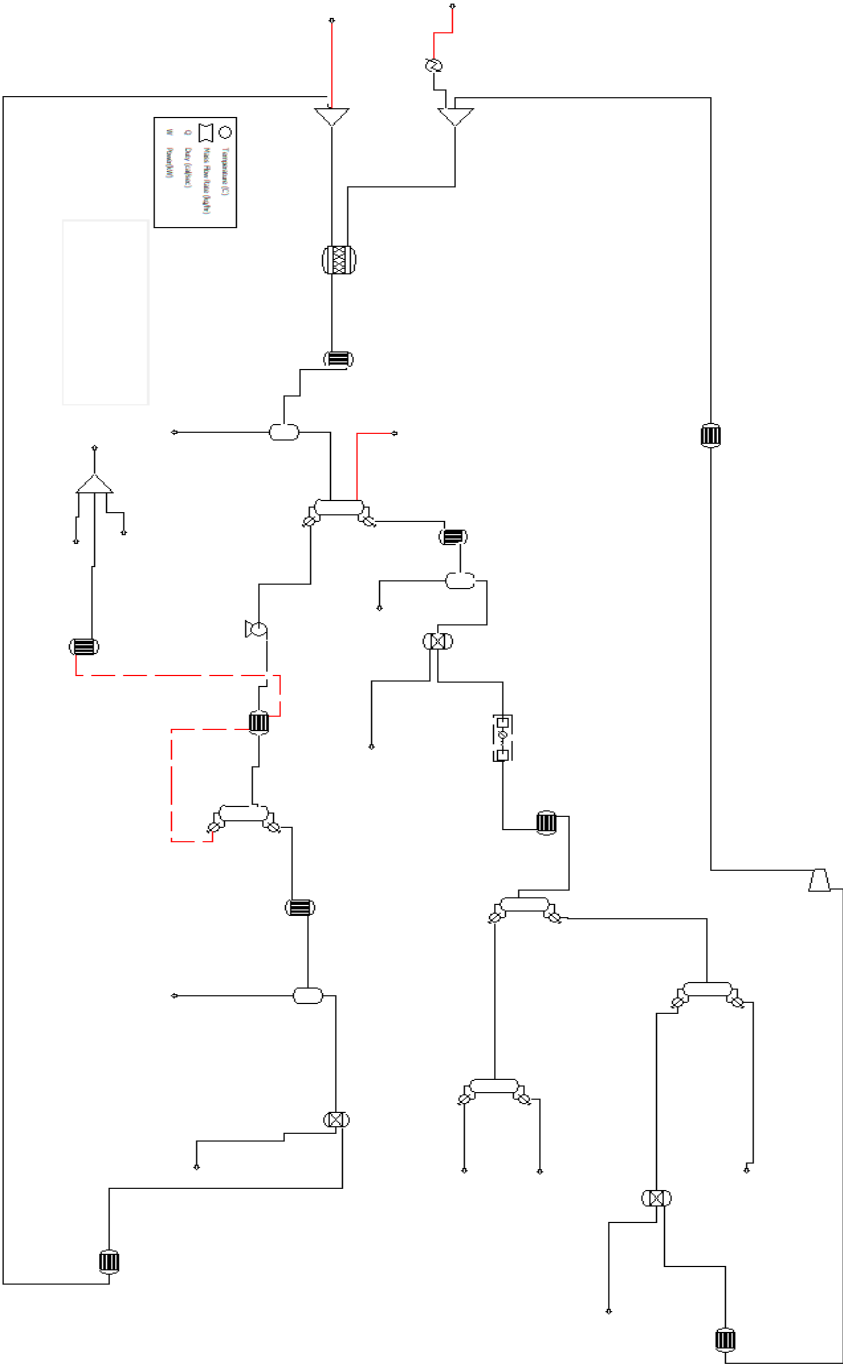
## Appendix A.1 CO<sub>2</sub>-OCM Catalysts

Appendix Table 1: list of CO<sub>2</sub>-OCM Catalysts

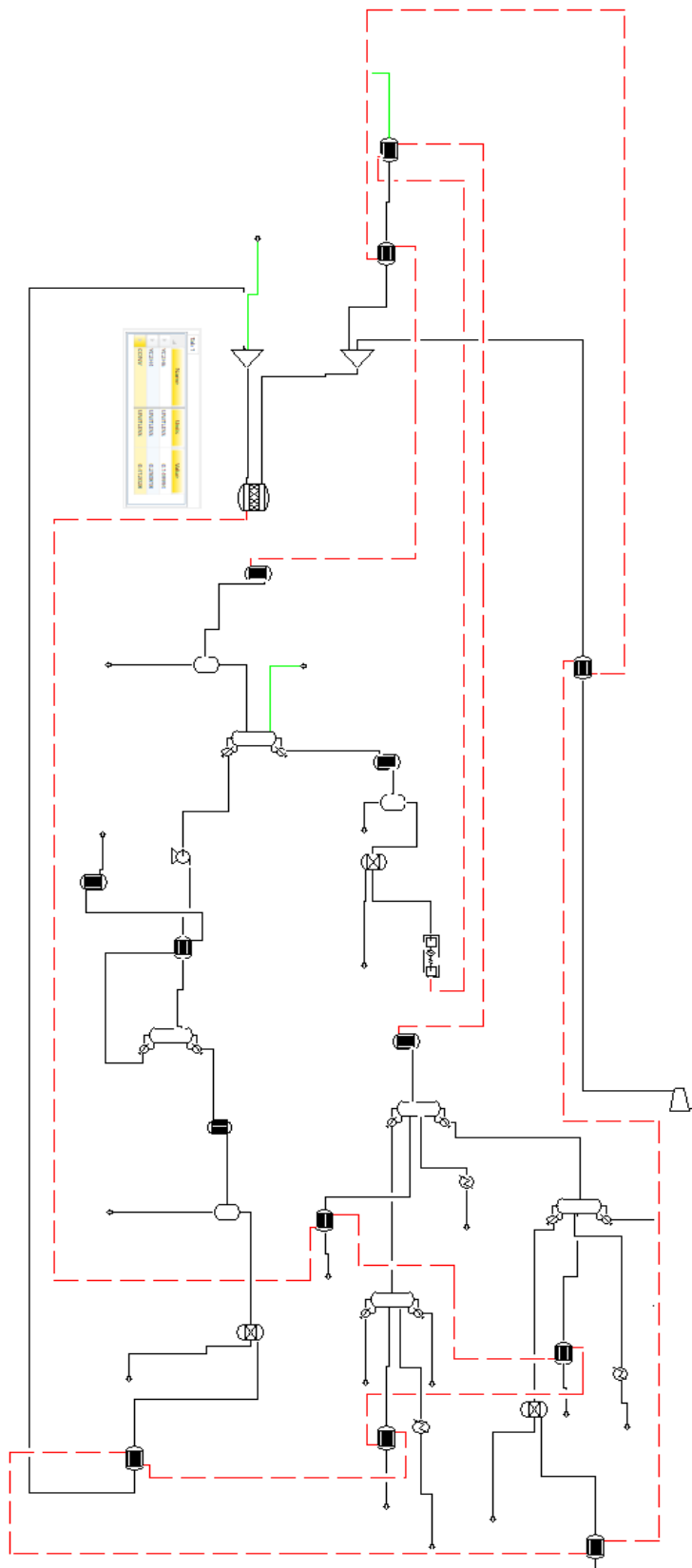
Catalyst	Temperature	Methane conversion (%)	C <sub>2</sub> selectivity (%)	Yield (%)	Source
Unsupported metal oxides: Co, Cu, La, Al, Sa et.al	850°C.			0.44%	(Cai and Hu 2019)
La <sub>2</sub> O <sub>3</sub> /ZnO	850°C.	3.1(2)	91(2)	2.80%	1) (Cai and Hu 2019) 2) (Wang and Zhu 2004)
CaO-CeO <sub>2</sub> solid solution	780-900°C 850 °C (2)	5 (2)	62 (2)	6% 3.2% (2)	1) (Cai and Hu 2019) 2) (Wang and Zhu 2004)
CaO-MnO/CeO <sub>2</sub>	700-925°C			3.74%	(Cai and Hu 2019)
CaO-ZnO	850°C 875°C (2)	5.4 (2)	80%	4.30%	1) (Cai and Hu 2019) 2) (Wang and Zhu 2004)
Nano-CeO <sub>2</sub> /ZnO	740-900°C		>80%.		(Cai and Hu 2019)
MnO-SrCO <sub>3</sub>	875°C	5.7 (2)	51	4.3% 4.5% (2)	1) (Cai and Hu 2019) 2) Wang, Zhu 2004
Mn-based binary oxides (Ca-Mn, Sr-Mn, and Ba-Mn)	850°C			4%	(Cai and Hu 2019)
Cr <sub>2</sub> O <sub>3</sub> -CaO	850°C	6.3	63	4	(Wang and Zhu 2004)
MnO <sub>2</sub> -CaO	850°C	3.9	68	2.7	(Wang and Zhu 2004)
Cr <sub>2</sub> O <sub>3</sub> -SrO	850°C	2.4	37	1.3	(Wang and Zhu 2004)
ZnO-SrO	850°C	2.8	79	2.2	(Wang and Zhu 2004)
CeO <sub>2</sub> -SrO	850°C	1.5	64	1	(Wang and Zhu 2004)
MnO <sub>2</sub> -SrO	850°C	3.9	85	3.3	(Wang and Zhu 2004)
ZnO-BaO	850°C	0.6	74	0.4	(Wang and Zhu 2004)
CeO <sub>2</sub> -BaO	850°C	0.4	55	0.2	(Wang and Zhu 2004)
Cr <sub>2</sub> O <sub>3</sub> -BaO	850°C	0.8	42	0.3	(Wang and Zhu 2004)
MnO <sub>2</sub> -BaO	850°C	3.8	67	2.6	(Wang and Zhu 2004)
Na <sub>2</sub> WO <sub>4</sub> -Mn/SiO <sub>2</sub>	820°C	4.7	94	4.5	(Wang and Zhu 2004)

# Appendix B

## Appendix B.1: Process Simulation



Appendix Figure 1: Process simulation before heat intergration



Appendix Figure 2: Process simulation after heat integration

## Appendix B.2: Stream results

Appendix Table 2: Stream results showing Temperature and Pressure (1)

Stream Name	From	To	Temperature	Pressure
Units			°C	bar
C2H4	C2SPLIT		-58.395785	8
C2H6	C2SPLIT		-39.7186331	8
CO	COSEP		-145.082036	28
CO2	B7	PURGE	4	1.77
CO2H2O	STRIPPER	COOLER3	109.532606	1.77
FEED-CH4		B4	-162	2
FEED-CO2		B8	25	1
LEAN		ABSORBER	42	1.15
MEA	SEP1		4	1
MEASOLN	STRIPPER	HEATER	124.33414	1.98
METHANE	COSEP	B2	-98.2710506	28
OFFGAS	QUENCH	ABSORBER	40	1
OFFGAS2	ABSORBER	B13	53.0762134	1
OFFGAS3	SEP1	B12	4	1
PURECO2	PURGE	B14	4	1.77
RICH	ABSORBER	PUMP	78.1790864	1
S1	B9	OCM	24.8076879	1
S2	B8	OCM	24.4102261	1
S3	OCM	B15	800	1
S4	COOLER1	QUENCH	40	1
S5	B12	B4	30	30.00000304
S6	QUENCH		40	1
S7	COOLER2	DEMTN	-90	30.00000304
S8	DEMTN	COSEP	-117.23164	29
S9	DEMTN	C2SPLIT	-6.87263277	29
S10	PUMP	HEATER	78.2125015	2.4
S11	HEATER	STRIPPER	96	2.4
S12	B2	B1	-98.2710506	28
S13	B2		-98.2710506	28
S14	COOLER3	B7	40	1.77
S15	B4	B10	-152.320611	2
S16	B14	B8	25	1.77
S17	B10	B9	25	2
S18	B1	B3	-90	28
S19	PURGE		4	1.77
S20	B3	B5	-161.299403	1
S21	B5	B9	25	1
S22	B4	COOLER2	-39.2946434	30.00000304
S23	B11		42	1.15
S24	DEMTN	B15	-8.0247548	29
S25	HEATER	B11	105.709922	1.98
S26	B6	SEP1	4	1
S27	B6		4	1
S28	B13	B6	40	1

Appendix Table 3: Stream results showing Temperature and Pressure (2)

Stream Name	From	To	Temperature	Pressure
Units			°C	bar
S29	B15		-6.87257294	29
S30	B15	B19	780.109622	1
S32	DEMTH	B18	-112.515166	29
S35	B18		-117.232	29
S36	COSEP	B19	-98.2763352	28
S37	B19		-98.2710233	28
S38	B19	B21	716.805718	1
S39	COSEP	B20	-144.971641	28
S40	B20		-145.082036	28
S41	C2SPLIT	B21	-40.0021825	8
S42	B21		-39.7156009	8
S43	C2SPLIT	B22	-58.3919781	8
S44	B22		-58.3958032	8
S45	B21	B14	689.502	1
S46	B14	B1	683.165787	1
S47	B1	B5	681.446178	1
S48	B5	B10	656.96581	1
S49	B10	COOLER1	642.527792	1
WASTEH2O	B7		4	1.77

Appendix Table 4: Stream results showing Mass and Mole Flows of the process (1)

Stream Name	From	To	Molar Vapor Fraction	Molar Liquid Fraction	Mole Flows	Mass Flows
Units					kmol/h	kg/h
C2H4	C2SPLIT		0.00	0.00	450.54	12639.30
C2H6	C2SPLIT		0.00	1.00	304.70	9187.55
CO	COSEP		1.00	0.00	3148.14	88114.92
CO2	B7	PURGE	1.00	0.00	6952.05	305175.79
CO2H2O	STRIPPER	COOLER3	1.00	0.00	22830.80	590949.27
FEED-CH4		B4	0.00	1.00	1997.00	32037.42
FEED-CO2		B8	1.00	0.00	2824.81	124319.39
LEAN		ABSORBER	0.00	1.00	190233.63	4518404.75
MEA	SEP1		0.00	1.00	38.35	721.07
MEASOLN	STRIPPER	HEATER	0.00	1.00	174210.22	4235227.14
METHANE	COSEP	B2	0.00	1.00	2836.32	45508.21
OFFGAS	QUENCH	ABSORBER	1.00	0.00	14654.63	480637.51
OFFGAS2	ABSORBER	B13	1.00	0.00	7704.94	172865.86

Appendix Table 5: Stream results showing Mass and Mole Flows of the process (2)

Stream Name	From	To	Molar Vapor Fraction	Molar Liquid Fraction	Mole Flows	Mass Flows
Units					kmol/h	kg/h
OFFGAS3	SEP1	B12	1.00	0.00	6739.69	155449.98
PURECO2	PURGE	B14	1.00	0.00	6915.80	302942.75
RICH	ABSORBER	PUMP	0.00	1.00	190196.72	4826176.40
S1	B9	OCM	1.00	0.00	4832.84	77532.05
S2	B8	OCM	1.00	0.00	9740.61	427261.91
S3	OCM	B15	1.00	0.00	15995.45	504793.96
S4	COOLER1	QUENCH	0.92	0.08	15995.45	504793.96
S5	B12	B4	1.00	0.00	6739.69	155449.98
S6	QUENCH		0.00	1.00	1340.82	24156.45
S7	COOLER2	DEMTH	0.90	0.10	6739.69	155449.98
S8	DEMTH	COSEP	1.00	0.00	5984.46	133623.13
S9	DEMTH	C2SPLIT	0.00	1.00	755.23	21826.85
S10	PUMP	HEATER	0.00	1.00	190196.78	4826176.40
S11	HEATER	STRIPPER	0.00	1.00	190256.64	4826176.40
S12	B2	B1	1.00	0.00	2835.84	45494.64
S13	B2		0.00	1.00	0.48	13.57
S14	COOLER3	B7	0.31	0.69	22812.69	590949.27
S15	B4	B10	1.00	0.00	1997.00	32037.42
S16	B14	B8	1.00	0.00	6915.80	302942.75
S17	B10	B9	1.00	0.00	1997.00	32037.42
S18	B1	B3	1.00	0.00	2835.84	45494.64
S19	PURGE		0.00	1.00	36.25	2233.05
S20	B3	B5	0.88	0.12	2835.84	45494.64
S21	B5	B9	1.00	0.00	2835.84	45494.64
S22	B4	COOLER2	1.00	0.00	6739.69	155449.98
S23	B11		0.00	1.00	174208.04	4235227.14
S24	DEMTH	B15	0.00	1.00	3010.16	86625.68
S25	HEATER	B11	0.00	1.00	174208.61	4235227.14
S26	B6	SEP1	1.00	0.00	6778.04	156171.05
S27	B6		0.00	1.00	926.68	16694.81
S28	B13	B6	0.94	0.06	7704.72	172865.86
S29	B15		0.75	0.25	3010.16	86625.68
S30	B15	B19	1.00	0.00	15995.45	504793.96
S32	DEMTH	B18	1.00	0.00	10861.75	228525.69
S35	B18		0.55	0.45	10861.75	228525.69

Appendix Table 6: Stream results showing Mass and Mole Flows of the process (3)

Stream Name	From	To	Molar Vapor Fraction	Molar Liquid Fraction	Mole Flows	Mass Flows
Units					kmol/h	kg/h
S36	COSEP	B19	0.00	1.00	15118.37	242555.27
S37	B19		0.81	0.19	15118.37	242555.27
S38	B19	B21	1.00	0.00	15995.45	504793.96
S39	COSEP	B20	1.00	0.00	33510.11	937247.18
S40	B20		0.09	0.91	33510.11	937247.18
S41	C2SPLIT	B21	0.00	1.00	2162.20	65066.52
S42	B21		0.86	0.14	2162.20	65066.52
S43	C2SPLIT	B22	1.00	0.00	2304.21	64646.33
S44	B22		0.19	0.81	2304.21	64646.33
S45	B21	B14	1.00	0.00	15995.45	504793.96
S46	B14	B1	1.00	0.00	15995.45	504793.96
S47	B1	B5	1.00	0.00	15995.45	504793.96
S48	B5	B10	1.00	0.00	15995.45	504793.96
S49	B10	COOLER1	1.00	0.00	15995.45	504793.96
WASTEH2O	B7		0.00	1.00	15860.64	285773.47

Appendix Table 7: Summary of stream results showing mass fractions (1a)

Stream Name	From	To	CH4	CO2	H2O	C2H4
Units						
C2H4	C2SPLIT		9.59E-05	2.03E-04	3.30E-75	1.00E+00
C2H6	C2SPLIT		8.26E-29	4.89E-03	1.18E-06	1.39E-02
CO	COSEP		1.00E-03	1.63E-49	0.00E+00	1.65E-39
CO2	B7	PURGE	8.79E-06	9.87E-01	1.31E-03	4.05E-03
CO2H2O	STRIPPER	COOLER3	4.54E-06	5.11E-01	4.85E-01	2.09E-03
FEED-CH4		B4	1.00E+00	0.00E+00	0.00E+00	0.00E+00
FEED-CO2		B8	0.00E+00	1.00E+00	0.00E+00	0.00E+00
LEAN		ABSORBER	0.00E+00	3.47E-08	6.70E-01	0.00E+00
MEA	SEP1		0.00E+00	0.00E+00	9.41E-01	0.00E+00
MEASOLN	STRIPPER	HEATER	1.93E-28	2.27E-05	6.46E-01	6.96E-16
METHANE	COSEP	B2	1.00E+00	3.95E-09	0.00E+00	2.81E-04
OFFGAS	QUENCH	ABSORBER	9.48E-02	6.42E-01	3.21E-02	2.92E-02
OFFGAS2	ABSORBER	B13	2.64E-01	3.31E-04	1.01E-01	7.39E-02
OFFGAS3	SEP1	B12	2.93E-01	3.06E-04	6.98E-08	8.22E-02
PURECO2	PURGE	B14	8.85E-06	9.94E-01	1.32E-03	4.08E-03
RICH	ABSORBER	PUMP	5.56E-07	1.68E-04	6.24E-01	2.56E-04
S1	B9	OCM	1.00E+00	0.00E+00	0.00E+00	0.00E+00
S2	B8	OCM	6.28E-06	9.96E-01	9.36E-04	2.89E-03

Appendix Table 8: Summary of stream results showing mass fractions (1b)

Stream Name	From	To	CH4	CO2	H2O	C2H4
Units						
S3	OCM	B15	9.03E-02	6.11E-01	7.85E-02	2.78E-02
S4	COOLER1	QUENCH	9.03E-02	6.11E-01	7.85E-02	2.78E-02
S5	B12	B4	2.93E-01	3.06E-04	6.98E-08	8.22E-02
S6	QUENCH		1.75E-07	8.07E-05	1.00E+00	9.33E-08
S7	COOLER2	DEMTN	2.93E-01	3.06E-04	6.98E-08	8.22E-02
S8	DEMTN	COSEP	3.41E-01	1.34E-09	6.35E-44	9.56E-05
S9	DEMTN	C2SPLIT	5.55E-05	2.18E-03	4.97E-07	5.85E-01
S10	PUMP	HEATER	5.56E-07	1.68E-04	6.24E-01	2.56E-04
S11	HEATER	STRIPPER	5.56E-07	7.14E-04	6.24E-01	2.56E-04
S12	B2	B1	1.00E+00	0.00E+00	0.00E+00	0.00E+00
S13	B2		0.00E+00	1.32E-05	0.00E+00	9.41E-01
S14	COOLER3	B7	4.54E-06	5.10E-01	4.84E-01	2.09E-03
S15	B4	B10	1.00E+00	0.00E+00	0.00E+00	0.00E+00
S16	B14	B8	8.85E-06	9.94E-01	1.32E-03	4.08E-03
S17	B10	B9	1.00E+00	0.00E+00	0.00E+00	0.00E+00
S18	B1	B3	1.00E+00	0.00E+00	0.00E+00	0.00E+00
S19	PURGE		0.00E+00	0.00E+00	0.00E+00	0.00E+00
S20	B3	B5	1.00E+00	0.00E+00	0.00E+00	0.00E+00
S21	B5	B9	1.00E+00	0.00E+00	0.00E+00	0.00E+00
S22	B4	COOLER2	2.93E-01	3.06E-04	6.98E-08	8.22E-02
S23	B11		0.00E+00	3.72E-08	6.46E-01	6.96E-16
S24	DEMTN	B15	1.41E-04	2.27E-03	1.68E-07	6.37E-01
S25	HEATER	B11	0.00E+00	5.97E-06	6.46E-01	6.96E-16
S26	B6	SEP1	2.92E-01	3.04E-04	4.34E-03	8.18E-02
S27	B6		9.84E-08	2.13E-08	1.00E+00	4.89E-08
S28	B13	B6	2.64E-01	2.75E-04	1.00E-01	7.39E-02
S29	B15		1.41E-04	2.27E-03	1.68E-07	6.37E-01
S30	B15	B19	9.03E-02	6.11E-01	7.85E-02	2.78E-02
S32	DEMTN	B18	4.44E-01	8.37E-09	1.26E-41	4.55E-04
S35	B18		4.44E-01	8.37E-09	1.26E-41	4.55E-04
S36	COSEP	B19	1.00E+00	1.33E-09	0.00E+00	1.06E-04
S37	B19		1.00E+00	1.33E-09	0.00E+00	1.06E-04
S38	B19	B21	9.03E-02	6.11E-01	7.85E-02	2.78E-02
S39	COSEP	B20	1.98E-03	1.56E-48	0.00E+00	1.33E-38
S40	B20		1.98E-03	1.56E-48	0.00E+00	1.33E-38
S41	C2SPLIT	B21	6.94E-28	6.33E-03	1.92E-07	2.22E-02
S42	B21		6.94E-28	6.33E-03	1.92E-07	2.22E-02
S43	C2SPLIT	B22	2.86E-05	2.54E-04	2.96E-73	1.00E+00
S44	B22		2.86E-05	2.54E-04	2.96E-73	1.00E+00
S45	B21	B14	9.03E-02	6.11E-01	7.85E-02	2.78E-02
S46	B14	B1	9.03E-02	6.11E-01	7.85E-02	2.78E-02
S47	B1	B5	9.03E-02	6.11E-01	7.85E-02	2.78E-02
S48	B5	B10	9.03E-02	6.11E-01	7.85E-02	2.78E-02
S49	B10	COOLER1	9.03E-02	6.11E-01	7.85E-02	2.78E-02
WASTEH2O	B7		9.99E-12	2.32E-04	1.00E+00	8.10E-09

Appendix Table 9: Summary of stream results showing mass fractions (2a)

Stream Name	From	To	C2H4	C2H6	CO	MEA	MEA+
Units							
C2H4	C2SPLIT		1.00E+00	2.93E-06	6.46E-08	0.00E+00	1.00E-70
C2H6	C2SPLIT		1.39E-02	9.77E-01	1.46E-45	0.00E+00	1.67E-03
CO	COSEP		1.65E-39	6.06E-56	9.99E-01	0.00E+00	0.00E+00
CO2	B7	PURGE	4.05E-03	1.84E-06	7.78E-04	4.49E-06	3.69E-03
CO2H20	STRIPPER	COOLER3	2.09E-03	9.52E-07	4.02E-04	1.88E-03	0.00E+00
FEED-CH4		B4	0.00E+00	0.00E+00	0.00E+00	0.00E+00	0.00E+00
FEED-CO2		B8	0.00E+00	0.00E+00	0.00E+00	0.00E+00	0.00E+00
LEAN		ABSORBER	0.00E+00	0.00E+00	0.00E+00	2.17E-01	4.33E-02
MEA	SEP1		0.00E+00	0.00E+00	0.00E+00	5.93E-02	0.00E+00
MEASOLN	STRIPPER	HEATER	6.96E-16	6.64E-28	1.15E-30	2.28E-01	4.74E-02
METHANE	COSEP	B2	2.81E-04	5.67E-09	1.75E-05	0.00E+00	0.00E+00
OFFGAS	QUENCH	ABSORBER	2.92E-02	1.87E-02	1.84E-01	0.00E+00	0.00E+00
OFFGAS2	ABSORBER	B13	7.39E-02	5.20E-02	5.09E-01	3.85E-04	0.00E+00
OFFGAS3	SEP1	B12	8.22E-02	5.78E-02	5.66E-01	9.12E-31	9.85E-05
PURECO2	PURGE	B14	4.08E-03	1.86E-06	7.84E-04	0.00E+00	0.00E+00
RICH	ABSORBER	PUMP	2.56E-04	1.17E-07	4.92E-05	3.45E-02	1.30E-01
S1	B9	OCM	0.00E+00	0.00E+00	0.00E+00	0.00E+00	0.00E+00
S2	B8	OCM	2.89E-03	1.32E-06	5.56E-04	0.00E+00	0.00E+00
S3	OCM	B15	2.78E-02	1.78E-02	1.75E-01	0.00E+00	0.00E+00
S4	COOLER1	QUENCH	2.78E-02	1.78E-02	1.75E-01	0.00E+00	0.00E+00
S5	B12	B4	8.22E-02	5.78E-02	5.66E-01	9.12E-31	9.85E-05
S6	QUENCH		9.33E-08	4.35E-08	4.22E-08	0.00E+00	0.00E+00
S7	COOLER2	DEMTN	8.22E-02	5.78E-02	5.66E-01	9.12E-31	9.85E-05
S8	DEMTN	COSEP	9.56E-05	1.93E-09	6.59E-01	0.00E+00	1.47E-40
S9	DEMTN	C2SPLIT	5.85E-01	4.11E-01	3.74E-08	0.00E+00	7.02E-04
S10	PUMP	HEATER	2.56E-04	1.17E-07	4.92E-05	3.45E-02	1.30E-01
S11	HEATER	STRIPPER	2.56E-04	1.17E-07	4.92E-05	3.74E-02	1.29E-01
S12	B2	B1	0.00E+00	0.00E+00	0.00E+00	0.00E+00	0.00E+00
S13	B2		9.41E-01	1.90E-05	5.85E-02	0.00E+00	0.00E+00
S14	COOLER3	B7	2.09E-03	9.52E-07	4.02E-04	3.26E-06	1.90E-03
S15	B4	B10	0.00E+00	0.00E+00	0.00E+00	0.00E+00	0.00E+00
S16	B14	B8	4.08E-03	1.86E-06	7.84E-04	0.00E+00	0.00E+00
S17	B10	B9	0.00E+00	0.00E+00	0.00E+00	0.00E+00	0.00E+00
S18	B1	B3	0.00E+00	0.00E+00	0.00E+00	0.00E+00	0.00E+00
S19	PURGE		0.00E+00	0.00E+00	0.00E+00	6.14E-04	5.04E-01
S20	B3	B5	0.00E+00	0.00E+00	0.00E+00	0.00E+00	0.00E+00
S21	B5	B9	0.00E+00	0.00E+00	0.00E+00	0.00E+00	0.00E+00
S22	B4	COOLER2	8.22E-02	5.78E-02	5.66E-01	9.12E-31	9.85E-05
S23	B11		6.96E-16	0.00E+00	0.00E+00	2.27E-01	4.83E-02
S24	DEMTN	B15	6.37E-01	3.60E-01	1.71E-07	0.00E+00	2.25E-04
S25	HEATER	B11	6.96E-16	0.00E+00	0.00E+00	2.28E-01	4.75E-02
S26	B6	SEP1	8.18E-02	5.75E-02	5.64E-01	2.74E-04	9.81E-05
S27	B6		4.89E-08	2.20E-08	1.79E-08	3.69E-05	3.42E-11
S28	B13	B6	7.39E-02	5.20E-02	5.09E-01	2.51E-04	8.86E-05
S29	B15		6.37E-01	3.60E-01	1.71E-07	0.00E+00	2.25E-04
S30	B15	B19	2.78E-02	1.78E-02	1.75E-01	0.00E+00	0.00E+00

Appendix Table 10: Summary of stream results showing mass fractions (2b)

Stream Name	From	To	C2H4	C2H6	CO	MEA	MEA+
Units							
S32	DEMTN	B18	4.55E-04	1.66E-08	5.55E-01	0.00E+00	4.13E-38
S35	B18		4.55E-04	1.66E-08	5.55E-01	0.00E+00	4.13E-38
S36	COSEP	B19	1.06E-04	1.67E-09	3.75E-05	0.00E+00	0.00E+00
S37	B19		1.06E-04	1.67E-09	3.75E-05	0.00E+00	0.00E+00
S38	B19	B21	2.78E-02	1.78E-02	1.75E-01	0.00E+00	0.00E+00
S39	COSEP	B20	1.33E-38	7.60E-55	9.98E-01	0.00E+00	0.00E+00
S40	B20		1.33E-38	7.60E-55	9.98E-01	0.00E+00	0.00E+00
S41	C2SPLIT	B21	2.22E-02	9.71E-01	3.78E-44	0.00E+00	2.71E-04
S42	B21		2.22E-02	9.71E-01	3.78E-44	0.00E+00	2.71E-04
S43	C2SPLIT	B22	1.00E+00	4.68E-06	1.47E-08	0.00E+00	8.24E-69
S44	B22		1.00E+00	4.68E-06	1.47E-08	0.00E+00	8.24E-69
S45	B21	B14	2.78E-02	1.78E-02	1.75E-01	0.00E+00	0.00E+00
S46	B14	B1	2.78E-02	1.78E-02	1.75E-01	0.00E+00	0.00E+00
S47	B1	B5	2.78E-02	1.78E-02	1.75E-01	0.00E+00	0.00E+00
S48	B5	B10	2.78E-02	1.78E-02	1.75E-01	0.00E+00	0.00E+00
S49	B10	COOLER1	2.78E-02	1.78E-02	1.75E-01	0.00E+00	0.00E+00
WASTEH2O	B7		8.10E-09	2.36E-12	8.35E-11	1.93E-06	4.23E-09

Appendix Table 11: Summary of stream results showing mass fractions (3a)

Stream Name	From	To	OH-	HCO3-	CO3-2	MEACOO
Units						
C2H4	C2SPLIT		1.17E-73	2.50E-71	1.00E-71	9.03E-71
C2H6	C2SPLIT		1.93E-06	4.15E-04	1.66E-04	1.50E-03
CO	COSEP		0.00E+00	0.00E+00	0.00E+00	0.00E+00
CO2	B7	PURGE	1.48E-09	3.61E-03	1.11E-06	1.59E-05
CO2H2O	STRIPPER	COOLER3	0.00E+00	0.00E+00	0.00E+00	0.00E+00
FEED-CH4		B4	0.00E+00	0.00E+00	0.00E+00	0.00E+00
FEED-CO2		B8	0.00E+00	0.00E+00	0.00E+00	0.00E+00
LEAN		ABSORBER	5.72E-06	3.81E-04	9.20E-04	6.87E-02
MEA	SEP1		0.00E+00	0.00E+00	0.00E+00	0.00E+00
MEASOLN	STRIPPER	HEATER	4.64E-06	1.43E-03	1.01E-04	7.66E-02
METHANE	COSEP	B2	0.00E+00	0.00E+00	0.00E+00	0.00E+00
OFFGAS	QUENCH	ABSORBER	0.00E+00	0.00E+00	0.00E+00	0.00E+00
OFFGAS2	ABSORBER	B13	0.00E+00	0.00E+00	0.00E+00	0.00E+00
OFFGAS3	SEP1	B12	1.14E-07	2.45E-05	9.83E-06	8.86E-05
PURECO2	PURGE	B14	0.00E+00	0.00E+00	0.00E+00	0.00E+00

Appendix Table 12: Summary of stream results showing mass fractions (3b)

Stream Name	From	To	OH-	HCO3-	CO3-2	MEACOO -
Units						
RICH	ABSORBER	PUMP	3.29E-07	8.47E-03	4.85E-04	2.02E-01
S1	B9	OCM	0.00E+00	0.00E+00	0.00E+00	0.00E+00
S2	B8	OCM	0.00E+00	0.00E+00	0.00E+00	0.00E+00
S3	OCM	B15	0.00E+00	0.00E+00	0.00E+00	0.00E+00
S4	COOLER1	QUENCH	0.00E+00	0.00E+00	0.00E+00	0.00E+00
S5	B12	B4	1.14E-07	2.45E-05	9.83E-06	8.86E-05
S6	QUENCH		0.00E+00	0.00E+00	0.00E+00	0.00E+00
S7	COOLER2	DEMTN	1.14E-07	2.45E-05	9.83E-06	8.86E-05
S8	DEMTN	COSEP	1.70E-43	3.66E-41	1.47E-41	1.32E-40
S9	DEMTN	C2SPLIT	8.14E-07	1.75E-04	7.00E-05	6.31E-04
S10	PUMP	HEATER	3.29E-07	8.47E-03	4.84E-04	2.02E-01
S11	HEATER	STRIPPER	3.42E-07	9.80E-03	3.03E-04	1.99E-01
S12	B2	B1	0.00E+00	0.00E+00	0.00E+00	0.00E+00
S13	B2		0.00E+00	0.00E+00	0.00E+00	0.00E+00
S14	COOLER3	B7	7.63E-10	1.86E-03	5.72E-07	8.20E-06
S15	B4	B10	0.00E+00	0.00E+00	0.00E+00	0.00E+00
S16	B14	B8	0.00E+00	0.00E+00	0.00E+00	0.00E+00
S17	B10	B9	0.00E+00	0.00E+00	0.00E+00	0.00E+00
S18	B1	B3	0.00E+00	0.00E+00	0.00E+00	0.00E+00
S19	PURGE		2.02E-07	4.93E-01	1.51E-04	2.17E-03
S20	B3	B5	0.00E+00	0.00E+00	0.00E+00	0.00E+00
S21	B5	B9	0.00E+00	0.00E+00	0.00E+00	0.00E+00
S22	B4	COOLER2	1.14E-07	2.45E-05	9.83E-06	8.86E-05
S23	B11		5.27E-06	3.94E-04	9.38E-04	7.69E-02
S24	DEMTN	B15	2.61E-07	5.60E-05	2.25E-05	2.02E-04
S25	HEATER	B11	5.09E-06	1.12E-03	1.71E-04	7.70E-02
S26	B6	SEP1	1.14E-07	2.44E-05	9.78E-06	8.81E-05
S27	B6		3.97E-14	8.52E-12	3.41E-12	3.08E-11
S28	B13	B6	1.03E-07	2.20E-05	8.84E-06	7.96E-05
S29	B15		2.61E-07	5.60E-05	2.25E-05	2.02E-04
S30	B15	B19	0.00E+00	0.00E+00	0.00E+00	0.00E+00
S32	DEMTN	B18	4.79E-41	1.03E-38	4.12E-39	3.72E-38
S35	B18		4.79E-41	1.03E-38	4.12E-39	3.72E-38
S36	COSEP	B19	0.00E+00	0.00E+00	0.00E+00	0.00E+00
S37	B19		0.00E+00	0.00E+00	0.00E+00	0.00E+00

Appendix Table 13: Summary of stream results showing mass fractions (3c)

Stream Name	From	To	OH-	HCO <sub>3</sub> <sup>-</sup>	CO <sub>3</sub> <sup>-2</sup>	MEACOO -
Units						
S38	B19	B21	0.00E+00	0.00E+00	0.00E+00	0.00E+00
S39	COSEP	B20	0.00E+00	0.00E+00	0.00E+00	0.00E+00
S40	B20		0.00E+00	0.00E+00	0.00E+00	0.00E+00
S41	C2SPLIT	B21	3.14E-07	6.74E-05	2.70E-05	2.43E-04
S42	B21		3.14E-07	6.74E-05	2.70E-05	2.43E-04
S43	C2SPLIT	B22	9.56E-72	2.05E-69	8.22E-70	7.41E-69
S44	B22		9.56E-72	2.05E-69	8.22E-70	7.41E-69
S45	B21	B14	0.00E+00	0.00E+00	0.00E+00	0.00E+00
S46	B14	B1	0.00E+00	0.00E+00	0.00E+00	0.00E+00
S47	B1	B5	0.00E+00	0.00E+00	0.00E+00	0.00E+00
S48	B5	B10	0.00E+00	0.00E+00	0.00E+00	0.00E+00
S49	B10	COOLER1	0.00E+00	0.00E+00	0.00E+00	0.00E+00
WASTEH2O	B7		1.70E-15	4.14E-09	1.27E-12	1.82E-11

## Appendix B.3: Energy Analysis

Appendix Table 14: Energy savings calculation of the process (1)

Equipment	Base Duty (cal/sec)	Optimized Duty (cal/sec)
Cooler1	4.19E+07	3.29E+07
OCM_HX	5.95E+07	5.95E+07
Reboiler_COSEP	3.66E+06	0
B10	1.95E+06	0
Reboiler_C2Split	1.55E+06	0
B5	1.38E+06	0
Reboiler_DEMTH	1.16E+06	0
B14	3.59E+05	0
B1	9.76E+04	0
Heater	1.90E+07	0
Condenser_C2split	1.43E+06	1.43E+06
COND_COSEP	4.64E+06	4.64E+06

Appendix Table 15: Energy savings calculation of the process (2)

<b>Equipment</b>	<b>Base Duty (cal/sec)</b>	<b>Optimized Duty (cal/sec)</b>
COND_DEMTH	1.52E+06	1.52E+06
COND_Stripper	2.29E+07	2.29E+07
B6_Flash_HX	2.37E+06	2.37E+06
B7_Flash_HX	6.46E+06	6.46E+06
Cooler3	4.87E+07	4.87E+07
B11	6.23E+07	6.23E+07
Cooler2	2.43E+06	1.28E+06
Reboiler_stripper	1.25E+08	1.25E+08
B13	1.67E+06	1.67E+06
Total	4.10E+08	3.70E+08
<b>Energy savings</b>		<b>10%</b>

# Appendix C

## Appendix C.1 Equipment sizing and costing

Appendix Table 16: Equipment sizing for Heat exchanger and OCM reactor

Heat exchanger	U (W/m <sup>2</sup> /K)	$\Delta T_{ln}$	Q (W)	A (m <sup>2</sup> )
B10	425	709.9	3374245.2	11.1
Cooler1	750	174.0	68823831.1	527.0
B13	750	23.8	6092737.0	341.1
Heater	2850	27.9	39450184.5	496.0
B11	2500	45.1	65363568.6	578.8
Cooler3	750	44.7	18547698.0	552.3
B14	425	671.4	1500898.5	5.2
Cooler2	425	92.7	5368245.7	136.1
B5	425	734.0	5762842.1	18.4
B1	425	776.2	406747.6	1.2
B4	425	150.5	4819836.7	75.3
OCM Reactor	750	278.8	124853018.3	597.0

The power duty of each stage of the multi-compressor (B12a – B12c) was split into two in order to fit into the correlation range of the cost estimation chart for compressors.

Appendix Table 17: Power duty for multi-compressor, pump and expander

Equipment	Power (kW)
Pump	236
B3	1657.6
B12a	3904.265
B12a1	3904.265
B12b	4250
B12b1	4250
B12c	4237.12
B12c1	4237.12

Appendix Table 18 – 7 shows the sizing of the distillation columns in the simulation, Appendix Table 21 shows the sizing of the flash drums.

Appendix Table 18: Distillation column sizing (1)

Equipment	Vv (kmol/s)	Vl (kmol/s)	Mg	MI	U <sub>f</sub> (m/s)	Pressure (Pa)	Temp (K)
CO <sub>2</sub> Absorber	2.59	19.47	22.37	25.37	12.42	100000	327.39
Stripper	3.14	15.18	25.89	24.31	9.269	177000	382.65
DEMTH	3.01	1.34	22.30	28.90	0.715	2900000	156.01
COSEP	3.10	2.81	27.98	16.04	0.359	2800000	128.06
C2SPLIT	0.64	0.51	28.05	30.16	2.081	800000	214.75

Appendix Table 19: distillation column sizing (2)

Equipment	R (J/kg. k)	Pi	P <sub>g</sub>	P <sub>l</sub>	F <sub>v1</sub>	Ad/A	C
CO <sub>2</sub> Absorber	8314	3.1416	0.823467	926.2541	0.254016	0.117113	0.137447
Stripper	8314	3.1416	1.454125	910.5248	0.181168	0.109019	0.137447
DEMTH	8314	3.1416	75.82791	358.2259	0.267102	0.118567	0.137447
COSEP	8314	3.1416	137.718	267.25	0.373072	0.130341	0.137447
C2SPLIT	8314	3.1416	14.49885	471.5548	0.152278	0.105809	0.137447

Appendix Table 20: distillation sizing (3)

Equipment	Diameter (m)	Stages	Tray spacing (m)	Space at Cond (m)	Space at Reb (m)	Height(m)	Volume (m <sup>3</sup> )
CO <sub>2</sub> Absorber	3.19	10	0.60	1.21	3.048	9.75	78.29
Stripper	3.28	12	0.60	1.21	3.048	10.97	93.01
DEMTH	1.49	26	0.60	1.21	3.048	19.50	34.26
COSEP	1.79	58	0.60	1.21	3.048	39.01	98.55
C2SPLIT	1.03	60	0.60	1.21	3.048	40.23	33.63

Appendix Table 21: Flash drum sizing

	Vl (kmol/s)	MI	PI	Vol (m <sup>3</sup> )
Quench	0.368	18.016	946.981	4.212
B6	0.275	18.015	977.436	3.044
B7	4.400	18.017	977.510	48.667

## Appendix C.2 sensitivity analysis

*Appendix Table 22: effect of plant operational hours on the price of ethylene*

<b>Operational Hours</b>	<b>Ethylene Price \$/kg</b>
1500	18.5798779
2500	17.6810736
3500	17.2958717
4500	17.0818707
5500	16.9456882
6500	16.851408
8000	16.7541816

*Appendix Table 23: comparison of ethylene prices from different production pathways*

<b>Production pathways</b>	<b>Ethylene Price \$/kg</b>
BG-OCM (2018)	0.51
Fossil Ethylene (2022)	1.235
SNG_2050	1.641543
Biomethane	1.861902
Best case	3.2703
Base case	16.85332